PB88-224332

Development of a Breadboard CO2 Laser Photoacoustic Toxic Vapor Monitor

Aerospace Corp., El Segundo, CA

Prepared for

Environmental Protection Agency
Research Triangle Park, NC

Jun 88

U.S. Department of Commerce
National Technical Information Service
NTIS

TECHNICAL REPORT DATA
(Please read Instructions on the reverse before completing)

1. REPORT NO. EPA/600/7-88/011	2.
3. RECIPIENT'S ACCESSION NO. PB88 224332/AS	
4. TITLE AND SUBTITLE Development of a Breadboard CO_2 Laser Photoacoustic Toxic Vapor Monitor	5. REPORT DATE June 1988
	6. PERFORMING ORGANIZATION CODE
7. AUTHOR(S) G. L. Loper, R. C. Corbin, M. L. Takayama, R. A. Clifton, J. A. Gelbwachs, and S. M. Beck	8. PERFORMING ORGANIZATION REPORT NO.
9. PERFORMING ORGANIZATION NAME AND ADDRESS The Aerospace Corporation El Segundo, California 90245	10. PROGRAM ELEMENT NO.
	11. CONTRACT/GRANT NO. 68-03-3171, Task 3, and CR812715-01
12. SPONSORING AGENCY NAME AND ADDRESS EPA, Office of Research and Development Air and Energy Engineering Research Laboratory Research Triangle Park, NC 27711	13. TYPE OF REPORT AND PERIOD COVERED Final Report; 1984-1987
	14. SPONSORING AGENCY CODE EPA/600/13

15. SUPPLEMENTARY NOTES AEERL project officer is Merrill D. Jackson, Mail Drop 54, 919/541-2559.

16. ABSTRACT The report describes the development of a breadboard version of a CO2 laser photoacoustic (LPA) detector. The CO2 LPA technique has been demonstrated to be capable of detecting, with high specificity, a variety of toxic compounds at low parts-per-billion (ppb) levels in multicomponent air samples. The technique can be used for monitoring trace levels of various hazardous compounds in ambient air samples. Key achievements during the program included: (1) Determination of CO2 laser absorption cross-section data for seven compounds of EPA concern that are volatile constituents of hazardous chemical waste. These data show that the LPA method can detect these compounds in ambient air at levels well below their most stringent TLVs. (2) Development of an acoustic-frequency-tracking device that allows the use of a resonant photoacoustic cell for the first time under field conditions of changing temperature and humidity. (3) Identification of nonadsorptive materials for use in air sampling lines and for coating the cell's interior to minimize sample adsorption and reaction losses. (4) Development of a pyro-electronic device that automatically determines the wavelength of a CO2 laser transition, allowing the laser-wavelength selection to be placed under closed-loop control. (5) Analysis of laboratory-prepared air mixtures to determine the instrument's performance.

17. KEY WORDS AND DOCUMENT ANALYSIS

a. DESCRIPTORS	b. IDENTIFIERS/OPEN ENDED TERMS	c. COSATI Field/Group
Pollution Toxicity Hydrazines Carbon Dioxide Lasers Acoustic Detection Monitors Vapors	Pollution Control Stationary Sources CO_2 Laser Photoacoustic Monitors	13B 06T 07C 20E 17A 14G 07D

18. DISTRIBUTION STATEMENT **Release to Public**	19. SECURITY CLASS *(This Report)* **Unclassified**	21. NO. OF PAGES 113
	20. SECURITY CLASS *(This page)* **Unclassified**	22. PRICE PC$19.95/MF$6.95

EPA Form 2220-1 (9-73)

PB88-224332

EPA/600/7-88/011
June 1988

DEVELOPMENT OF A BREADBOARD CO_2 LASER PHOTOACOUSTIC TOXIC VAPOR MONITOR

by

G. L. LOPER, R. C. CORBIN, M. L. TAKAYAMA,
R. A. CLIFTON, J. A. GELBWACHS, and S. M. BECK

THE AEROSPACE CORPORATION
El Segundo, California 90245

Contract 68-03-3171
Work Assignment 3

and

Cooperative Agreement
CR812715-01

EPA Project Officer
Merrill D. Jackson

Air and Energy Engineering Research Laboratory
Research Triangle Park, North Carolina 27711

AIR AND ENERGY ENGINEERING RESEARCH LABORATORY
OFFICE OF RESEARCH AND DEVELOPMENT
U.S. ENVIRONMENTAL PROTECTION AGENCY
RESEARCH TRIANGLE PARK, NC 27711

REPRODUCED BY
U.S. DEPARTMENT OF COMMERCE
National Technical Information Service
SPRINGFIELD, VA. 22161

NOTICE

This document has been reviewed in accordance with U.S. Environmental Protection Agency policy and approved for publication. Mention of trade names or commercial products does not constitute endorsement or recommendation for use.

ABSTRACT

This report describes progress made during FYs 1984 through 1987 toward the development of a breadboard version of a CO_2 laser photoacoustic detector. The work was carried out as part of EPA contract 68-03-3171 and cooperative agreement CR812715-01. The CO_2 laser photoacoustic technique has been demonstrated to be capable of detecting, with high specificity, a variety of toxic compounds at low parts-per-billion (ppb) levels in multicomponent air samples. Both the U.S. Air Force and the EPA could use the detection technique for monitoring trace levels of various hazardous compounds in ambient air samples.

Key achievements during the program included: (1) The determination of CO_2 laser absorption cross-section data for seven compounds of EPA concern that are volatile constituents of hazardous chemical waste. These data show that the laser photoacoustic method could detect these compounds in the ambient air at levels well below their most stringent Threshold Limit Values. (2) The development of an acoustic-frequency-tracking device that allows the use of a resonant photoacoustic cell for the first time under field conditions of changing temperature and humidity. (3) The identification of nonadsorptive materials for use in air sampling lines and for coating the cell's interior to minimize sample adsorption and reaction losses. (4) The development of a pyro-electronic device that automatically determines the wavelength of a CO_2 laser transition. This device allows the laser-wavelength selection process to be placed under closed-loop control. (5) The placement of a breadboard detector under microcomputer control such that all wavelength selection procedures and the calculation and display of the unknown concentrations of the gases in the air sample are performed automatically. (6) The analysis of laboratory-prepared air mixtures to determine the performance capability of the instrument.

Experiments performed on the laboratory-prepared mixtures showed that the fully automated breadboard instrument can detect hydrazine, a toxic rocket fuel used by the Air Force, at concentrations as low as 5 ppb in the presence of three interfering gases at concentrations as much as 600 times greater.

TABLE OF CONTENTS

ABSTRACT iii

TABLES v

FIGURES vi

INTRODUCTION 1

CHAPTER I. BACKGROUND 3

A. CO_2 LASER PHOTOACOUSTIC TECHNIQUE OPERATING PRINCIPLES . . . 3

B. AIR FORCE AND EPA NEED FOR IMPROVED TOXIC VAPOR DETECTORS . . 5

C. RESULTS FROM PREVIOUS AEROSPACE STUDIES 10

D. ADVANCES MADE DURING PROGRAM TO DEVELOP BREADBOARD INSTRUMENT 11

CHAPTER II. DETERMINATION OF PRACTICAL PHOTOACOUSTIC CELL DESIGN (TASK 1) 13

CHAPTER III. PHOTOACOUSTIC CELL AND SAMPLING LINE MATERIALS (TASK 2) 18

CHAPTER IV. ABSORPTION CROSS-SECTION MEASUREMENTS (TASK 3) 20

CHAPTER V. AUTOMATION OF BREADBOARD DETECTOR (TASK 4) 22

A. AUTOMATIC WAVELENGTH VERIFICATION DEVICE 23

B. COMPUTER CONTROL OF LASER WAVELENGTH 25

C. MATRIX INVERSION PROGRAM FOR CALCULATING UNKNOWN GAS CONCENTRATIONS 27

CHAPTER VI. LABORATORY DEMONSTRATION OF BREADBOARD INSTRUMENT . . . 29

CHAPTER VII. SUMMARY, CONCLUSIONS AND RECOMMENDATIONS FOR FUTURE WORK 42

REFERENCES 46

APPENDIX A. QUALITY ASSURANCE PROCEDURES A-1

A. PHOTOACOUSTIC CELL DESIGN (TASK 1) AND CELL MATERIALS (TASK 2) A-1

B. PHOTOACOUSTIC CELL MATERIALS (TASK 2) A-5

C. ABSORPTION CROSS-SECTION MEASUREMENTS (TASK 3) A-6

APPENDIX B. ELECTRONIC DEVICE TO TRACK RESONANT CELL FREQUENCY . . . B-1

APPENDIX C. C-1

A. CELL COATINGS TO MINIMIZE SAMPLE (NH_3 AND N_2H_4) ADSORPTION FOR LOW-LEVEL PHOTOACOUSTIC DETECTION C-1

B. HYDRAZINE SAMPLING LINE TESTS C-11

APPENDIX D. CO_2 LASER ABSORPTION SPECTRA OF VOLATILE CONSTITUENTS OF HAZARDOUS WASTE D-1

TABLES

Number		Page
1.	Comparison of air monitoring methods for hydrazine fuels	6
2	Results of consecutive mixture analyse: Static mixture concentrations	37
3	Results of consecutive mixture analyses: Changing mixture concentrations	38
4	Results of analyses of a mixture in which the hydrazine concentration was varied by changing its relative flow rate into the gas mixing system. The concentrations of other components were held constant	40

FIGURES

Number		Page
1	Calculation of concentrations of species in a mixture.....	8
2	Resonant photoacoustic cell for the breadboard detector.....	15
3	Log-Log plot of the resonance cell response versus ethylene concentration in nitrogen. Also shown are the noise floors due to several contributing sources which limit the ethylene detection level to 1.8 ppb at one watt of laser power and a 1.2 liters/min gas sample flow rate	17
4	Chemical structures for compounds studied in task 3	21
5	Pyro-electronic device for verifying CO_2 laser wavelength.....	24
6	Schematic diagram of flow system for producing mixtures of various relative concentrations	30
7	CO_2 laser absorption spectrum for hydrazine	31
8	CO_2 laser absorption spectrum for methyl bromide	32
9	CO_2 laser absorption spectrum for ammonia	33
10	CO_2 laser absorption spectrum for ethylene	35
11	Superimposed CO_2 laser absorption spectra of hydrazine, methyl bromide, ammonia and ethylene	36
12	Plot of hydrazine concentration detected by photo-acoustic apparatus as a function of the relative flow rate of the hydrazine into the gas mixing manifold	41

INTRODUCTION

A breadboard version of a CO_2 laser photoacoustic detector has been developed for the U. S. Air Force Space Division (AFSD) and the Environmental Protection Agency as part of EPA contract 68-03-3171 and EPA cooperative agreement CR812715-01. This detector can automatically and simultaneously monitor low parts-per-billion (ppb) level concentrations of several gases in laboratory-prepared air samples with high specificity. For example, the instrument has been demonstrated to be able to detect hydrazine at concentrations as low as 5 ppb in gas mixtures in nitrogen containing as much as 500 ppb of the interfering gases ethylene and ammonia and 3 parts-per-million (ppm) methyl bromide.

When fully-developed, this detector will be capable of monitoring areas that have potential hazards from toxic compounds and will provide personnel protection not possible at this time. The Air Force has an interest in using a fully-developed version of this instrument for the rapid detection, at their threshold-limit-values (TLVs), of various toxic or carcinogenic compounds that may inadvertently be present in air samples at satellite launch sites. These compounds could include the extensively used hydrazine-based rocket fuels and some of their air-oxidation products. The results obtained in this study will assist EPA in developing a prototype TLV-level detector for various toxic gases that can be used in on-site environmental evaluations. Such a detector will assist EPA in obtaining, on schedule, required contamination data on toxic vapors in the vicinity of energy conversion and hazardous waste incineration projects. This report describes the work performed during FYs 1984 through 1987 leading to the development of the breadboard CO_2 laser photoacoustic detector.

The development of the breadboard instrument has required completion of important research and development tasks: (1) Work needed to be carried out to determine the optimum photoacoustic cell design for use in a practical field instrument. (2) The photoacoustic cell materials and geometry, as well as sample flow rates, had to be selected to minimize adsorption or reaction losses of sampled gases on the cell walls. (3) CO_2 laser absorption cross-section data had to be measured for several compounds whose detection are of interest by this technique. (4) The detection system needed to be interfaced to a microcomputer to allow automatic wavelength selection and the calculation of the concentrations of the various components in the mixture.

The principles of operation of the CO_2 laser photoacoustic technique are described in Section I. Also outlined here is the background to the need by the Air Force and EPA for an instrument that can specifically and simultaneously detect a variety of toxic vapors at low ppb levels. The results obtained on tasks (1) through (4) above are described in Sections II through V, respectively. The results of experiments to determine the performance capabilities of the breadboard instrument are described in Section VI. Conclusions to the study and recommendations for future detection system development work are described in Section VII. Quality assurance procedures employed in the experimental tasks are outlined in Appendix A. Appendixes B through E provide further detail on the procedures and results obtained in tasks 1 through 4, respectively.

I. BACKGROUND

A. CO_2 Laser Photoacoustic Technique Operating Principles

By the CO_2 laser photoacoustic technique[1-3], an intensity-modulated beam of CO_2 laser radiation is passed through a cell containing the gas mixture to be analyzed. The wavelength of this radiation is chosen to be coincident with an infrared absorption feature of the species to be detected. The radiation periodically absorbed by the species of interest is transferred, through collisions with the nonabsorbing surrounding gas molecules (N_2 and O_2), into thermal motion of the entire gas mixture. This produces a modulated pressure rise in the cell which can be sensitively detected by a pressure transducer used in combination with a lock-in amplifier. If the laser intensity is modulated at frequencies in the audio region, a microphone can be used as the pressure transducer.

The CO_2 laser portion of the detection system can provide highly specific detection of species in multicomponent air samples. The CO_2 laser provides an output of numerous, discretely tunable lines within the 9-11 micrometer wavelength region[4]. Many organic and inorganic compounds possess strong absorption bands due to skeletal stretching and bending vibrational modes in this region[5,6]. The wavelength positions, shapes, and intensities of these bands are highly dependent on the molecule's size, geometry, and type of bonding. Thus a molecule's CO_2 laser absorption spectrum can serve to uniquely identify it. In addition, interferences due to the atmospheric constituents water vapor and CO_2 are minimized in this wavelength region due to the presence of an atmospheric transmission window in the 8-

12 micrometer region[7-9].

The photoacoustic detector portion of the instrument is responsible for the high detection sensitivities. Photoacoustic detection methods are inherently more sensitive than conventional long-path absorption techniques. The sensitivity of conventional long-path absorption techniques is limited by the difficulty in measuring the small difference in the intensities of the incident and transmitted laser beams through the absorber of interest. The photoacoustic method, on the other hand, measures small absorption signals against a null background. The photoacoustic signal is directly proportional to the optical power absorbed. Photoacoustic detectors routinely provide minimum detectable absorptivity values of 10^{-8} $cm^{-1}W$. When equipped with a CO_2 laser that provides output powers of a few watts, these detectors can provide interference-free detection limits of 1 ppb for molecules with moderate (about 5 $cm^{-1}atm^{-1}$) absorption strengths.

B. Air Force and EPA Need for Improved Toxic Vapor Detectors

The Air Force needs a single analytical instrument for rapidly and reliably monitoring a variety of toxic compounds (including the hydrazine-based rocket fuels and their atmospheric degradation products) at low ppb levels in the air at various locations at satellite and missile launch sites, near fuel production facilities, or during fuel transport. It is desired that the detector will have a dynamic range of response of greater than 10^4. This would allow the Air Force to monitor the hydrazine fuels at concentrations all the way from one-half of their ACGIH threshold limit values, TLVs, (TLVs are 100, 200, and 500 ppb for hydrazine, monomethylhydrazine (MMH), and unsymmetrical dimethylhydrazine (UDMH), respectively) as they are now required to do, up to levels that would allow both protection of payloads during payload integration activities (5-10 ppm) and detection of the fuels at their lower explosion limits, LELs, (1000 ppm). An instrument is desired that is sufficiently general that it will be able to detect, at their TLVs, hazardous compounds that may be increasingly used in future launch operations. Examples might include various epoxide curing agents, and the volatile constituents of solid propellants used in future launch vehicles.

Table I compares the performance characteristics of the various detectors under development for monitoring the hydrazine fuels at their TLVs. The different detectors possess various advantages and disadvantages. However, only the CO_2 laser photoacoustic detector possesses all the desired attributes listed. In particular, this instrument is the only one under development for the hydrazine fuels that can carry out highly specific, multicomponent analysis on mixtures containing a large number of different compounds. A

TABLE I.

COMPARISON OF AIR MONITORING METHODS FOR HYDRAZINE FUELS

METHOD	SENSITIVITY	GENERALITY	MULTIGAS CAPABILITY	INTERFERENCE DISCRIMINATION	DYNAMIC RANGE	PORTABILITY
ELECTROCHEMICAL CELL	LOW PPB	POOR	POOR	POOR	POOR	HAND CARRY
CHEMICALLY IMPREG. TAPE	LOW PPB	POOR	POOR	MODERATE	POOR	FIXED
UV LAMP-INDUCED PHOTOIONIZATION	LOW PPB	POOR	POOR	MODERATE	VERY GOOD	HAND CARRY
RXS. OF DERIVATIZED FUELS LEADING TO NO_2 LUMINESCENCE	LOW PPB	POOR	POOR	GOOD	VERY GOOD	FIXED
CO_2 LASER PHOTOACOUSTIC	LOW PPB	GOOD	EXCELLENT	GOOD	VERY GOOD	CART

detector of this type would also be useful to EPA in applications such as monitoring TLV concentrations of toxic gases in the air near hazardous waste dumps.

By properly selecting the CO_2 laser wavelengths used in the analysis of a gas mixture it is possible to determine the concentrations of the various absorbing components in the mixture. For example, first consider the case of a sample containing the three hydrazine fuels and no other species. It would be possible to determine the concentrations of each of the hydrazines by performing absorption measurements at three or more CO_2 laser wavelengths if the absorption cross sections at these wavelengths are known for each of the hydrazines. (Here each hydrazine must have a non-zero cross section for at least one of the monitoring wavelengths). The concentrations of these species are determined by solving a set of three simultaneous equations (see Fig. 1a). These simultaneous equations can readily be solved on a microcomputer by matrix inversion techniques.

Next consider the case of a sample containing the three hydrazines as well as two other components that absorb at CO_2 laser wavelengths. In this case it would be possible to determine the concentrations of all five species in the mixture by carrying out the analysis at five or more CO_2 laser wavelengths assuming the CO_2 laser absorption cross sections are known for each species at the monitoring wavelengths. Thus, the detection of n additional compounds in a mixture only requires that both absorption cross section data be available and absorption measurements be carried out at n or more additional CO_2 laser wavelengths (see Fig. 1b). The use of the CO_2 laser photoacoustic detection method for toxic vapor monitoring applications could minimize future detector development costs. It would not be necessary to develop a new detector, or even a new colorimetric reagent or new electrochemical cell as in the

CALCULATION OF CONCENTRATIONS OF SPECIES IN A MIXTURE

FIG. 1A

FOR MIXTURE OF 3 HYDRAZINE FUELS:

$$ABS(\lambda_1) = L(\sigma_{1H}C_H + \sigma_{1M}C_M + \sigma_{1U}C_U)$$

$$ABS(\lambda_2) = L(\sigma_{2H}C_H + \sigma_{2M}C_M + \sigma_{2U}C_U)$$

$$ABS(\lambda_3) = L(\sigma_{3H}C_H + \sigma_{3M}C_M + \sigma_{3U}C_U)$$

$$\begin{bmatrix} C_H \\ C_M \\ C_U \end{bmatrix} = \begin{bmatrix} \sigma_{1H} & \sigma_{1M} & \sigma_{1U} \\ \sigma_{2H} & \sigma_{2M} & \sigma_{2U} \\ \sigma_{3H} & \sigma_{3M} & \sigma_{3U} \end{bmatrix}^{-1} \begin{bmatrix} \frac{ABS(\lambda_1)}{L} \\ \frac{ABS(\lambda_2)}{L} \\ \frac{ABS(\lambda_3)}{L} \end{bmatrix}$$

FIG. 1B

FOR MIXTURE OF 3 HYDRAZINE FUELS
PLUS 2 ADDITIONAL COMPONENTS (A AND B):

$$ABS(\lambda_1) = L(\sigma_{1H}C_H + \sigma_{1M}C_M + \sigma_{1U}C_U + \sigma_{1A}C_A + \sigma_{1B}C_B)$$

$$ABS(\lambda_2) = L(\sigma_{2H}C_H + \sigma_{2M}C_M + \sigma_{2U}C_U + \sigma_{2A}C_A + \sigma_{2B}C_B)$$

$$\vdots$$

$$ABS(\lambda_5) = L(\sigma_{5H}C_H + \sigma_{5M}C_M + \sigma_{5U}C_U + \sigma_{5A}C_A + \sigma_{5B}C_B)$$

$$\begin{bmatrix} C_H \\ C_M \\ C_U \\ C_A \\ C_B \end{bmatrix} = \begin{bmatrix} \sigma_{1H} & \sigma_{1M} & \sigma_{1U} & \sigma_{1A} & \sigma_{1B} \\ \sigma_{2H} & \sigma_{2M} & \cdot & \cdot & \cdot \\ \sigma_{3H} & \cdot & \cdot & \cdot & \cdot \\ \sigma_{4H} & \cdot & \cdot & \cdot & \cdot \\ \sigma_{5H} & \sigma_{5M} & \cdot & \cdot & \sigma_{5B} \end{bmatrix}^{-1} \begin{bmatrix} \frac{ABS(\lambda_1)}{L} \\ \cdot \\ \cdot \\ \cdot \\ \frac{ABS(\lambda_5)}{L} \end{bmatrix}$$

case of detectors based on colorimetric or electrochemical techniques, respectively, each time a new compound needs to be detected.

C. Results from Previous Aerospace Studies

In earlier Aerospace studies[10,11], the CO_2 laser photoacoustic technique was demonstrated to provide a linear response for UDMH over greater than a 10^4 dynamic range of concentrations down to below its TLV level. Estimates made from CO_2 laser absorption cross section data for the hydrazines indicate that the hydrazines should be detectable below their TLV levels by the photoacoustic technique even in the presence of possible concentrations of pollutants and water vapor found in urban atmospheres[10,11]. It was also shown[12] that the hazardous compounds acrolein, styrene, ethyl acrylate, trichloroethylene, vinyl bromide, and vinylidene chloride should be detectable at concentrations of 40 ppb or less in the presence of anticipated interferences by the CO_2 laser photoacoustic technique. The latter compounds were further shown not to be important interferences to the detection of the hydrazine fuels.

D. Advances Made During Program to Develop Breadboard Instrument

Several technological advances have been made and key components developed in our work to produce the breadboard detector. This progress, described in detail in Sections II through V and in the Appendixes, is summarized below.

(1) The determination that resonant photoacoustic cell designs have distinct advantages over nonresonant cell designs in terms of smaller sample adsorption or reaction losses and greater immunity to background noise and unwanted window absorption.

(2) The identification of nonadsorptive materials that can be used to coat the interior surfaces of the photoacoustic cell to minimize further adsorption or reaction losses of the sample.

(3) The development of a novel electronic device that automatically tracks the acoustic resonance frequency of a resonant photoacoustic cell and continuously and precisely maintains the modulation frequency of the laser at that frequency. This device will allow resonant photoacoustic cell designs to be used for the first time in field environments where temperature- and humidity- induced changes in the cell's resonant frequency would otherwise make the use of a resonant cell impractical.

(4) The development of an pyro-electronic device that determines the wavelength of the CO_2 laser transition. This device makes it possible to scan the laser automatically to any laser transition wavelength by adjusting the angle of the laser's grating with a stepper motor that is under computer control.

(5) The detector has been automated by interfacing the laser wavelength verification device and the laser's grating controller to a microcomputer. The computer rapidly calculates the concentrations of n components in a mixture from absorption measurements at $m \geq n$ different CO_2 laser lines. The computer makes use of a library of absorption cross-section data determined at the various monitoring wavelengths. CO_2 laser absorption cross-section data have been determined by us at greater than 60 CO_2 laser wavelengths each for the three hydrazine fuels and 16 other compounds. These and other literature data are stored in the computer's library of spectra.

II. DETERMINATION OF PRACTICAL PHOTOACOUSTIC CELL DESIGN (TASK 1)

The usefulness of a laser photoacoustic detection system for trace vapor monitoring depends critically upon detector cell performance. The cell must efficiently transmit the sound wave from the laser beam, where it is produced, to the cell's pressure transducer while minimizing spurious acoustic noise detected by the transducer. Other important considerations in cell performance are unique to trace detection of adsorptive compounds. These compounds can adhere to detector feed lines and cell surfaces, depleting the vapor concentration and thus causing erroneous concentration measurements. Cells must be designed and operated to minimize the interaction between detector surfaces and the sample.

Both acoustically resonant and nonresonant photoacoustic cells have been investigated for use in gas phase photoacoustic spectroscopy. Each of these cell types has a different optimum geometry, which leads to performance trade-offs[13-17]. Upon analyzing these trade-offs, we have concluded that the resonant cell design is more suitable for trace ambient air detection of adsorptive compounds than the nonresonant cell design. We outline some of these considerations here.

The pressure fluctuations produced in a nonresonant photoacoustic cell are a function of the energy absorbed in a given illumination cycle[18]. Energy remaining from previous illumination cycles only contributes noise to the desired signal. The responsivity of a cylindrical nonresonant cell varies inversely with the square of the cell radius[19] and decreases with increasing exciting light modulation frequency[16,17]. Thus, nonresonant cells are designed to be of as small a diameter as practicable and use illumination sources that are modulated at low frequencies.

Resonant cells are designed to accumulate the absorbed energy in a standing acoustic wave when the exciting laser light is modulated at a cell resonant frequency[18]. The resonant cell acts as an amplifier such that the energy stored in the standing wave is many times greater than the energy absorbed per illumination cycle. Longitudinal, azimuthal, and radial acoustic modes may be excited in a resonant cell. Cells that use either predominantly radial or longitudinal acoustic modes have been investigated. The modulation frequencies used for resonant cells depend upon the cell dimensions. Resonant cells, designed to operate at high modulation frequencies, provide no substantial reduction in the responsivity obtainable with nonresonant cells operating in the low-frequency regime[16,17]. Since the power spectrum of

external acoustic and electrical noise usually exhibits an inverse frequency dependence, resonant photoacoustic cells are expected to provide inherently higher signal-to-noise ratios than nonresonant cells operated at lower modulation frequencies[16,17].

An important noise source in photoacoustic cells is the small amount of absorption that occurs at the cell windows which is independent of the absorbing gas concentration. Work by several groups has been directed at designing photoacoustic cells for which windows absorption effects are minimized. For nonresonant cells, this has primarily included the design of cells with: [1] carefully matched, optically tandem reference and sample chambers to allow sample chamber window absorption to be nulled out with that of the reference chamber[19,20] or [2] acoustic dampers inside the cell to minimize transmission of window absorption signals to the cell pressure transducer[21].

Resonant photoacoustic cells have been designed that employ radial[22] or longitudinal[21] acoustic modes that nearly eliminate coupling of background window absorption signals to the cell pressure transducer. This is accomplished by placing the cell windows at stationary nodal positions of the acoustic mode being excited. These resonant cells can provide greater inherent immunity from background window absorption than nonresonant cells.

Sample adsorption losses would be expected to be minimized for low surface-to-volume ratio cell designs that also allow the rapid, continuous flow of the sample gas through the cell. Resonant cells typically have surface-to-volume ratios as much as an order of magnitude lower than those of nonresonant cells. Resonant cells can be successfully operated in a continuous-flow mode at much higher flow rates than nonresonant cells. This is because background acoustic noise resulting from gas turbulence can be suppressed in a resonant cell, just as window absorption is minimized, by locating the gas sample inlet and outlet ports at the resonant cell's acoustical node positions[22] (see Fig. 2). Nonresonant cells provide acceptable responsivities in a continuous-flow mode only if the gas sample enters and exits the cell through small bore inlet and outlet orifices. The flow rates that can be obtained with nonresonant cells are thus generally much lower than those that can be obtained with resonant cells. Sample adsorption losses for a given sample residence time should thus be significantly lower in a resonant cell than in a nonresonant cell.

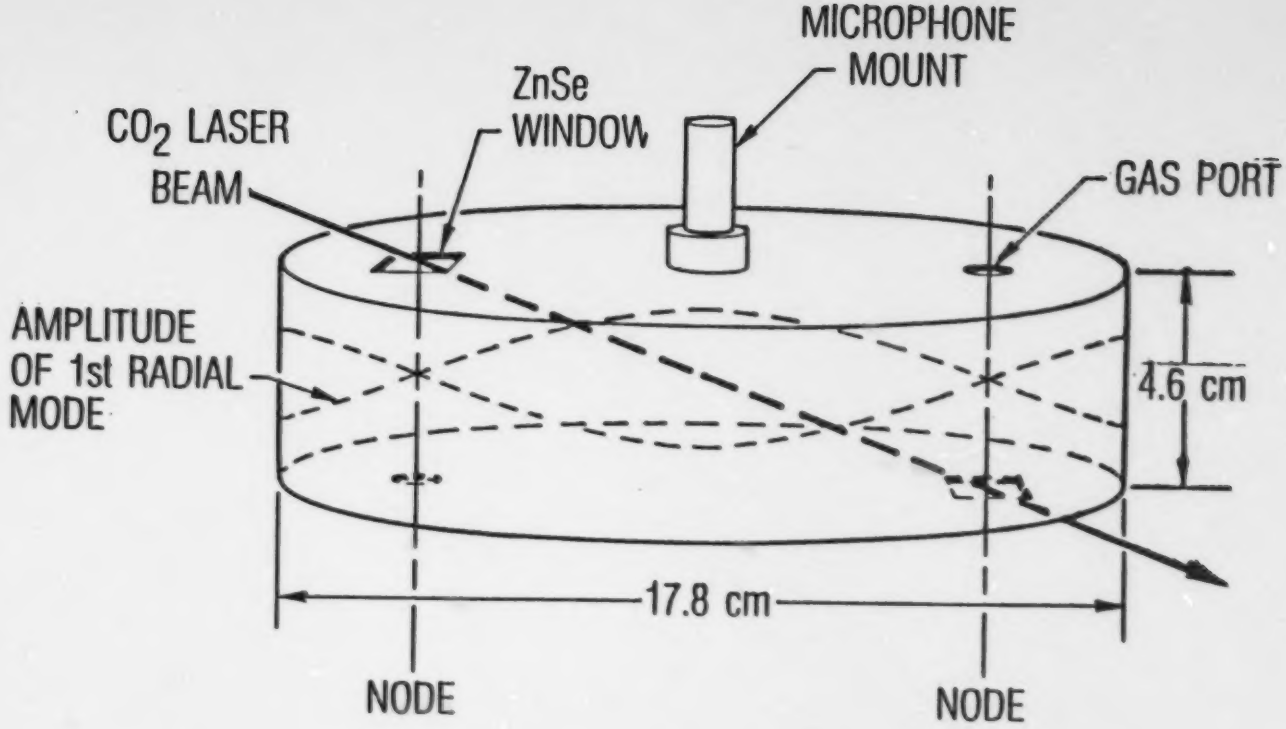

Figure 2. Resonant photoacoustic cell for the breadboard detector. The thin dashed curves represent first radial mode amplitudes of the cell, separated in phase from each other by 180°. The placement of the laser beam entrance windows and gas ports at the node of this mode minimizes coupling between noise generated at thee positions and the detected radial pressure wave. The microphone is placed at the point of maximum amplitude of the first radial mode. Cell based on design of Gerlach and Amer.[13,15,22]

The advantages of smaller expected adsorption losses and greater immunity to background noise and unwanted window absorption offered by a resonant cell compared to a nonresonant cell are offset by the fact that the resonance frequency of a resonant cell is a sensitive function of gas temperature and composition [15]. If a resonant cell is to be used in a practical detection system the laser light modulation frequency must be continuously maintained at the cell's acoustical resonance frequency. This is necessary if a constant photoacoustic response is to be obtained for the same gas concentration at different ambient conditions.

We have developed an electronic circuit device that automatically tracks the resonance frequency of a resonant cell under changing temperature and composition of the gas sample. (This frequency tracking device is described in detail in Appendix B). The device uses the high gain bandpass filter properties of the cell to detect changes in the acoustic resonance frequency and adjusts the laser light modulator to this frequency to maintain the peak photoacoustic signal. This device eliminates the major disadvantage in using a resonant photoacoustic cell for ambient air monitoring. We have chosen a resonant photoacoustic cell based upon the design of Gerlach and Amer[22] for use in our photoacoustic detection system. The performance characteristics of this stainless steel resonant cell when used uncoated are shown in Fig. 3. Under our experimental conditions, the ambient background noise in a 20 Hz bandwidth centered at the acoustic resonance frequency was 0.6 μV. The combined noise from the chopper (0.35 μV), the laser (0.20 μV/W), and the gas sample flow (0.08 μV at 1.2 liters/min.) added only 0.63 μV, when the laser output power was 1W, indicating the effectiveness of the design. With a laser output power of 1W, the minimum detectable flowing ethylene concentration monitored at the P(14) 10 μm band CO_2 laser line was 1.8 ppb which corresponds to a minimum detectable level of hydrazine of about 10 ppb in the absence of interferences when monitored at the 10 μm band P(22) laser line[23]. Similar detection limits would be obtained with MMH, UDMH, and the olefins[10-12]. When used with a CO_2 laser that provides a several watt output, this cell should provide detection limits for the hydrazines or olefins of a few ppb in the absence of interferences and below 100 ppb in high humidity air samples containing likely interferences.

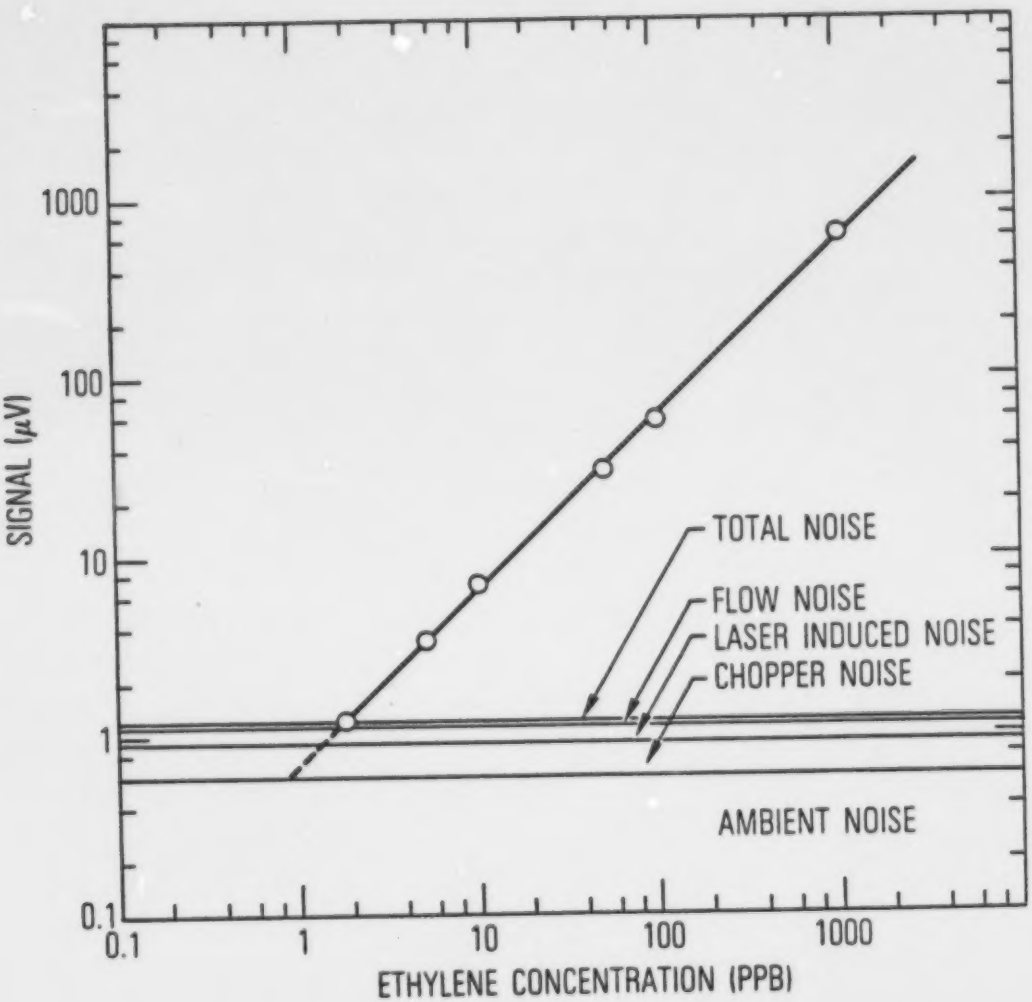

Figure 3. Log-log plot of the resonance cell response versus ethylene concentration in nitrogen. Also shown are the noise floors due to several contributing sources which limit the ethylene detection level to 1.8 ppb at one watt of laser power and a 1.2 liters/min gas sample flow rate.

III. PHOTOACOUSTIC CELL AND SAMPLING LINE MATERIALS (TASK 2)

The detection of polar compounds, and especially compounds that can form hydrogen bonds, is complicated since at the trace levels of interest significant amounts of these compounds can adsorb on the surfaces of the sampling lines and detector cells. To develop a detector that can accurately measure and rapidly respond to low concentrations of adsorptive compounds, detector and sampling line materials must be chosen to minimize these surface effects. The hydrazine fuels, due to their polar nature and ability to form strong hydrogen bonds, are among the most adsorptive of all compounds. The hydrazines may also undergo surface catalyzed degradations on certain materials. Materials that provide small adsorption and reaction losses for the hydrazines should thus be suitable for use with most other compounds.

Photoacoustic signal rise-time experiments were carried out to evaluate the suitability of several detector cell surface materials for minimizing hydrazine adsorption losses in a trace-level toxic vapor monitor. Four cell materials, 304 stainless steel, gold, paraffin wax, and TFE-Teflon were tested. The results showed that both metals interact strongly with hydrazine. The paraffin and TFE-Teflon cell coatings were found to provide the resonant photoacoustic cell with accurate real-time responses for hydrazine flows.

Tests were also carried out to evaluate various types of plastic tubing (viz., TFE-Teflon, FEP-Teflon, PFA-Teflon, high density polyethylene, Polyflo-polyethylene, and polypropylene) for suitability as trace level toxic vapor detector sampling lines. The goal of these tests was to determine which commercially available plastic tubing would be most suitable for remote sampling of the hydrazine fuels and other polar compounds through as much as 200 feet of tubing.

These tests were carried out using the photoacoustic detector to monitor the risetimes of 1 ppm hydrazine flows at 1.2 liters/min in nitrogen (dry or 80% relative humidity). These tests, described in detail in Appendix C, indicated that TFE-Teflon was the most suitable sampling line material in that it possessed the fastest and most consistent hydrazine signal risetimes of all tubing types. High density polyethylene and FEP Teflon also possessed acceptable risetimes. Polyflo-polyethylene and PFA-Teflon provided irreproducible risetimes. Polypropylene risetimes were longer than desired.

In additional studies, air was substituted for nitrogen as a diluent to determine whether oxygen increases the amount of hydrazine decomposition

inside TFE-Teflon tubing. No change was observed for 1 ppm hydrazine concentrations. It was further shown that both 100 foot TFE-Teflon coils and the TFE-Teflon coated resonant cell recovered the ability to measure 1 ppm hydrazine levels, under normal sampling flow rates, two hours after exposure to saturation vapor pressures of hydrazine.

IV. ABSORPTION CROSS-SECTION MEASUREMENTS (TASK 3)

To determine the concentrations of species in a multicomponent air mixture, photoacoustic measurements need to be performed at each of a sequence of CO_2 laser wavelengths. The photoacoustic signal produced at the various excitation wavelengths by the air sample is directly related to the concentrations of the various species in the sample. To obtain the concentrations of n components in an air sample, photoacoustic measurements are required at $m \geq n$ different wavelengths. The concentrations of the n absorbing components in the mixture can then be determined by solving a set of n simultaneous equations. This requires knowledge of the absorption cross sections of the n components in the mixture at the different CO_2 laser wavelengths used. A library of CO_2 laser absorption spectra will thus be needed for the compounds whose detection are of interest as well as for possible interferences.

Absorption cross-section data of this type, at greater than 70 $C^{12}O_2^{16}$ laser wavelengths, have been determined in our previous work for the hydrazines,[10,11] for expected hydrazine-fuel degradation products (methanol, dimethylamine, and trimethylamine),[10,11] as well as for other anticipated interferences (acrolein, styrene, ethyl acrylate, trichloroethylene, vinyl bromide, and vinylidene chloride).[12] Such data were determined in this program for seven additional compounds of EPA interest (acrylonitrile, allyl alcohol, methacrylonitrile, methyl methacrylate, carbonyl difluoride, methyl bromide, and methyl chloride) that are to be detected by the CO_2 laser photoacoustic technique. The chemical structures of these compounds are shown in Figure 4. These species are among the large number of hazardous compounds that are volatile constituents of chemical waste for which improved ambient air detection methods are needed.[23]

As described fully in Appendix D, some of the same vibrational modes are responsible for absorption in the CO_2 laser region for acrylonitrile, allyl alcohol, methacrylonitrile, and methyl methacrylate. A similar situation exists for methyl bromide and methyl chloride. Nonetheless, as shown in Appendix D, the seven compounds under study here can readily be distinguished

from each other and from expected ambient air interferences by their CO_2 laser absorption spectra. The observation that these structurally and vibrationally very similar compounds possess unique CO_2 laser spectra, indicates the CO_2 photoacoustic technique should provide highly specific detection for almost any compound with absorption in the 9- to 11-μm region.

Based on the magnitudes of their CO_2 laser absorption cross sections, we estimate that methyl bromide and methyl chloride should be detectable in typically polluted urban air at concentrations below 100 and 250 ppb, respectively, by the CO_2 laser photoacoustic technique. The other five compounds should all be detectable at concentrations of 25 ppb or below in urban air by this method. The experimental procedures employed to obtain accurate CO_2 laser absorption cross-section data for these compounds are also described in Appendix D.

CO_2 LASER ABSORPTION
CROSS-SECTIONS NEEDED FOR:

ACRYLONITRILE	$H_2C=CH-C\equiv N$	CARBONYL DIFLUORIDE	$F-\overset{\overset{O}{\|}}{C}-F$
ALLYL ALCOHOL	$H_2C=CH-CH_2OH$	METHYL BROMIDE	CH_3Br
METHACRYLONITRILE	$H_2C=C(CH_3)-C\equiv N$	METHYL CHLORIDE	CH_3Cl
METHYL METHACRYLATE	$H_2C=C(CH_3)-CO_2CH_3$		

Fig. 4. Chemical Structures for Compounds Studied in Task 3

V. AUTOMATION OF BREADBOARD DETECTOR (TASK 4)

The breadboard photoacoustic detection system was placed under microcomputer control so that all wavelength selection procedures could be performed automatically. The microcomputer was provided with a library of CO_2 laser absorption cross-section data for compounds whose detection are of interest and for several possible interferences. As described in Section I, the microcomputer calculates the concentrations of the various species in the air sample by solving sets of simultaneous equations through the use of matrix inversion schemes. The calculated concentration data are displayed on the computer's monitor or are output to it's printer. Although the instrument is capable of performing measurements at all available CO_2 laser wavelengths, it is shown in the following section that highly accurate and reproducible detection of four compounds is possible in laboratory synthetic mixtures using no more than seven laser lines. It is similarly anticipated that the detection of up to eight compounds in real field samples should be possible with no more than about 12 laser lines.

The CO_2 laser photoacoustic detection system was interfaced to an IBM PC-XT microcomputer system. The computer was equipped with an Intel 8087 Numeric Data Coprocessor chip and an AST Six Pack Plus memory expansion board (640 kilobytes of total RAM). The computer employed an Intel 8088 16-bit microprocessor and was equipped with a Winchester hard disk with 10-megabyte storage capacity. The arithmetic calculation speeds and memory size of the system were adequate to allow the unknown gas concentrations to be calculated within a few seconds following completion of the absorption measurements. The 8-bit input/output architecture of the Intel 8088 chip allowed it to be coupled easily to well-developed A/D and D/A converters, timer/counters, and

other interface hardware such as stepper motor controllers and piezoelectric drive systems. This hardware was used to control wavelength selection operations.

The detector automation task requires the capability of controlling the CO_2 laser to any of its discretely tunable wavelengths. A critical portion of this task involves developing an automatic means of spectrally verifying the laser wavelength. Work was completed toward the development of a pyro-electronic device for this purpose.

A. Automatic Wavelength Verification Device

This device, shown schematically in Fig. 5, requires the use of only a small fraction of the laser output. A grating, placed in front of an 80-element thermal sensor array, displaces the incident laser light by different discrete angles that depend on the laser wavelength. Detecting thermistors, placed at the angular positions of the different diffracted laser lines, can be used to determine the laser wavelength.

Each detecting thermistor has been paired with a reference resistor as one of 80 different voltage divider circuits. The resistances of the detecting thermistor and reference resistor in each voltage divider circuit, R_T and R_{REF}, respectively, have been matched to be within 5 percent of each other. When a given detecting thermistor is not exposed to laser light, the voltage output of the corresponding divider circuit is 2.5 V (1/2 the supply voltage). This voltage is monitored at a center junction between the detecting thermistor and reference resistor. When one of the detecting thermistors is exposed to a small amount of laser light the thermistor resistance decreases by 20 percent or more. This gives rise to an output of 3.0 V or more from the corresponding divider circuit.

The output of any of the different divider circuits can

Figure 5. Pyro-electronic device for verifying CO_2 laser wavelength.

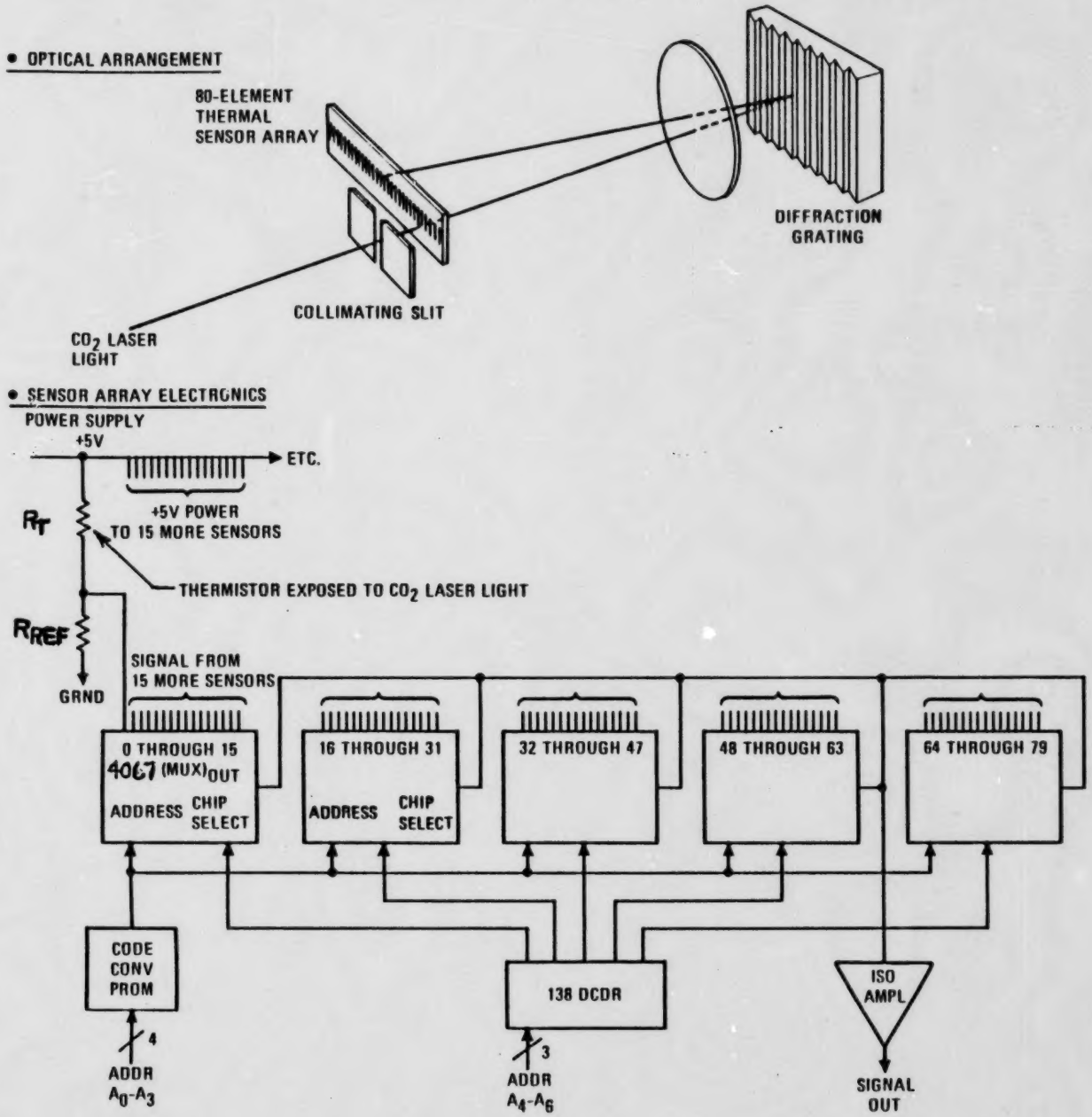

be examined by a series of electronically controlled switches addressed by the detector system's microcomputer. Address positions A_4 through A_6 select any one of five 4067 chips. Each of these chips monitor the output of sixteen different divider circuits. Address positions A_0 through A_3 select the output of any one of the sixteen divider circuits monitored by a particular 4067 chip. The isolation buffer amplifier provides the output of the addressed divider circuit.

The foregoing pyro-electronic device allows the CO_2 laser's wavelength to be determined automatically. The device can be used to verify that a laser, placed under computer control as described below, has been tuned to a particular wavelength detected by the addressed divider circuit in the sensor array.

B. Computer Control of Laser Wavelength

In the detector automation effort hardware and software also had to be developed to tune the CO_2 laser to any desired set of lasing transitions in order to determine the absorbance of the air sample at each transition.

Initial instrument automation work was carried out on a photoacoustic detection system equipped with an air-cooled, waveguide CO_2 laser. The unsatisfactory performance of the waveguide laser led to long analysis times. Excessive thermal equilibration times of the laser cavity as the laser was tuned from one transition to another resulted in the tendency of the laser to lase simultaneously on more than one transition. This also contributed to poor amplitude stability and spatial mode quality of the laser. The poor spatial mode quality required careful spatial filtering of the laser beam to minimize spurious absorption signals due to misalignment of the beam through the photoacoustic cell. This often significantly reduced the usable laser power.

Iterative, computer-controlled adjustments of the angle of the laser's grating, with a motor-micrometer, and of the laser's cavity length, with a piezoelectric translation element (PZT), were required in order to minimize the laser line purity, amplitude stability, and mode quality problems. Analysis times of greater than 3 minutes per laser transition used were required with this detection system.

The detection system's waveguide laser was replaced with a CO_2 laser equipped with a water-cooled plasma tube. The thermal equilibration time of this laser's cavity was sufficiently rapid that the laser provided good line purity, amplitude stability, and spatial mode quality as the laser wavelength was tuned. These enhancements in laser performance resulted in improved analysis accuracy and precision. In addition, the analysis time was decreased to slightly greater than one minute per laser line.

Both hardware-modification- and software-development-work had to be carried out in order to place the plasma-tube-equipped laser under computer control. Hardware modifications included: (1) coupling a computer-controlled stepper motor to a drive to adjust the angular position of the laser's grating, (2) modifying the laser's PZT driver to allow computer adjustment of the PZT voltage, and (3) interfacing the wavelength verification device described above to the detection system to provide automatic control of the line position.

Rapid coarse tuning of the laser to various lines is possible by making use of computer-stored, stepper motor positions of each line. However, small amounts of mechanical slippage in the coupling between the stepper motor and the laser's grating angle as well as PZT adjustment errors prevented complete repeatability in the stepper motor positions and PZT voltage settings of the different laser lines. An algorithm was developed to make the fine

adjustments necessary to select a particular laser line. The algorithm controls the following sequence of steps: (1) The laser line position is examined with the wavelength verification device. (2) If lines are not detected, the PZT voltage is swept through it's operating range. If lines are still not detected the grating position is dithered until a line is found. (3) If the wrong line is detected, the grating is tuned to the desired line. (4) If the desired line is found, the grating position is adjusted slightly to maximize the line purity and power. The PZT is adjusted in a similar manner. (5) If the line is not found, the line is skipped.

Using this algorithm with the better performing laser in the detection system it is possible to analyze a four-component mixture in about 8 minutes when seven laser lines are employed. This is close to a three-fold reduction in analysis time compared to that possible when the system employed the waveguide laser. It should be possible to make further significant improvements in the analysis times of this detection system (to less than 15 seconds per line) by minimizing slippage in the coupling between stepper motor and the grating adjustment mechanism and reducing PZT errors.

C. Matrix Inversion Program for Calculating Unknown Gas Concentrations

A FORTRAN matrix inversion program, developed by Green and Steinfeld[8b], for use in CO_2 laser spectroscopy was adapted to run on the PC-XT. This program can calculate, within a few seconds, the unknown concentrations of specific gases, given a library of known absorption cross-sections of the species in the gas sample and the absorption values of the sample measured at the different CO_2 laser detection wavelengths.

Work was performed to determine how uncertainties in the measured sample absorbances at the monitoring laser lines, as well as in the cross-section data for the components in the mixture, influence the uncertainties in the calculated concentrations of the components. Average concentration errors were calculated as a function of average errors in the cross sections and absorbances for three different hypothetical mixtures containing hydrazine, MMH, and UDMH, and three other components. One mixture contained the hydrazines[10,11], ethyl acrylate[12], trichloroethylene[12], and vinyl bromide[12]. Another mixture contained the hydrazines, methanol[10,11], acrolein[12], and styrene[12]. The third mixture contained the hydrazines, dimethylamine[10,11], trimethylamine[10,11], and vinylidene chloride[12]. Methanol, dimethylamine, and trimethylamine are important hydrazine-fuel air-oxidation products. All gases were assumed to be present in equal concentrations. Random errors were then induced in our previously measured cross sections for these compounds and the sample absorbance values predicted from the original cross-section data.

This simulation showed that the average concentration errors increase in nearly a linear manner with an increase in the magnitude of the average error in the cross-section data and the sample-absorbance values. For the three hypothetical mixtures, when the random induced errors averaged 5%, the average concentration error was predicted to be less than 10% when 18 or more monitoring lines were used, and less than 20% when as few as six lines were used. The components of a mixture can thus be determined with satisfactory accuracy in cases where the average absorbance and cross-section errors are 5% or less, even when the minimum number of laser lines are used for monitoring.

VI. LABORATORY DEMONSTRATION OF BREADBOARD INSTRUMENT

In order to test the ability of the breadboard detector to obtain accurate and reproducible concentrations of gases in mixtures a gas flow and mixing system was assembled. The use of mass-flow controllers in this system allowed the concentrations of four different gases to be independently varied in nitrogen from low ppb to high ppm values. A sample of this gas mixture was then continuously drawn through the photoacoustic cell. The concentration of any of the gases in the mixture could be quantitatively changed by adjusting the appropriate flow controller. A schematic diagram of this flow system is shown in Fig. 6.

The four gases chosen for the mixture were hydrazine, methyl bromide, ammonia, and ethylene. The CO_2 laser absorption spectrum for hydrazine, shown in Fig. 7, consists of a series of sharp peaks and valleys. Hydrazine was chosen for use in the mixture since it is the most reactive and adsorptive of the hydrazine-fuels.

The CO_2 laser absorption spectrum for methyl bromide is shown in Fig. 8. Methyl bromide is widely used as a fumigant. It is among toxic compounds for which improved detection capability is desired by EPA. This compound also was chosen to test the discrimination capability of the instrument. Methyl bromide's spectrum consists of a series of peaks and valleys, that in many instances, are located at the same wavelength positions as peaks and valleys in the spectrum for hydrazine.

Ammonia's CO_2 laser absorption spectrum is shown in Fig. 9. Ammonia may be present at hydrazine-fuel monitoring locations since it is an important air oxidation product of

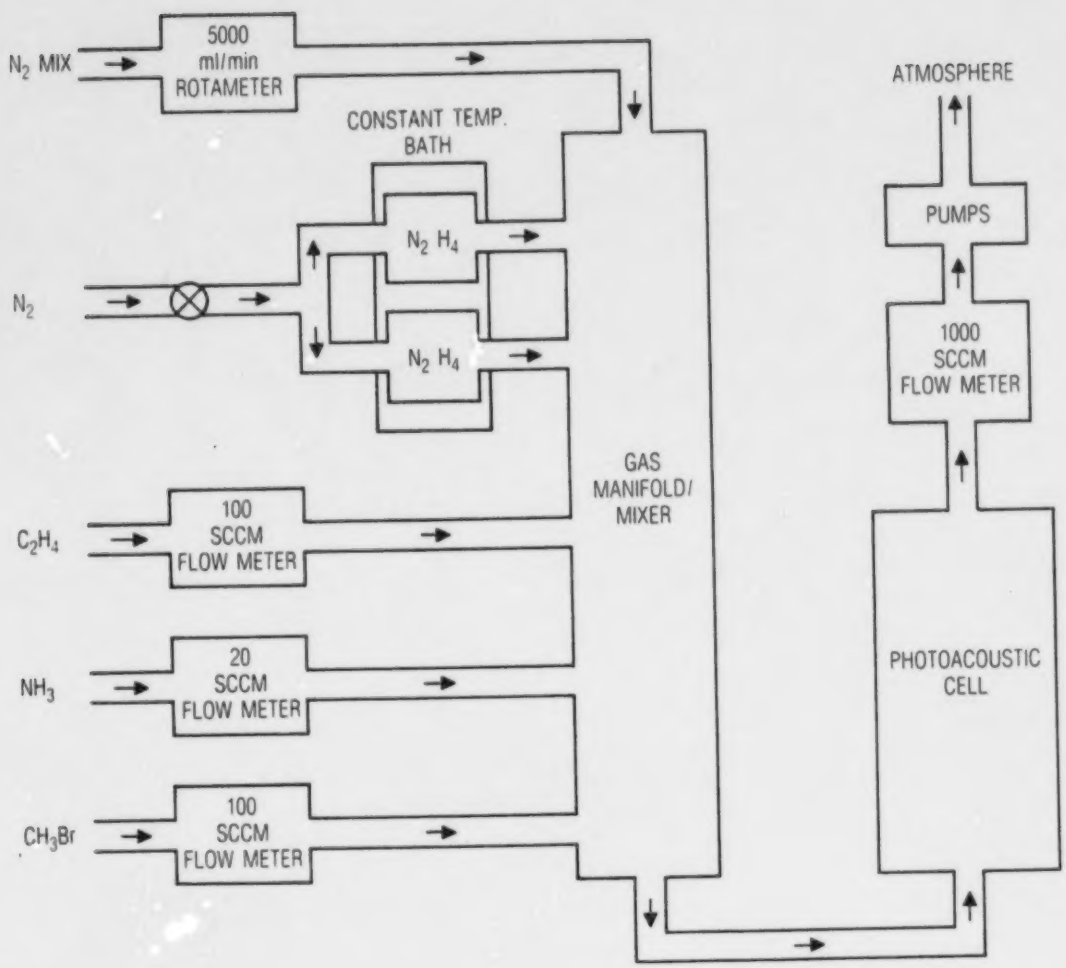

Fig. 6. Schematic Diagram of flow system for producing mixtures of various relative concentrations.

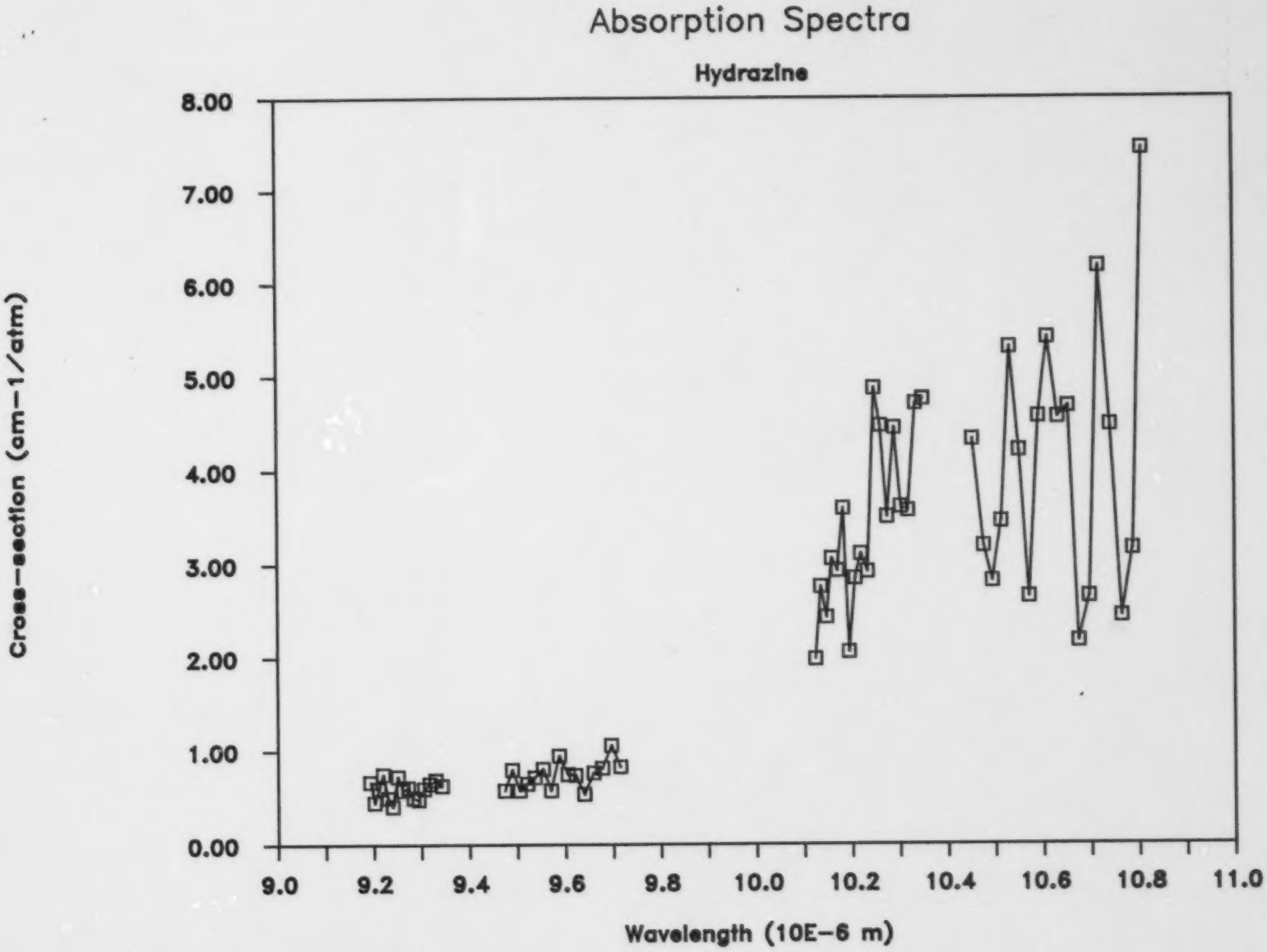

Fig. 7. CO_2 Laser Absorption Spectrum for Hydrazine.

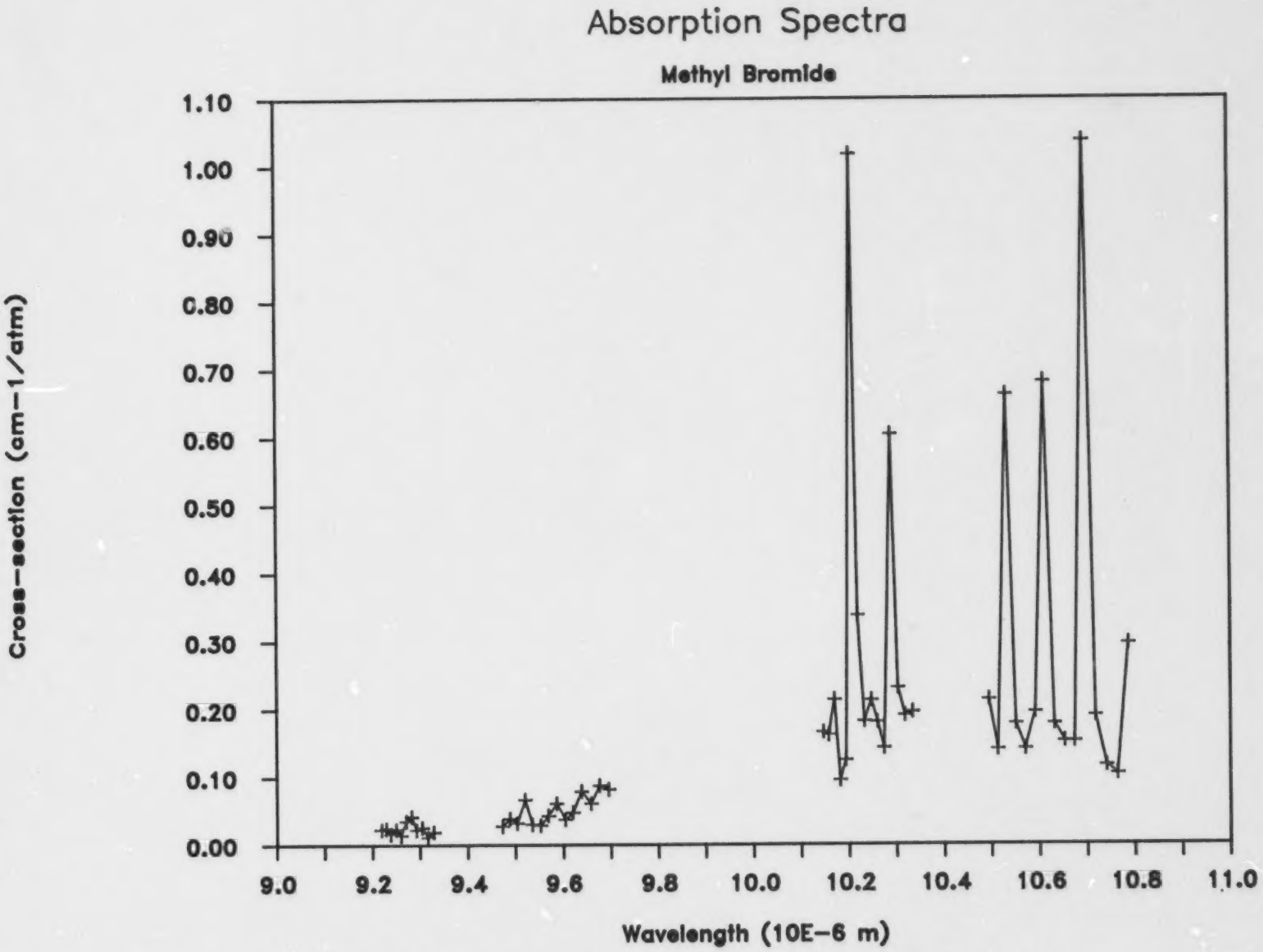

Fig. 8. CO_2 Laser Absorption Spectrum for Methyl Bromide.

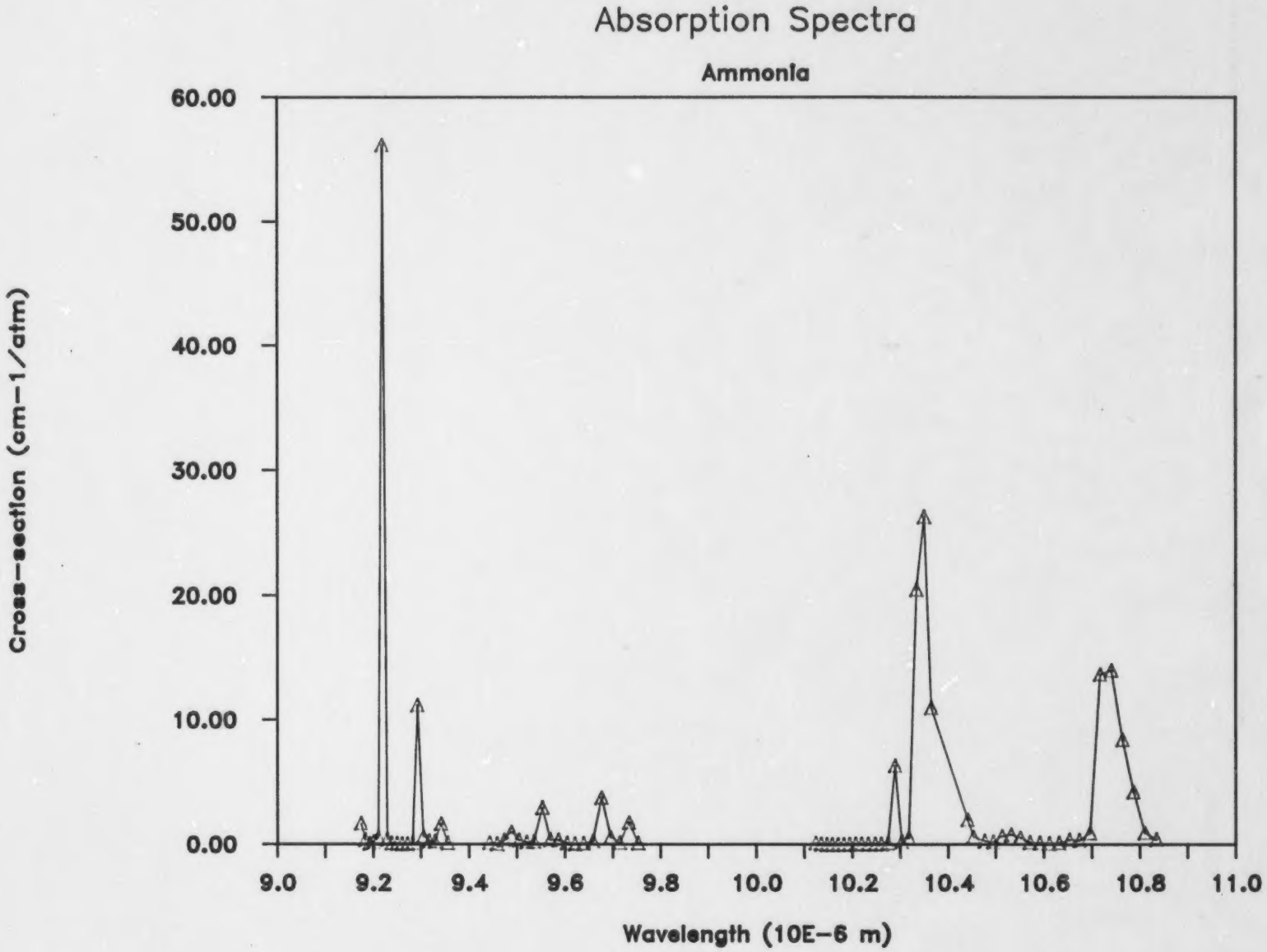

Fig. 9. CO_2 Laser Absorption Spectrum for Ammonia.

the hydrazines and it is used as a refrigerant on the Shuttle Transporter.

Ethylene's CO_2 laser absorption spectrum is shown in Fig. 10. Ethylene is present in typically polluted urban air samples.

When superimposed, as shown in Fig. 11, the spectra of these four gases give rise to a dense and complex pattern of absorption features. Seven CO_2 laser lines [10 μm band lines R(16), R(14), P(14), P(22), P(28), P(30), and P(32)] were selected in order to determine the concentrations of each of these four species in the gas mixtures prepared. These wavelengths are designated by the hash marks in Fig. 11.

Table II lists the results of five sequential analyses performed on a flowing gas mixture in which the mixture composition was held constant. Any variance in the measured concentrations for these gases reflects instrumental uncertainties and real variances in the gas concentrations. The good repeatability in the measured concentrations here (in all cases less than $\pm$4% standard deviation) indicates the good reproducibility of the technique.

Table III shows results for samples where the concentrations of various components were changed. The first two rows give the results of analyses performed on a mixture of constant composition. The third row shows the results obtained following hydrazine flow termination. The analysis in this case was performed after a several minute delay so that adsorbed hydrazine was completely depleted from the mass flow controller and gas inlet lines. The constant concentrations observed for ethylene, ammonia, and methyl bromide in the first three rows of Table III indicate that the technique can uniquely identify the mixture's components with minimal interference from the other gases present. These results also indicate that the absorption cross-

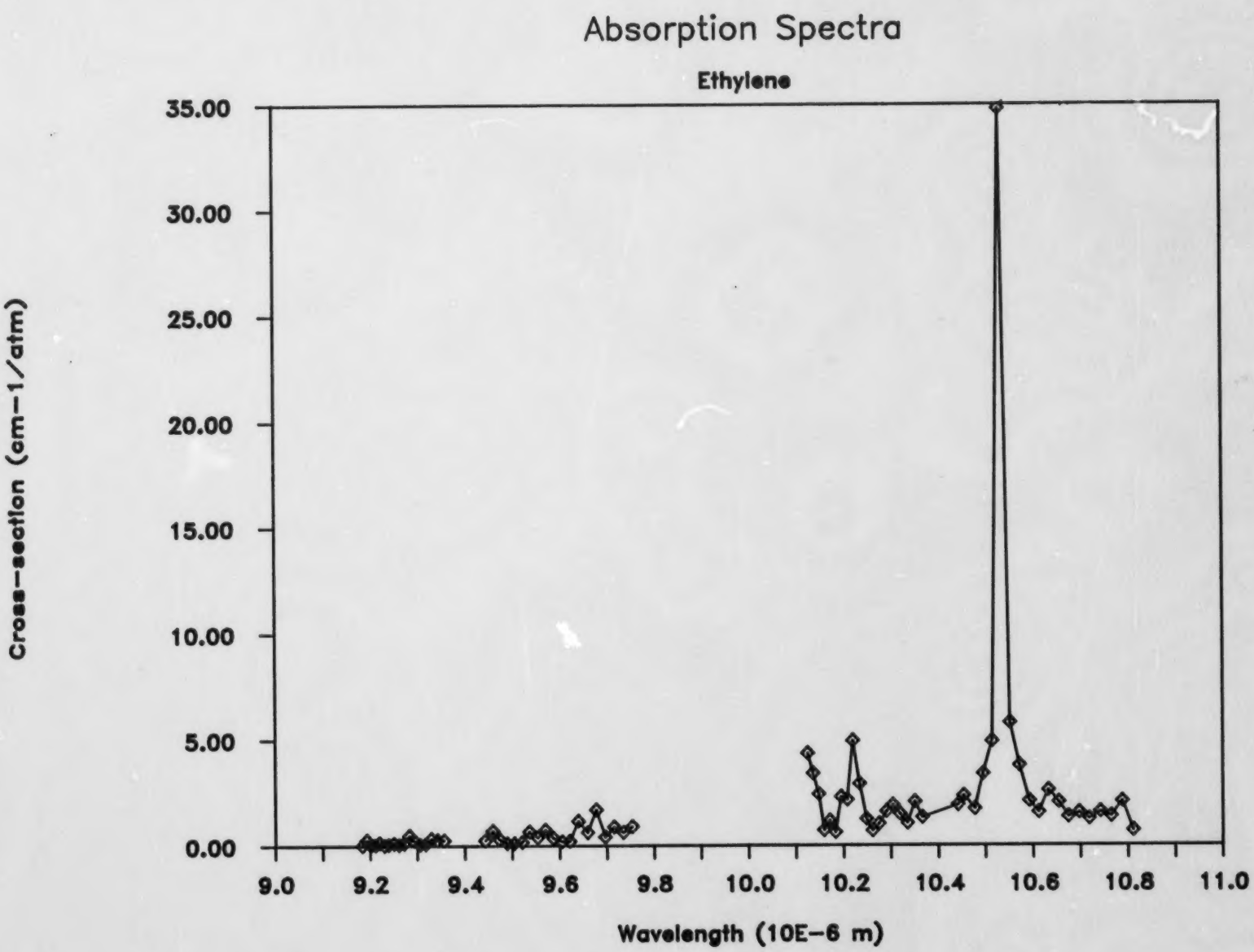

Fig. 10. CO_2 Laser Absorption Spectrum for Ethylene.

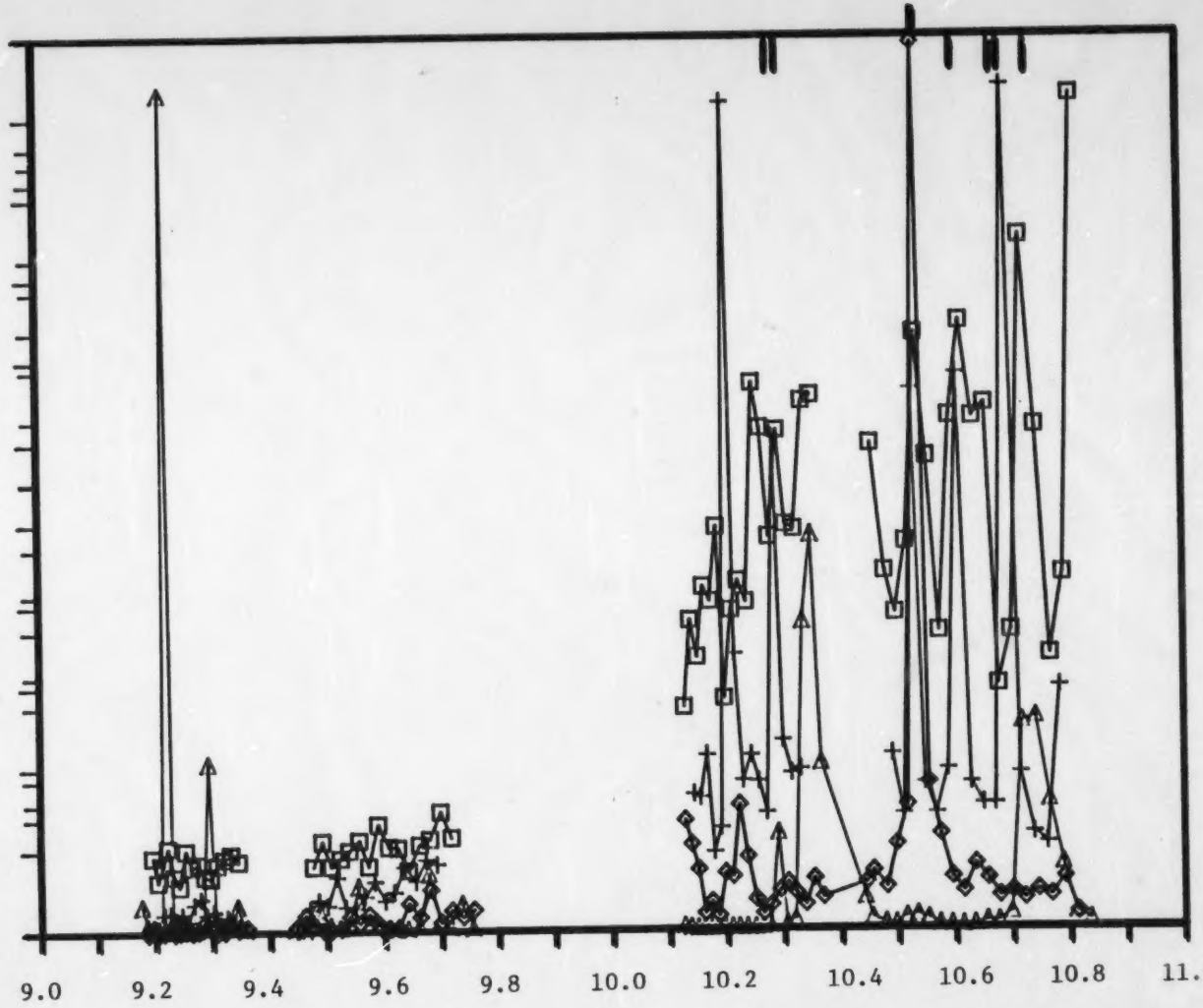

Fig. 11. Superimposed CO_2 Laser Absorption Spectra of Hydrazine, Methyl Bromide, Ammonia and Ethylene.

TABLE II.

Results of Consecutive Mixture Analyses:
Static Mixture Concentrations

RUN	C_2H_4 (ppb)	N_2H_4 (ppb)	NH_3 (ppb)	CH_3Br (ppm)
1.	269	164	270	1957
2.	260	180	255	2036
3.	268	174	275	2003
4.	250	178	280	1976
5.	257	171	269	2003
Ave.	260.8 ±7.9(3.0%)	173.4 ±6.3(3.6%)	269.8 ±6.3(2.3%)	1995 ±9.4(0.5%)

TABLE III.

Results of Consecutive Mixture Analyses:
Changing Mixture Concentrations

RUN	C_2H_4(ppb)	N_2H_4(ppb)	NH_3(ppb)	CH_3Br(ppm)
1.	250	82	157	1.80
2.	243	84	155	1.79
N_2H_4 FLOW TERMINATED				
3.	253	0	162	1.76
REDUCED BY ~1/2, C_2H_4, NH_3 AND CH_3Br CONCENTRATIONS				
4.	121	0	99	1.04
5.	120	0	97	1.02

section data used to calculate the concentrations of these four gases have been accurately determined.

The last two rows of Table III show the results of the mixture analysis after the input flows of ethylene, ammonia, and methyl bromide have been reduced by a factor of about two. Precise control of the flows is difficult so the concentration of each gas does not fall by exactly one-half. The analysis results, however, are in good agreement with the expected concentrations. Reproducibility is also quite good.

Table IV shows the results of analyses of another mixture in which the ethylene, ammonia, and methyl bromide concentrations were held constant but the hydrazine concentration was varied by changing its flow rate into the gas mixing system. The hydrazine results are plotted in Fig. 12. Here the measured hydrazine concentration is observed to vary linearly with the hydrazine flow rate set on the mass flow controller. The non-zero intercept and slightly greater than unit slope suggest the presence of small calibration errors in the flow system. Nonetheless, the results shown indicate the accurate detection of hydrazine at concentrations down to below 5 ppb in the presence of 238 ppb of ethylene, 134 ppb of ammonia, and 1.73 ppm of methyl bromide in this mixture. In similar experiments hydrazine was detected in mixtures containing as much as a 600-fold excess of methyl bromide.

TABLE IV.

Results of Analyses of a Mixture in which the Hydrazine Concentration was Varied by Changing its Relative Flow Rate into the Gas Mixing System. The Concentrations of Other Components were Held Constant.

Relative Hydrazine Flow Rate into Mixing System	N_2H_4(ppb)	C_2H_4(ppb)	NH_3(ppb)	CH_3Br(ppm)
1.00	97	228	120	1.68
0.75	63	241	140	1.72
0.50	36	238	133	1.74
0.25	14	237	138	1.79
0.125	6	239	133	1.71
0.058	0	246	139	1.76

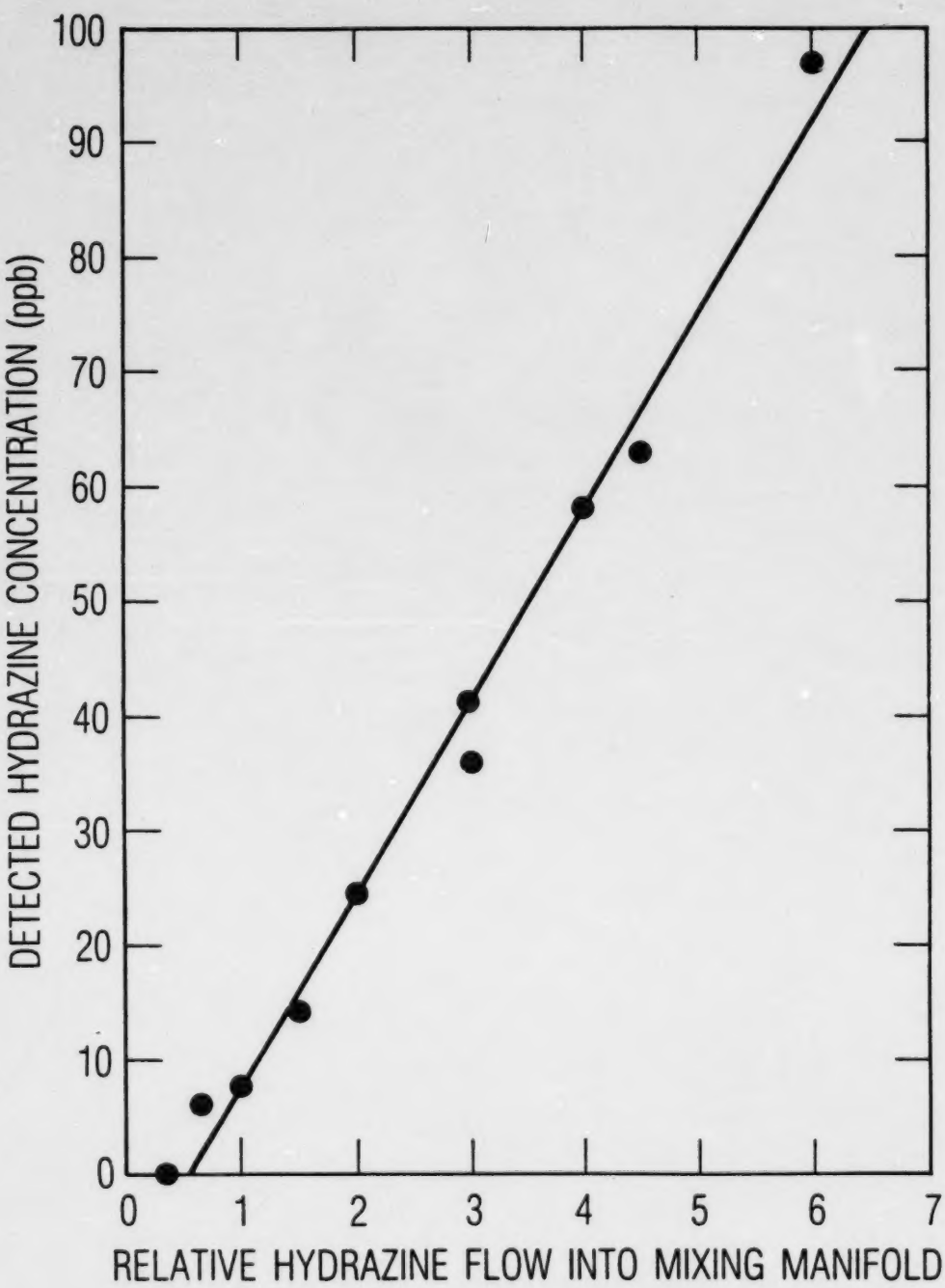

Figure 12 Plot of hydrazine concentration detected by photoacoustic apparatus as a function of the relative flow rate of the hydrazine into the gas mixing manifold. The measurement is in the presence of 238 ppb of ethylene, 134 ppb of ammonia, and 1.7 ppm methyl bromide.

VII. SUMMARY, CONCLUSIONS AND RECOMMENDATIONS FOR FUTURE WORK

The breadboard CO_2 laser photoacoustic detector has been demonstrated in laboratory experiments to provide highly specific detection of various toxic gases at levels as low as 5 ppb in multicomponent mixtures.

Several key results were achieved in the program. (1) Resonant photoacoustic cell designs were shown to offer advantages over nonresonant cells in terms of discriminating against window absorption and sample flow noise as well as minimizing the adsorption of polar compounds. (2) Signal risetime experiments carried out with the photoacoustic detector using 1 ppm hydrazine flows indicated that TFE Teflon is suitable as a cell-coating- and sampling-line-material to minimize adsorption losses of sampled gases. (3) An electronic device was developed that automatically maintains the modulation frequency of the laser at the acoustic resonance frequency of a resonant photoacoustic cell. This allows resonant cell designs to be used for the first time in field environments where the sample gas temperature and humidity may change often. (4) A pyro-electronic device was developed that can be used to determine the CO_2 laser wavelength. (5) This wavelength verification device allowed the laser's grating and PZT drive to be placed under computer control such that sample absorbance measurements can be automatically performed at any desired set of laser lines. The computer can then make use of the absorbance data at m different laser lines to calculate the concentrations of $n \leq m$ components in a mixture using a matrix inversion program. The program employs a library of data containing absorption cross sections for the n compounds of interest at the m laser lines used for monitoring.

The program goal of developing and demonstrating an automated, breadboard detector that can selectively detect a variety of toxic gases in air samples at levels below 100 ppb has been successfully met. The instrument's analysis time is presently slightly more than 1 minute per laser line used. It is expected, by improving the reproducibility in the control of the laser's grating angle and PZT element, that analysis times can be reduced to less than 15 seconds per laser line used. This would allow analyses on mixtures containing as many as 8 components (requiring the use of perhaps 12 laser lines) to be performed in 3 minutes or less.

Based on present microcomputer and CO_2 laser technology, a fully-automated detection system capable of detecting species at levels below 100 ppb in multicomponent mixtures should be produced at a cost of below $25,000. Such a detector would have dimensions of less than 60 x 80 x 140 cm and weigh less than 80 kg. The detector could thus be readily mounted on a cart for semi-portable operation. As microcomputer and CO_2 laser technology continue to evolve, reductions in the detector's cost, size, and weight are likely.

It should also be possible to use the detector in multipoint monitoring applications. One way that the instrument could be used as a multipoint monitor would be to have a central laser source that would feed laser light to photoacoustic cells located at detection sites greater than 200 feet away. This can be accomplished by transmitting the laser beams to these locations with the appropriate collimation optics. These beams could be transmitted through enclosed tubes if desired. Time-multiplexed laser output could be used to provide excitation of the gas samples in the cells at several remote locations. The electrical output of the microphone in each photoacoustic cell at each remote site is then carried back to the monitoring station by wires

for signal processing by a central microcomputer. Compared to the conventional monitoring network in which the laser source, photoacoustic cell, and computer are contiguously located at each monitoring point, the configuration that employs a centralized laser source with beam transmitting optics offers advantages of significantly lower cost, greater ease of maintenance, and smaller size and weight of equipment located at the remote monitoring location. This is due to the fact that roughly 80% of the cost, size, and weight of a CO_2 laser photoacoustic detection system in the conventional configuration is due to the CO_2 laser.

The following experimental tasks will need to be carried out in order to develop a prototype version of the instrument for use in multipoint-detection applications:

(1) Demonstrate feasibility of using CO_2 laser photoacoustic detection concept in multipoint detection applications. Show in the laboratory that light from a central laser source can be propagated over distances of greater than 100 feet to two different photoacoustic cells.

(2) Improve the response time of the instrument so that it can provide a 90% full scale response in less than 2 minutes for two hydrazine fuels (or two compounds of EPA concern) at concentrations of 200 ppb in the presence of two interferences.

(3) Perform additional studies on the effects of humidity on the instrument's detection limits. A weak, continuous background absorption that is associated with water vapor exists in the CO_2 laser wavelength region. This absorption must be properly accounted for in order to obtain accurate concentrations for toxic gases at low levels.

(4) Study the effects of aerosols that may be present in the air at monitoring locations on the instrument's detection limits.

(5) Measure CO_2 laser absorption cross-section data, if not previously determined, for new compounds of Air Force or EPA concern and for unexpected interfering compounds that may be present at monitoring locations.

(6) To verify that the water continuum, aerosol, and unexpected interferent effects described in (3) through (5) above are adequately addressed, perform analyses on mixtures prepared with air from El Segundo, California (location of The Aerospace Corporation) and Vandenberg Air Force Base (VAFB), or a site selected by EPA. Follow these experiments with field evaluations of the instrument at VAFB or the EPA site.

REFERENCES

1. E. L. Kerr and J. G. Atwood, Appl. Opt. 7, 915 (1968).

2. L. B. Kreuzer, N. D. Kenyon, and C. K. N. Patel, Science 177, 347 (1972); L. B. Kreuzer, Anal. Chem. 46, 239A (1974).

3. R. J. Brewer and C. W. Bruce, Appl. Opt. 17, 3746 (1978).

4. R. Beck, W. English, and K. Gurs, Table of Laser Lines in Gases and Vapors, Vol. 2, Springer, Berlin (1978).

5.

6. C. J. Pouchert, The Aldrich Library of Infrared Spectra, Edition III, Aldrich Chemical Co., Inc., Milwaukee (1981).

7. G. L. Loper, M. A. O'Neill, and J. A. Gelbwachs, Appl. Opt., 22, 3701 (1983).

8. (a) R. R. Patty, G. M. Russwurm, W. A. McClenny, and D. R. Morgan, Appl. Opt. 13, 2850 (1974); (b) B. D. Green and J. I. Steinfeld, Environ. Sci. Technol., 10, 1134 (1976); (c) A. Mayer, J. Comera, H. Charpentier, and C. Jaussaud, Appl. Opt. 17, 391 (1978); (d) P. Andersson and U. Persson, Appl. Opt. 23, 192 (1984).

9. R. A. McClatchey, W. S. Benedict, S. A. Clough, D. E. Burch, R. F. Calfee, K. Fox, L. S. Rothman, J. S. Garing, "AFCRL Atmospheric Absorption Line Parameters Compilation," AFCRL-TR-73-0096, Bedford, Mass. (1973).

10. G. L. Loper, A. R. Calloway, M. A. Stamps, and J. A. Gelbwachs, Appl. Opt. 19, 2726 (1980).

11. G. L. Loper, A. R. Calloway, M. A. Stamps, and J. A. Gelbwachs, Expected Detection Limits of Hydrazine-Based Rocket Fuels and Their Selected Oxidation Products by $C^{12}O_2^{16}$ Laser Spectroscopic Techniques. TR-0080 (5970-09)-1, The Aerospace Corp. (15 August 1980).

12. G. L. Loper, G. R. Sasaki, and M. A. Stamps, Appl. Opt. 21, 1648 (1982).

13. R. Gerlach and N. M. Amer, Appl. Phys. Lett. 32, 228 (1978).

14. L. J. Thomas III, M. J. Kelly, and N. M. Amer, Appl. Phys. Lett. 32, 736 (1978).

15. D. R. Wake and N. M. Amer, Appl. Phys. Lett. 34, 379 (1979).

16. S. Shtrikman and M. Slatkine, Appl. Phys. Lett. 31, 830 (1977).

17. E. Kritchman, S. Shtrikman, and M. Slatkine, J. Opt. Soc. Am. 68, 1257 (1978).

REFERENCES

1. E. L. Kerr and J. G. Atwood, Appl. Opt. 7, 915 (1968).

2. L. B. Kreuzer, N. D. Kenyon, and C. K. N. Patel, Science 177, 347 (1972); L. B. Kreuzer, Anal. Chem. 46, 239A (1974).

3. R. J. Brewer and C. W. Bruce, Appl. Opt. 17, 3746 (1978).

4. R. Beck, W. English, and K. Gurs, Table of Laser Lines in Gases and Vapors, Vol. 2, Springer, Berlin (1978).

5.

6. C. J. Pouchert, The Aldrich Library of Infrared Spectra, Edition III, Aldrich Chemical Co., Inc., Milwaukee (1981).

7. G. L. Loper, M. A. O'Neill, and J. A. Gelbwachs, Appl. Opt., 22, 3701 (1983).

8. (a) R. R. Patty, G. M. Russwurm, W. A. McClenny, and D. R. Morgan, Appl. Opt. 13, 2850 (1974); (b) B. D. Green and J. I. Steinfeld, Environ. Sci. Technol., 10, 1134 (1976); (c) A. Mayer, J. Comera, H. Charpentier, and C. Jaussaud, Appl. Opt. 17, 391 (1978); (d) P. Andersson and U. Persson, Appl. Opt. 23, 192 (1984).

9. R. A. McClatchey, W. S. Benedict, S. A. Clough, D. E. Burch, R. F. Calfee, K. Fox, L. S. Rothman, J. S. Garing, "AFCRL Atmospheric Absorption Line Parameters Compilation," AFCRL-TR-73-0096, Bedford, Mass. (1973).

10. G. L. Loper, A. R. Calloway, M. A. Stamps, and J. A. Gelbwachs, Appl. Opt. 19, 2726 (1980).

11. G. L. Loper, A. R. Calloway, M. A. Stamps, and J. A. Gelbwachs, Expected Detection Limits of Hydrazine-Based Rocket Fuels and Their Selected Oxidation Products by $C^{12}O_2^{16}$ Laser Spectroscopic Techniques. TR-0080 (5970-09)-1, The Aerospace Corp. (15 August 1980).

12. G. L. Loper, G. R. Sasaki, and M. A. Stamps, Appl. Opt. 21, 1648 (1982).

13. R. Gerlach and N. M. Amer, Appl. Phys. Lett. 32, 228 (1978).

14. L. J. Thomas III, M. J. Kelly, and N. M. Amer, Appl. Phys. Lett. 32, 736 (1978).

15. D. R. Wake and N. M. Amer, Appl. Phys. Lett. 34, 379 (1979).

16. S. Shtrikman and M. Slatkine, Appl. Phys. Lett. 31, 830 (1977).

17. E. Kritchman, S. Shtrikman, and M. Slatkine, J. Opt. Soc. Am. 68, 1257 (1978).

18. C. F. Dewey, Jr., R. D. Kamm, and C. E. Hackett, Appl. Phys. Lett. 23, 633 (1973); R. D. Kamm, J. Appl. Phys. 47, 355 (1976).

19. M. S. Shumate, U. S. Patent 4,067,653 (10 Jan. 1978).

20. T. F. Deaton, D. A. Depatie, and T. W. Walker, Appl. Phys. Lett. 26, 300 (1975).

21. C. W. Bruce, B. Z. Sojka, B. G. Hurd, W. R. Watkins, K. O. White, and Z. Derzko, Appl. Optics 15, 2970 (1976).

22. R. Gerlach and N. M. Amer, Appl. Phys. 23, 319 (1980).

23. Hazardous Constituents of Waste Streams, Appendix VIII, Federal Register, Vol. 46, pp. 27477-480, 20 May 1981.

APPENDIX A

QUALITY ASSURANCE PROCEDURES

A. PHOTOACOUSTIC CELL DESIGN (TASK 1) AND CELL MATERIALS (TASK 2)

1. ABSOLUTE CALIBRATION OF CELL PHOTOACOUSTIC RESPONSE

The linearity of response of the resonant photoacoustic cell was measured over a several order of magnitude concentration range of ethylene in nitrogen, as shown in Figure A-1. Ethylene is well suited as a calibration gas for CO_2 laser photoacoustic systems due to its highly structured CO_2 laser absorption profile and its low adsorptivity on surfaces. Because the CO_2 laser adsorption cross-sections of ethylene are accurately known, these measurements allowed the absolute photoacoustic response of the resonant cell to be determined.

Ethylene absorption cross-section data have been carefully determined by Aerospace at selected CO_2 laser lines (Ref. A-1). The strongest absorption occurs at the 10.4-μm band P(14) laser line. The ethylene absorption at this line was used to calibrate the absolute response of the cell. The P(14) laser line cross section was shown to be independent of ethylene pressure and to remain constant (at 34.76 ± 0.27 cm^{-1} atm^{-1}) for twelve measurements over a 5 to 40 W/cm^2 laser intensity range. The latter observation indicates that ethylene and hydrazine absorption saturation effects are unimportant for intensities below 50 W/cm^2. (The hydrazine CO_2 laser absorption cross-sections are no larger than about 7.5 cm^{-1} atm^{-1}.) All photoacoustic responsivity measurements were performed at laser intensities below 50 W/cm^2. The ethylene absorption cross sections determined by Aerospace were in good agreement with similar data (generally within ± 10%) determined by three other groups (Refs. A-2 through A-4).

2. PREPARATION OF STANDARD ETHYLENE/NITROGEN MIXTURES

The ethylene/nitrogen dilution measurements described above were carried out by transferring a known pressure of ethylene to a small bulb (~ 100 ml) of

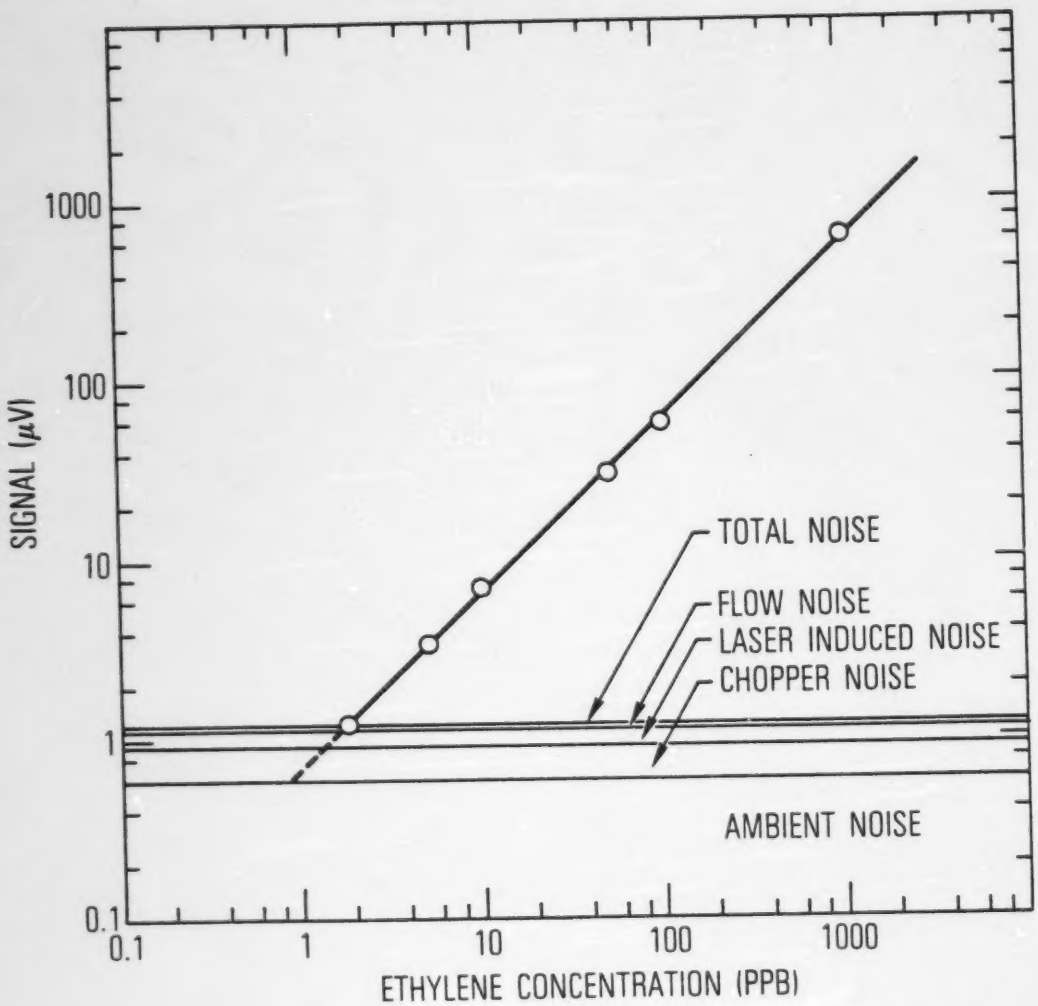

Fig. A-1. Photoacoustic Signal vs Ethylene Concentration

calibrated volume on a vacuum line. This gas aliquot was condensed at liquid nitrogen temperature into a calibrated 12-liter flask equipped with a convection mixing loop, and a known pressure (near 800 Torr) of pure nitrogen was added. One atmosphere of this gas mixture was expanded into the photoacoustic cell after thorough convection mixing.

Chemical purity ethylene (99.8% min) and research purity nitrogen (99.9995% min) was used in these dilution measurements. The volume of the small bulb on the vacuum line was calibrated gravimetrically. An analytical balance with a National Bureau of Standards (NBS) traceable sensitivity of 0.1 mg and a precision of 0.03 mg was used to determine the mass of the bulb when empty and when filled with distilled water. Water density reference data as a function of temperature were used to calculate the bulb volume to the nearest ± 0.03 ml. Standard gas expansion techniques allowed the volume of the 12-liter flask to be determined to the nearest ± 49 ml.

Ethylene pressures were measured with an MKS Baratron capacitance manometer with a 77 H-10 (10 Torr full range) pressure head. Ethylene/nitrogen mixtures were measured with a 0- to 800-Torr Wallace and Tiernan pressure gauge. The capacitance manometer provided an accuracy within 0.08% of reading. The manometer's calibration was checked by the Aerospace Calibration Lab against a reference capacitance manometer. This reference manometer is recalibrated and certified at periodic intervals by the manufacturer (MKS) against standards traceable to NBS. The Wallace and Tiernan gauge can be read with a precision of 1 Torr. Its accuracy was calibrated against the Baratron system.

Ethylene/nitrogen mixtures were prepared at concentrations near 1 ppm by the above procedures. By pumping off all but accurately known low pressures of these mixtures in the 12-liter flask and then diluting with nitrogen, it was possible to prepare concentrations as low as 1.0 ppb with tolerances of ± 5%.

3. PREPARATION OF HYDRAZINE/NITROGEN MIXTURES

Nitrogen was used to prepare hydrazine/nitrogen mixtures of known concentration and humidity. Hydrazine concentrations were determined from the

photoacoustic signals produced by making use of the cell response and our previously determined hydrazine CO_2 laser absorption cross sections (Ref. A-5). The CO_2 laser spectra obtained for these mixtures were in good agreement with our previously published hydrazine spectrum, indicating the absence of appreciable impurities in the hydrazine sample.

Preparation of hydrazine/nitrogen flows was as follows. A Kin Tek gas standards generator was used as a hydrazine source. Three Teflon permeation tubes containing liquid hydrazine were kept at a constant 70°C temperature and slowly purged with a 200 ml/min flow of N_2. Flow rates were determined by calibrated rotameters. The hydrazine flow was passed into a Teflon block where it was further diluted with N_2 to 1.0 ± 0.2 ppm in a total flow of 2000 ml/min. The hydrazine concentration was verified by a wet chemical colorimetric determination.

The hydrazine/N_2 flow is bubbled, using an impinger with a small orifice, through 100 ml of 0.1 N H_2SO_4 solution for 20 minutes. A 10-ml aliquot of this sample is transferred to a 25-ml volumetric. At this point the procedure follows exactly the calibration procedure described below starting at 1.3. After the absorbance of the sample has been measured, the amount of hydrazine in the 10-ml sample is read off the colorimetric analysis calibration curve. Knowing this amount and the flow rates, the concentration of hydrazine in the flow can be calculated. The hydrazine concentrations were also verified by the photoacoustic technique, using our previously calibrated cell responsivity and literature values for the hydrazine cross sections at specific CO_2 laser lines.

The procedures used to prepare calibration curves for determining, by colorimetric analysis, the concentration of hydrazine in a hydrazine/nitrogen mixture are summarized below:

1.0 Weigh out 0.4060 g of hydrazine sulfate ($N_2H_4.H_2SO_4$). Dissolve in 500 ml of 0.1N H_2SO_4 in a 1-liter volumetric flask. Bring to volume with 0.1N H_2SO_4. The resulting solution is 100 mg/ml in hydrazine. Calibration curves are prepared directly, using appropriate microliter pipettes and the following procedure:

1.1 Pipet 10 ml of 0.1N sulfuric acid into each of six 25-ml volumetric flasks.

1.2 Carefully pipet 10, 20, 30, 40, and 50 µl (1, 2, 3, 4, and 5 µg, respectively) of the standard hydrazine sulfate solution into the volumetric flasks. Process one flask as a blank.

1.3 Add 1.0 ml of HydraVer™ II para-dimethylaminobenzaldehyde reagent from Hach Chemical Company (Loveland, CO.) to each bottle.

1.4 Set timer for 8 minutes and swirl each flask intermittently.

1.5 After the 8-minute reaction period, bring each flask to 25 ml total volume with glacial acetic acid.

1.6 Place parafilm over mouth of bottles and invert 5 times.

1.7 Set timer for 4 minutes to allow bubbles to disappear (tap bottles lightly).

1.8 Adjust spectrophotometer (458 nm) or colorimeter (No. 5543 color filter) to 100-percent transmittance (100%T) using the blank solution (prepared in the same fashion as the unknown samples). Note that with some colorimeters, the color of the blank is too intense to set the spectrophotometer at 100%T and it is necessary to use a water blank. The reagent blank absorbance then must be subtracted from sample absorbance to get the true absorbance due to the unknown sample alone.

1.9 Sample %T is read within 15 minutes of HydraVer II addition. Convert %T to absorbance.

1.10 Construct a calibration curve by plotting absorbance against total µg of hydrazine in solution.

B. PHOTOACOUSTIC CELL MATERIALS (TASK 2)

1. CELL MATERIALS

The cell materials were traceable to a particular material manufacturer through Aerospace shop purchase records. The stainless steels of which the cells were constructed are standard alloys.

2. WINDOW MATERIAL

The windows used in the cells were made from ZnSe. They are supplied to Aerospace by Janos Corp.

C. ABSORPTION CROSS-SECTION MEASUREMENTS (TASK 3)

1. GASES

All of the gases used, either single component or mixtures, were of the highest purity commercially available. In some cases mixtures were made at Aerospace from stated purity gases using standard volumes and pressures (see task 1 of Appendix A). Matheson ammonia/nitrogen and ethylene/nitrogen gas mixtures were also used. These gas mixtures were quoted to be "primary standards" and had preparation tolerances of ± 1% of component and a NBS-traceable certification accuracy of ± 0.02% absolute. The concentrations of these mixtures were verified by CO_2 laser photoacoustic measurements using cell responsivities and the latest absorption cross sections found in the literature.

2. ELECTRONIC INSTRUMENTS

All electronic instruments used in experiments at Aerospace are calibrated annually by The Aerospace Corporation Calibration Lab, which is dedicated to ensuring that stringent Air Force calibration requirements are met.

3. CROSS-SECTION MEASUREMENT PROCEDURES (TASK 3)

High purity commercial compounds, further purified by bulb-to-bulb vacuum line distillation, were used in the absorption cross-section measurements. The compounds were degassed at liquid nitrogen and dry ice temperatures prior to use to remove entrapped air and carbon dioxide. The pressures of the compounds added to the absorption cell were determined with the MKS Baratron capacitance manometer described in task 1 of Appendix A. Buffer gas pressures were measured with the Wallace and Tiernan gauge. Transmission measurements were performed on the gas cell when it was filled with dry synthetic air to account accurately for the small amount of absorption by the cell windows. CO_2 laser absorption measurements were performed on ethylene, for which cross-section data have been reproducibly obtained by several groups (Refs. A-1 through A-5), to confirm the validity of our experimental procedures. The CO_2 laser absorption spectra obtained for the compounds studied were compared for consistency with their low-resolution standard infrared spectra.

4. CONSIDERATION OF POTENTIAL AMBIENT AIR INTERFERENCES

The types and concentrations of potential interferences to detection, by the CO_2 laser photoacoustic method, of the hydrazines and other compounds of Air Force concern and the seven compounds of EPA concern studied here vary with the detection location. The most likely interferences are expected to be those pollutants in urban air that primarily result from auto emissions. Additional interferences may become important if detection is to be carried out for these compounds near major chemical industry centers. The concentrations of pollutants typically found at nonurban installations where the hydrazines and other hazardous compounds are to be most often detected should be low compared with those found in urban and industrial locations.

The most abundant compounds in the ambient air, carbon dioxide (0.03 mole %) and water vapor (up to ~ 6 mole %) possess very weak absorption in the CO_2 laser region. The lasing action in CO_2 results from transitions between excited vibrational states. The laser output thus exhibits poor spectral overlap with CO_2 absorption transitions that originate in ground vibrational states. The very weak absorption due to vibrational hot-band transitions should readily be taken into account with available temperature-dependent cross-section data for CO_2.

The CO_2 laser spectra of water vapor consist of a few sharp absorption peaks on a broad continuum background. The dependences of the CO_2 laser absorption spectra of water vapor on temperature, water pressure, and atmospheric pressure have been carefully characterized in earlier studies (Refs. A-6 through A-8). Under conditions of high humidity (i.e., 70% RH at 23°C) the continuum possesses an absorption strength of ~ 10^{-6} cm^{-1} throughout the CO_2 laser region. The use of absorption measurements that are carefully ratioed to the sharp water peaks should allow the absorption profiles of the hydrazines and other species of interest to be detectable at absorption signals of 10^{-7} cm^{-1} or less. This would allow (see Appendix C) the detection of acrylonitrile, allyl alcohol, methacrylonitrile, methyl methacrylate, and carbonyl difluoride at concentrations of 25 ppb or less and methyl bromide and methyl chloride at concentrations of 100 and 250 ppb, respectively, in humid air. The use of a far more conservative detectable absorption value of

5.0×10^{-7} cm^{-1}, or 50% of the water continuum absorption strength, would increase the foregoing detection limits in humid air by a factor of 5. Nonetheless, these more conservative detection limits are still an order of magnitude or more below the current or proposed most stringent threshold levels for these compounds.

Of the inorganic pollutants CO, NO, NO_2, N_2O, O_3, NH_3, and SO_2 present in urban air, only the last three possess absorption within the wavelength intervals of CO_2 laser output. Ammonia possesses a highly distinctive CO_2 laser absorption spectrum (Refs. A-2, A-9). At the 2- to 20-ppb concentration range typically found in urban air, it is not expected to interfere severely with the detection of the hydrazines or other compounds of interest. Neither O_3[2] (20 to 200 ppb) nor SO_2 (Ref. A-10) (<2 ppm) exhibits significant absorption in the 10.4-μm CO_2 laser band and, thus, neither will appreciably increase the CO_2 laser spectroscopic detection limits estimated for the compounds of interest in the presence of water vapor only, since the strongest CO_2 laser absorbances for the latter compounds fall within the 10.4-μm laser band.

More than fifty different hydrocarbons have been found in typically polluted urban air samples (Ref. A-11). The most abundant hydrocarbons found in a series of 200 samples of air taken in the Los Angeles area during 1965 were as follows (Ref. A-11): methane (3.22 ppm); ethane (0.10 ppm); propane (0.05 ppm); n-butane (0.06 ppm); n-pentane (0.03 ppm); i-pentane (0.04 ppm); ethylene (0.06 ppm); benzene (0.03 ppm); and toluene (0.05 ppm). The average concentrations found for many of these compounds in the 1965 Los Angeles study tend to be larger than the highest concentrations found for these compounds in other urban air studies. Our analysis of the infrared spectral properties of these compounds indicate that, at their typical concentrations, these compounds should not significantly increase the estimated detection limits for the compounds of interest in the presence of ambient levels of water vapor.

Various fluorochlorocarbons including CCl_3F and CCl_2F_2 (Ref. A-10), C_2Cl_3F (Ref. A-12), and $C_2Cl_2F_4$ (Ref. A-13) possess moderate to strong absorption bands within the CO_2 laser 10.4-μm band where the hydrazines and

other compounds to be detected absorb. However, the background levels of these compounds in the ambient air are quite low (Ref. A-14), so that these compounds should not constitute interferences to the compounds to be detected unless they are in use on a local basis. The compounds CCl_4 and CH_3Cl (Ref. A-13) and CH_3CCl_3 (Ref. A-12) absorb negligibly in the 10.4-μm CO_2 laser band and should not interfere with detection of the compounds by CO_2 laser techniques.

REFERENCES

A-1. G. L. Loper, M. A. O'Neill, and J. A. Gelbwachs, Appl. Opt. 22, 3701 (1983).

A-2. R. R. Patty, G. M. Russwurm, W. A. McClenny, and D. R. Morgan, Appl. Opt. 13, 2850 (1974).

A-3. U. Persson, B. Marthinsson, J. Johansson, and S. T. Eng, Appl. Opt. 19, 1711 (1980).

A-4. E. H. Christy and K. H. Faller, Paper 23, Second Joint Conference on Sensing of Environmental Pollutants, 10-12 December 1973, Washington, D.C.

A-5. G. L. Loper, A. R. Calloway, M. A. Stamps, and J. A. Gelbwachs, Appl. Opt. 19, 2726 (1980).

A-6. M. S. Shumate, R. T. Menzies, J. S. Margolis, and L. G. Rosengren, Appl. Opt. 15, 2480 (1976).

A-7. J. C. Peterson, M. E. Thomas, R. J. Nordstorm, E. K. Damon, and R. K. Long, Appl. Opt. 18, 834 (1979).

A-8. G. L. Loper, M. A. O'Neill, and J. A. Gelbwachs, Appl. Opt. 22, 3701 (1983).

A-9. R. J. Brewer and C. W. Bruce, Appl. Opt. 17, 3746 (1978).

A-10. A. Mayer, J. Comera, H. Charpentier, and C. Jassaud, Appl. Opt. 17, 391 (1978).

A-11. U. S. Department of Health Education, and Welfare, Air Quality Criteria for Hydrocarbons, National Air Pollution Control Administration Publication AP-64 (NTIS PB 190489) (1970).

A-12. B. D. Green and J. I. Steinfeld, Enviro. Sci. Technol. 10, 1134 (1976).

A-13. Sadtler Standard Spectra, Gases and Vapors, Vol 1, Sadtler Research Laboratories, Philadelphia (1972).

A-14. H. B. Singh, L. J. Salas, and L. A. Cavanagh, Air Pollut. Control Assoc. 27, 332 (1977); D. R. Cronn, R. A. Rasmussen, E. Robinson, and D. A. Harsch, J. Geophys. Res. 82, 5935 (1977).

Appendix B

ELECTRONIC DEVICE TO TRACK RESONANT CELL FREQUENCY

As discussed in Section II, resonant photoacoustic cell designs offer several advantages over nonresonant cell designs for trace detection applications. Resonant cells, such as that designed by Gerlach and Amer (Refs. B-1, B-2, and B-3) and shown schematically in Fig. 2 of Section II, can provide greater inherent immunity from background window absorption than nonresonant cells. This is accomplished by placing the cell windows at stationary nodal positions of the acoustic mode being excited (1st radial mode in Fig. 2). Sample adsorption losses for a given sample residence time should also be significantly lower in a resonant cell than a nonresonant cell for two reasons. (1) Resonant cells typically have volume-to-surface ratios as much as an order of magnitude greater than those of nonresonant cells. (2) Resonant cells can be successfully operated in a continuous-flow mode at much higher flow rates than nonresonant cells. This is because acoustic noise due to gas turbulence can be suppressed in a resonant cell by locating the gas inlet and outlet ports at the resonant cell's acoustical node positions (see Fig. 2).

The use of resonant cell designs in practical photoacoustic detectors, however, has been limited by the fact that the resonant cell's response is more than 500 times greater at laser light modulation frequencies equal to the cell's acoustic resonance frequency than at slightly different frequencies (see Fig. B.1). This requires that the light modulation frequency be continuously maintained at the cell's acoustical resonance frequency. This is particularly difficult since the cell's resonant frequency is a sensitive function of gas temperature and humidity.

We have developed an electronic circuit device that automatically tracks the resonance frequency of a resonant cell under changing temperature and humidity of the gas sample. The device uses the high acoustical gain bandpass filter properties of the cell to detect changes in the acoustic resonance frequency and automatically adjusts the laser light modulator to this frequency to maintain the peak photoacoustic signal. The device also serves as the photoacoustic system's signal processing electronics. This device, shown schematically in Fig. B.2), eliminates the major disadvantage in using a resonant photoacoustic cell for ambient air monitoring.

Fig. B1. **Response vs Light Modulation Frequency for Nonresonant and Resonant Photoacoustic Cells**

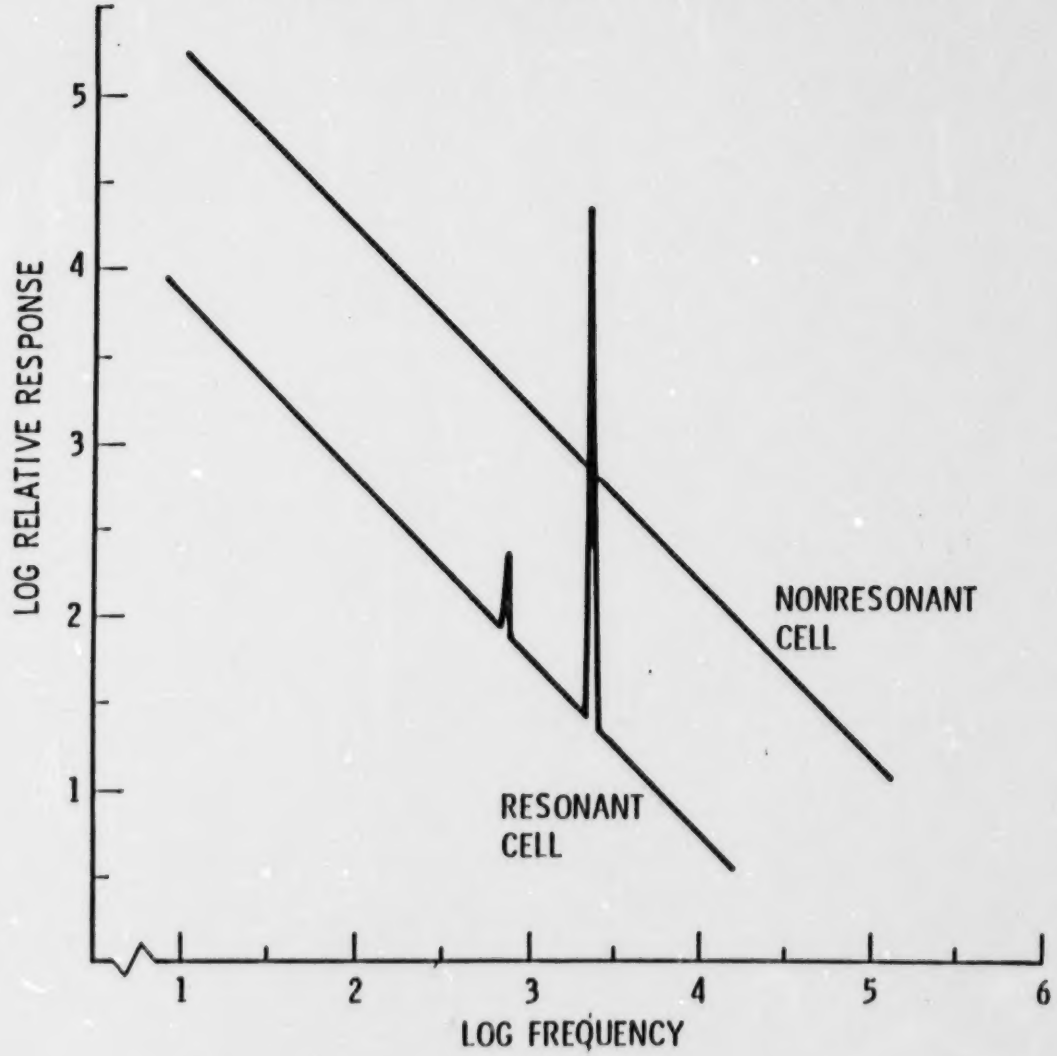

Fig. B1. **Response vs Light Modulation Frequency for Nonresonant and Resonant Photoacoustic Cells**

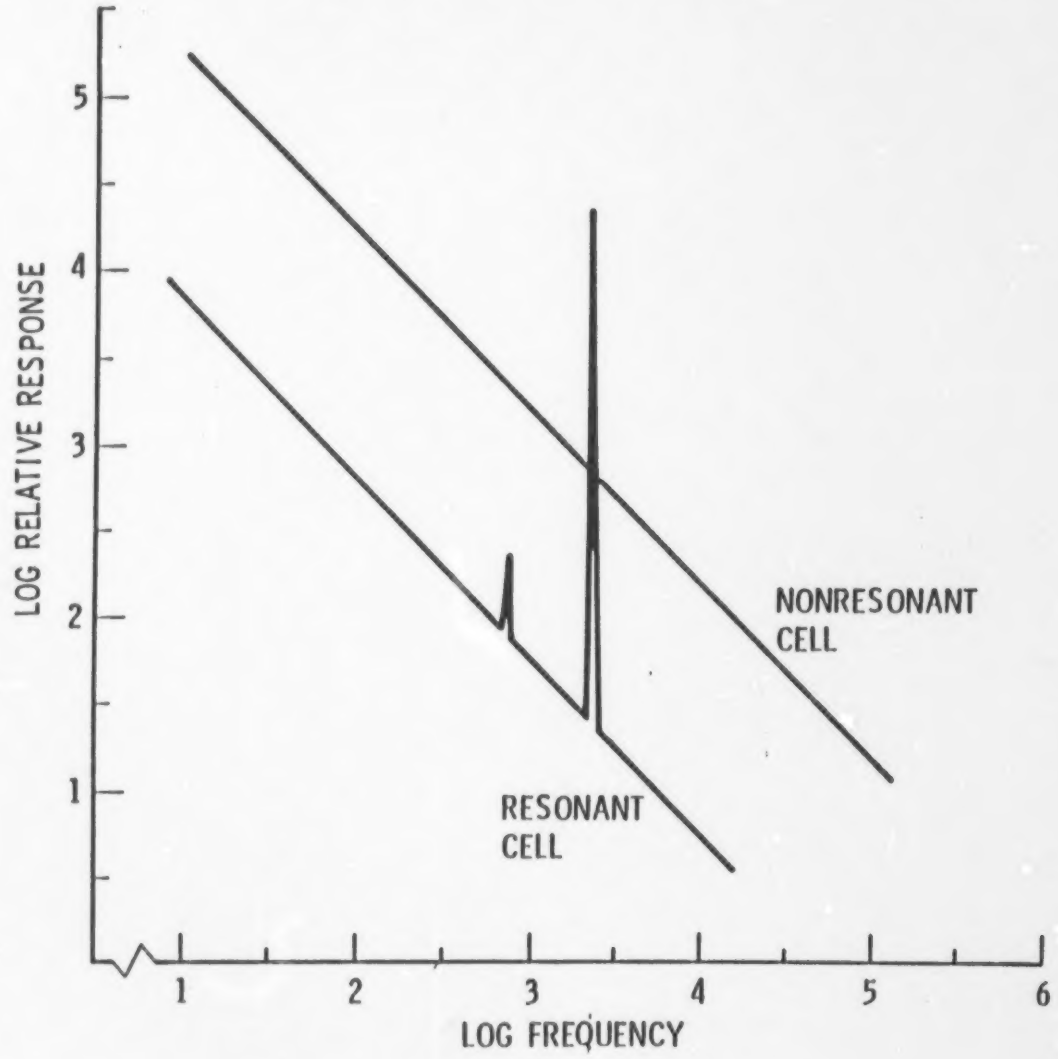

Fig. B2. **Resonant Cell Frequency Tracking and Signal Detection**

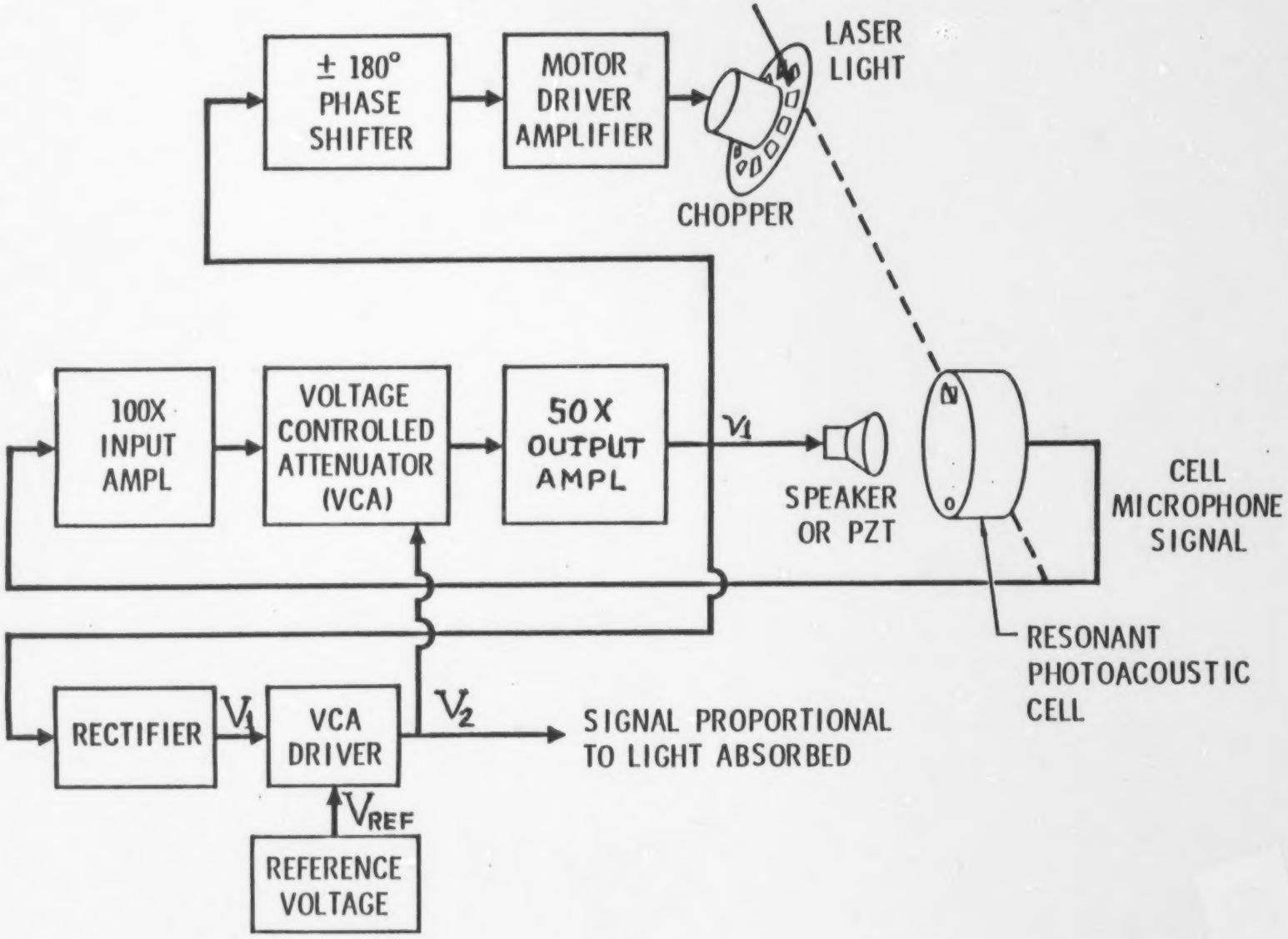

The device works as follows. A speaker, placed in front of the resonant cell, is initially made to emit a broad range of acoustic frequencies. The cell resonates preferentially at its acoustic resonance frequency. Acoustic energy is dissipated rapidly in the cell at nonresonant frequencies. The cell microphone thus selectively detects sound at the cell resonance frequency. The signal detected by the microphone is fed back into a 100X input amplifier, through a voltage controlled attenuator (VCA), and through a 50X output amplifier. The sinusoidal voltage signal ν_1 exiting the output amplifier has a frequency equal to the cell's acoustic resonance frequency. The speaker is driven by the signal at the cell's resonance frequency. The signal ν_1 is also fed into a rectifier to produce a DC voltage V_1 proportional to the amplitude of ν_1. V_1 is compared to a constant reference voltage V_{REF} by the VCA driver. The VCA driver produces a DC output voltage V_2 which is proportional to V_1-V_{REF}. The voltage V_2 controls the amount of attenuation produced by the VCA. The portion of the device described so far forms an acousto-electronic loop. The loop oscillates at the particular cell resonance frequency with a small, constant amount of acoustic energy in the cell. The DC output voltage V_2 rapidly adjusts to a constant value K in the absence of any light absorption by the gas in the cell.

The portion of device not yet described modulates the laser light intensity. The signal ν_1, whose frequency is equal to the cell resonance frequency, is phase-shifted by the amount needed to drive a mechanical chopper such that light absorption in the cell occurs in phase with the small acoustic signal produced in the cell by the speaker. Light absorption in the cell increases the magnitude of the signal ν_1 giving rise to an increase in its rectified DC signal V_1. V_2, which is proportional to V_1-V_{REF}, will then increase so that the amount of attenuation produced by the VCA increases in an attempt to reduce ν_1 to the constant, small value it had in the absence of light absorption by the gas sample. The quantity V_2-K at any time is thus directly proportional to the amount of light absorbed by the gas in the cell.

REFERENCES

B-1 R. Gerlach and N. M. Amer, Appl. Phys. Lett. 32, 228 (1978).

B-2 D. R. Wake and N. M. Amer, Appl. Phys. Lett. 34, 379 (1979).

B-3 R. Gerlach and N. M. Amer, Appl. Phys. 23, 319 (1980).

APPENDIX C

A. CELL COATINGS TO MINIMIZE SAMPLE (NH_3 AND N_2H_4) ADSORPTION FOR LOW-LEVEL PHOTOACOUSTIC DETECTION

ABSTRACT

A photoacoustic signal rise-time technique is used to evaluate the suitability of several surface materials for minimizing sample adsorption loss in a trace-level toxic vapor monitor. Four materials, 304 stainless steel, gold, paraffin wax, and tetrafluoroethylene (TFE-) Teflon are tested using ammonia as a sample. TFE-Teflon is also tested using hydrazine. The results show that both metals interact strongly with the sample. The TFE-Teflon coating is found to provide the resonant photoacoustic cell with accurate real-time response for both hydrazine and ammonia sample flows.

I. INTRODUCTION

CO_2 laser photoacoustic spectroscopy (PAS) provides a sensitive and general technique for monitoring trace-level toxic vapors (Refs. C-1, C-2). Many polar compounds of interest, however, are highly adsorptive and produce an error in real-time concentration measurements by adhering to detector surfaces. We report the effects of various surface coatings on the performance of a resonant photoacoustic cell for detection of trace levels of adsorptive compounds. It is important to note that both the problem of sample adsorption loss at detector surfaces and the resolution of the problem are not limited to PAS but are common to any trace-level detection cell.

One important class of toxic compounds that is especially adsorptive is hydrazine and its methylated derivatives. These molecules, by overlap of the nitrogen lone-pair electrons with surface atoms, interact strongly with most metals and many insulating materials. Often these compounds can also form hydrogen bonds with surface adsorbed species such as water. Ammonia is a good model compound for these molecules, as it shows the characteristic adsorptive behavior but is not a health hazard at low concentrations.

In the present study, adsorptive losses in a flowing resonant photoacoustic cell are measured as a function of time following flow introduction, by monitoring the photoacoustic signal rise time. Comparison of the ammonia and hydrazine results with those for ethylene, which interacts weakly with most surfaces, provides a measure of the cell-sample interaction. Ammonia rise times are measured for four different cell surface materials: 304 stainless steel, gold, TFE-Teflon, and paraffin wax. Also reported are the results for hydrazine in a TFE-Teflon coated cell.

II. EXPERIMENTAL

Experiments to measure the effectiveness of the cell coatings in reducing adsorptive losses are performed using a standard photoacoustic arrangement. Light from a line-tunable CO_2 waveguide laser is mechanically chopped and double-passed through a resonant PAS cell. Laser power is monitored by a thermopile after passing through the cell. Acoustic signals, detected by a microphone mounted in the cell wall, are amplified and demodulated by a lock-in amplifier referenced by the chopper motor. Both the cell and the chopper are mounted in separate sound-insulating boxes which reduce the coherent acoustic noise level.

The resonant cell, of the Amer design (Ref. C-3), is a cylinder with windows and gas ports located at the nodal position of the first radial mode. The laser beam enters and exits the cell at Brewster's angle. The microphone is mounted at the center of one cylinder face which is the position of the maximum pressure amplitude of the first radial mode. Both cylinder faces are easily removed to facilitate coating of the cell interior with various materials. The faces bolt to the cylinder body and are O-ring sealed. The 17.8-cm-diameter cell exhibits a strong acoustic resonance at 2034 Hz, close to the frequency calculated for the first radial mode (Ref. C-4). The performance characteristics of the uncoated stainless steel cell are given in Table C-1.

Ethylene and ammonia dilutions in nitrogen are produced by flowing standard gases through calibrated flow meters into a mixing chamber where turbulence mixes the gases. Hydrazine mixtures are produced by heating hydrazine-filled Teflon permeation tubes to 70°C and purging with a slow nitrogen flow. These tubes produce a steady mass flow of hydrazine which is diluted downstream with a turbulent N_2 flow. The concentration of hydrazine in the stream was verified by a wet chemical technique to be 1.0 ± 0.2 ppm. In all cases dry nitrogen is used as the diluting gas. The mixture is sampled from the mixing chamber at essentially atmospheric pressure by a small pump

which pulls the gas mixture through the PAS cell at a typical rate of 1.2 liters per minute. Provision is made for bypassing the cell with the gas mixture flow prior to a measurement in order to equilibrate the feedline surfaces. This ensures that measured rise times are a function of cell characteristics only. A rise time measurement is initiated by diverting the gas flow from the bypass through the cell and monitoring the photoacoustic signal rise that follows.

Ethylene is monitored at the 10.6-μm P(14) line of the CO_2 laser, where it has an absorption coefficient of 34.7 atm^{-1} cm^{-1} (Ref. C-5). Ammonia is monitored at the 10.6-μm P(32) line, at which wavelength its absorption coefficient is 13.7 atm^{-1} cm^{-1} (Ref. C-2). To avoid interferences from ammonia, a hydrazine thermal decomposition product, hydrazine is monitored at the 10.6-μm P(22) line. At P(22) hydrazine has an absorption coefficient of 6.18 atm^{-1} cm^{-1}, almost a factor of 77 larger than that of ammonia (Ref. C-6). All of the data reported are ror room temperature measurements.

Table C-1. Cell Performance Characteristics

Noise Source	RMS Level	Equivalent C_2H_4 Concentration
Ambient	0.6 μV†	
Flow (1.2 liter/mm)	0.08 μV†	
Coherent acoustic	0.35 μV	
Photoacoustic	0.2 μV/W	
Total Background	1.23 μV/W†	1.8 ppb

†20-Hz bandwidth

III. RESULTS AND DISCUSSION

A. RISE TIMES

The rate of change in concentration of a species i in a flowing cell is given by

$$\frac{d\,C_i(t)}{dt} = \frac{R}{V}\left[F_i - C_i(t)\right] \qquad (C\text{-}1)$$

where R is the gas flow rate, F_i is the feed concentration of species i, and V is the cell volume. Equation (C-1) assumes that the adsorption rate of i is zero and gas mixing inside the cell is instantaneous. Integrating Eq. (C-1) with the initial condition that $C_i(0) = 0$ gives

$$C_i(t) = F_i\left(1 - e^{-Rt/V}\right) \qquad (C\text{-}2)$$

The solid line in Figure C-1 shows the rise time curve predicted by Eq. (C-2) for the experimental parameter values. Also shown are the experimental ethylene and ammonia signal results for the various cell coatings. The values have been normalized to the same maximum signal level by factoring out the appropriate cell responsivity and absorption coefficient. The results are also summarized in Table C-2.

The rise times measured for ethylene are identical, within experimental error, for all four cell-surface coatings. This observation, along with the good agreement between the experimental curve and the rise time predicted by Eq. (C-2), confirms that ethylene does not strongly interact with the cell surface materials under consideration. The small discrepancy between the predicted and observed rise time for ethylene is attributed to a finite mixing time.

The rise time curve for ammonia in a gold plated cell (Figure C-1) shows significantly different behavior than for ethylene. The ammonia signal rises

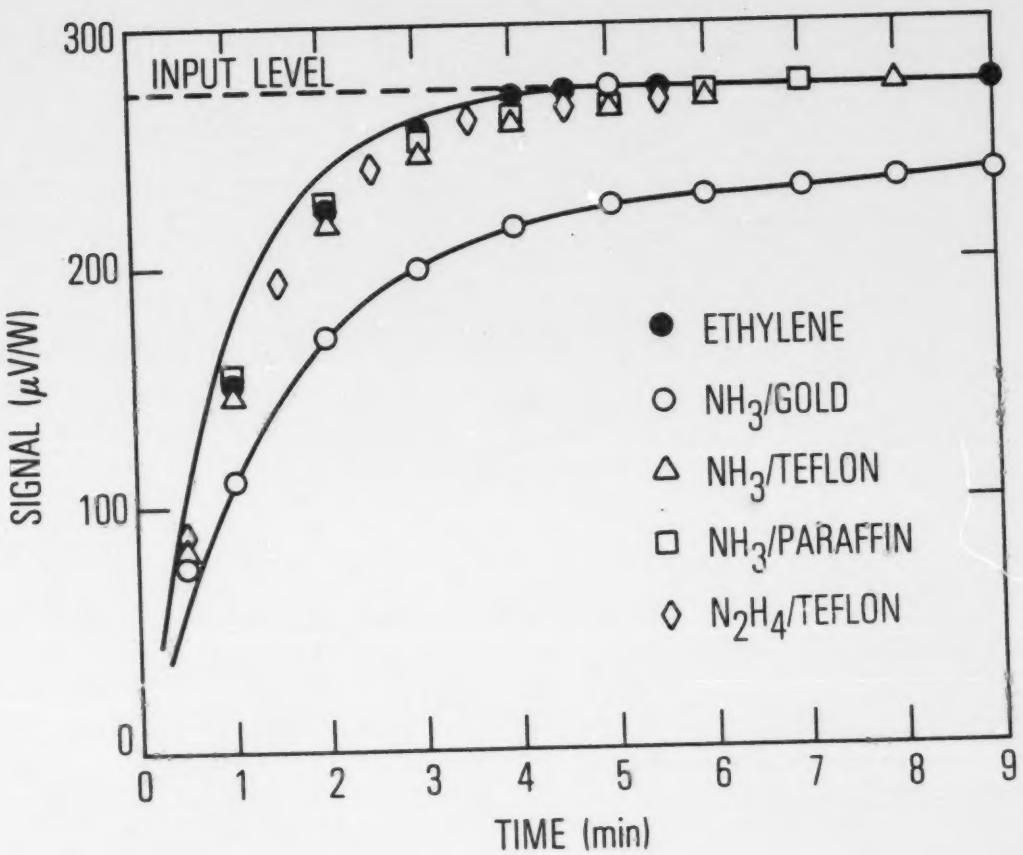

Fig. C-1. Photoacoustic Response as a Function of Time Following Flow Introduction Into the Cell for Various Cell Coatings and Gas Samples. The solid line is the response calculated from Eq. (C-2). Curves are normalized to a common maximum.

Table -2. Effect of Surface Coating on Signal Rise Time and Cell Q

Coating	Time to Reach 90% of Maximum Photoacoustic Signal Level		Cell Q
	NH_3	N_2H_4	
304 stainless steel	99 min		415
Gold	34 min		538
Paraffin	2.5 min		502
TFE-Teflon	2.8 min	2.8 min	545

Volume exchange = 2.3 min.

rapidly at first, but then slows to a steady rise which asymptotically approaches the feed concentration value after several hours. The slow rise is attributed to adsorption loss of ammonia in the cell to the walls. This is corroborated by the observation of a fast signal decay when the flow is terminated and the cell is isolated prior to the signal reaching its maximum value. No such decay is observed for ethylene.

Also shown in Figure C-1 are the ammonia rise times for the cell coated with paraffin wax and TFE-Teflon, respectively. In contrast to the results for the gold coated cell, both rise times closely follow that predicted for simple volume exchange and observed for ethylene. Also, no signal decay is observed following flow termination.

Lastly, Figure C-1 shows the rise time curve obtained for a 1-ppm flow of hydrazine through the Teflon coated cell. As was observed for ammonia, the hydrazine curve follows the volume exchange curve quite closely. This is strong support that the hydrazine is not adhering to or reacting at the TFE-Teflon surface.

B. Q MEASUREMENTS

For a cell coating material to be effective for PAS trace vapor detection, it must reduce sample-cell interaction. Additionally, the coatings

must not degrade the acoustic response of the cell. The cell Q, calculated by dividing the resonance frequency by its bandwidth at the 0.707 amplitude point, is listed in Table C-2 for each of the four cell coatings. A small decrease in the cavity Q is observed for the wax as compared to the gold coating. A decrease in Q is expected for a material which deforms easily under acoustic pressure and, thus, damps the acoustic wave. Apparently the coating is thin enough that the effects are minor. The Teflon coating actually increases the cell Q by a small amount. This is attributed to the smooth, slick surface obtained by Teflon coating, which would decrease any surface frictional or scattering loss of acoustic energy (Ref. C-7).

IV. CONCLUSIONS

We have demonstrated that, by the correct choice of surface coating material, the surface adsorptive loss of ammonia and hydrazine can be significantly reduced in a flowing PAS cell, with no reduction in acoustic response. Teflon and paraffin are found to be excellent materials for this purpose. Ammonia is found to be a good model compound for hydrazine surface studies, at least at room temperature.

Lastly, the technique of photoacoustic detection in a flowing system is demonstrated to be an efficient and sensitive method for monitoring surface adsorption loss.

REFERENCES

C-1. E. L. Kerr and J. G. Atwood, Appl. Opt. 7, 915 (1968); L. B. Kreuzer, N. D. Kenyon, and C. K. N. Patel, Science 177, 347 (1972); L. B. Kreuzer, Anal. Chem. 46, 239A (1974); G. L. Loper, R. A. Calloway, M. A. Stamps, and J. A. Gelbwachs, Appl. Opt. 19, 2726 (1980).

C-2. R. J. Brewer and C. W. Bruce, Appl. Opt. 17, 3746 (1978).

C-3. R. Gerlach and N. M. Amer, Appl. Phys. 23, 319 (1980).

C-4. P. M. Morse, Vibration and Sound, McGraw-Hill (1948), p. 398.

C-5. G. L. Loper, M. A. O'Neill, and J. A. Gelbwachs, Appl. Opt. 23, 3701 (1983).

C-6. G. L. Loper, A. R. Calloway, M. A. Stamps, and J. A. Gelbwachs, Appl. Opt. 19, 2726 (1980).

C-7. R. H. Johnson, R. Gerlach, L. J. Thomas III, and N. M. Amer, Appl. Opt. 21, 81 (1982).

APPENDIX C (Continued)

B. HYDRAZINE SAMPLING LINE TESTS

ABSTRACT

Six types of plastic tubing were experimentally evaluated for suitability as trace level hydrazine remote sampling lines. A photoacoustic technique was used to measure the hydrazine losses from a 1 ppm hydrazine/nitrogen flow through a 100 foot coil of the various plastic tubings. The plastics exhibited a wide range of behavior. It was determined that the TFE Teflon was the most suitable material.

Introduction

One proposal for low level hydrazine monitoring at a launch facility calls for a stationary detector which is able to remotely sample various site locations by pulling the gas sample through tubing from the site to the detector. A potential problem with such a scheme is loss of hydrazine concentration in the tubing due to adsorption or other mechanism. Hydrazine and its methylated derivatives are known to strongly adsorb to a large number of materials. For long lengths of tubing, even a material with moderate hydrazine adsorptivity could produce a dangerous error in the detected hydrazine concentration. Therefore, laboratory tests designed to evaluate the suitability of various plastic tubings as remote sampling lines have been carried out. We define "suitable" in terms of a tubing's ability to transport a 1 ppm hydrazine flow through 100 feet of tubing, losing not more than 25% of the initial hydrazine concentration within 10 minutes of flow initiation. The six different tubing types which were evaluated are listed in Table I along with the material manufacturers and tubing suppliers (Ref. C-8). The test results, as detailed below, showed a wide range of behavior between the different tubing materials. Recommendations as to the suitability of the various tubings are supplied later in this report.

Experimental

The experimental technique which was used in these tests is based upon photoacoustic (PAS) detection of hydrazine. This technique has previously proved useful for evaluation of cell coatings for hydrazine detectors (Ref. C-9). The PAS technique is unique in its ability to provide extreme sensitivity (< 5 ppb N_2H_4) for virtually any compound that has a moderate absorption coefficient at a laser accessable wavelength. For the present study this attribute has been indispensable, allowing comparison between flows of adsorptive compounds like hydrazine with more inert gases such as ethylene, at the same trace levels. Such comparisons are necessary to quantify or calibrate the interactions between the sample gas and the tubing material.

Other detection techniques offer similar sensitivity for selected compounds, but it is the generality of the PAS technique which sets it apart from the other methods.

In the present study, hydrazine adsorptive losses in a 100 foot coil of tubing are measured as a function of time following flow introduction by monitoring the photoacoustic signal risetime. Comparison of the hydrazine results with and without the plastic coil provides a measure of the tubing-sample interaction.

Experiments were performed using a standard photoacoustic arrangement. Light from a line tunable CO_2 waveguide laser was mechanically chopped and double passed through a resonant PAS cell. Laser power was monitored by a thermopile after passing through the cell. Acoustic signals, detected by a microphone mounted in the cell wall, were amplified and demodulated by a lock-in amplifier referenced by the chopper motor. Both the cell and the chopper were mounted in separate sound insulating boxes which reduced the coherent acoustic noise level.

The resonant cell, of the Amer design (Ref. C-10), was a cylinder with windows and gas ports located at the nodal position of the first radial mode. Positioning the ports and windows in this manner provides a high degree of immunity from noise produced by flow turbulence or laser light absorption at the windows. Sample flows of up to two liters per minute were used in this cell without significantly affecting the cell's sensitivity. The laser beam entered and exited the cell at Brewster's angle. The microphone was mounted at the center of one cylinder face which is the position of the maximum pressure amplitude of the first radial mode. The 17.8 cm diameter cell exhibited a strong acoustic resonance at 2434 Hz, close to the frequency calculated for the first radial mode.

Hydrazine dilutions were produced by heating hydrazine filled Teflon permeation tubes to 70°C and purging with a slow nitrogen flow. These tubes produced a steady mass flow of hydrazine which was diluted downstream with a turbulent N_2 flow. The concentration of hydrazine in the stream was verified by a wet chemical technique to be $1.0 \pm .2$ ppm. In all cases nitrogen was used as the diluting gas. The mixture was sampled from the mixing chamber at

essentially atmospheric pressure by a small pump which pulled the gas mixture through the PAS cell at a rate of 1.2 liters per minute. Provision was made for directing the gas flow either through a 100 foot coil of the 1/4 inch diameter plastic tubing being tested and then to the PAS cell or directly to the PAS cell, bypassing the coil. The flow system is diagrammed in Fig. B-1. Humidity was controlled by saturating the diluting N_2 flow with water at a specific temperature and then warming the nitrogen back to room temperature. Tests were performed at either zero or 80 percent relative humidity. All tubing coils were pumped by a vacuum system for several hours prior to testing. No other preparations, except where specified later in the report, were performed.

Results

Fig. B-2 shows a typical risetime measured for hydrazine flowing through just the cell (dotted line) and flowing through a 100 foot coil of polyflo tubing before flowing into the cell (solid line). Several interesting features can be observed in the figure. First, following flow introduction through the coil, there is an induction period where no signal is observed. This period is much longer than that calculated for simple volume exchange of the coil and observed for ethylene flows. The induction period indicates a strong tubing - sample interaction, but this saturates rather quickly as evidenced by the signal rise. The fact that the "coil" curve continues to rise more slowly than the "no coil" curve, however, means that after the induction period there is still an active hydrazine loss mechanism. Finally, it should be noted that the maximum signal level for the two curves is not the same. The "no coil" curve levels off at the value expected for a 1 ppm hydrazine concentration based upon the known hydrazine absorption cross-section and cell responsivity. However, the risetime curve for the case in which the flow is directed through the coil never reaches this expected value. This is true even after flowing the hydrazine through the coil for long periods of time. Apparently, another loss mechanism does not saturate at the hydrazine concentration used. The level of hydrazine loss depends upon the tubing material. No such loss was observed for ethylene flows which showed the same final level for both coil and no coil configurations.

Risetime results for the various materials tested are summarized in Table II. Table II lists the plastics in descending order of recommended suitability as hydrazine sampling lines. Two of the table categories require clarification. The time to reach 80% of maximum signal is the time to reach a detected 0.8 ppm concentration of hydrazine in the PAS cell. It should be noted that simple volume exchange accounts for 2.5 minutes of the observed risetimes. "Percent of maximum signal at 10 minutes" means the percentage of 1 ppm hydrazine concentration reached in the PAS cell after 10 minutes of flowing the mixture through the coil into the cell. The values reported are an average of values from two or three different coils of the same material except for the tubings where the data was not reproducible from coil to coil, specifically Polyflo and FEP Teflon. For these cases the data for each coil is reported.

Additional Tests

Several tests besides the risetime measurements already described were performed on a few of the tubing materials. The results of these tests are summarized in Table III and described below.

Two samples of Kodak Polyflo polyethylene tubing which had previously shown very different hydrazine risetime behavior were subjected to first an acid and then a carbon tetrachloride wash in an effort to determine whether metal ions or plasticizers left in the tubing after extrusion were acting as hydrazine sinks. No change in the hydrazine risetime for either tubing was observed after the acid and solvent rinses.

Air was substituted for nitrogen as a diluent to determine whether oxygen increases the amount of hydrazine decomposition inside the tubing. No change was observed for 1 ppm hydrazine concentrations.

Additionally, the effect of lower hydrazine concentration on the risetime was investigated. A 250 ppb hydrazine in nitrogen mixture was flowed through a 100 foot Teflon TFE coil. The signal risetime was very close to that measured for a 1 ppm hydrazine concentration through the same coil.

Lastly, a test to determine the recovery time of a sampling line system following exposure to high levels of hydrazine was performed. A 0.1% hydrazine in nitrogen mixture was flowed through 100 feet of TFE Teflon tubing for about 10 minutes. The flow was then switched to pure N_2 and the signal decay was monitored. The system recovered to the 1 ppm sensitivity level within 2 hours of hydrazine flow termination.

Discussion

Two tubing materials proved suitable for remote sampling of low level hydrazine vapor, TFE Teflon and high density polyethylene. We recommend TFE Teflon as the most suitable. The FEP Teflon from one manufacturer (ZEUS) was a good material, however, the same material from the second supplier (PLASTIC CENTER) was not suitable. Kodak's Polyflo (polyethylene) showed inconsistent behavior from one coil to the next, even though the coils had been taken from the same large spool. Risetimes measured for the same Polyflo coil were very reproducible. We presently can offer no explanation for this inconsistent behavior. The least suitable material was found to be PFA Teflon, which gave consistently poor risetimes. PFA Teflon has a molecular structure which contains oxygen atoms. We believe the lone pair electrons on the oxygen atoms provide a likely binding site for the hydrazine molecule.

REFERENCES

C-8) The six materials were specified by the Air Force Space Division Propellant Office.

C-9) S. M. Beck, "Cell Coatings to Minimize Sample (NH_3 and N_2H_4) Adsorption for Low-level Photoacoustic Detection," Appl. Opt. 24, 1761 (1985).

C-10) R. Gerlach, N. M. Amer, "Brewster Window and Windowless Resonant Spectrophones for Intracavity Operation," Appl. Phys. 23, 319 (1980).

TABLE 1

TYPES OF TUBINGS TESTED

	MATERIAL	MANUFACTURER	SOURCE
1.	TFE TEFLON	DUPONT	ZEUS, PLASTIC CENTER
2.	PFA TEFLON	DUPONT	PLASTIC CENTER
3.	FEP TEFLON	DUPONT	ZEUS, PLASTIC CENTER
4.	HIGH DENSITY POLYETHYLENE	?	PLASTIC SALES
5.	POLYPROPYLENE	?	PLASTIC SALES
6.	POLYFLO (POLYETHYLENE)	KODAK	AEROSPACE

TABLE II

1 PPH HYDRAZINE RISETIME RESULTS FOR VARIOUS PLASTIC TUBINGS

# OF COILS AVERAGED	TUBING MATERIAL	SOURCE	HUMIDITY	TIME TO 80% MAXIMUM LEVEL	% OF MAXIMUM LEVEL AFTER 10 MIN
3	TFE TEFLON	ZEUS, PLASTIC CENTER	0%, 80%	10 MIN	80%
3	HDPE	PLASTIC SALES	0%, 80%	10 MIN	80%
2	POLYPROPYLENE	PLASTIC SALES	0%	17 MIN	70%
1	FEP TEFLON	ZEUS	0%	17 MIN	75%
1	FEP TEFLON	PLASTIC CENTER	0%	12 MIN	50%
1	FEP TEFLON	PLASTIC CENTER	80%	48 MIN	40%
1	POLYFLO	AEROSPACE	0%	8 MIN	85%
1	POLYFLO	AEROSPACE	0%	20 MIN	70%
1	POLYFLO	AEROSPACE	0%	60 MIN	35%
2	PFA TEFLON	PLASTIC CENTER		62 MIN	20%

TABLE III

ADDITIONAL TESTS AND TEST RESULTS

TEST	RESULT
1 m ACID ETCH OF POLYFLO	NO CHANGE
CCl_4 WASH OF POLYFLO	NO CHANGE
AIR DILUTION INSTEAD OF N_2	NO CHANGE
LOW LEVEL (250 ppb) HYDRAZINE	NO CHANGE FROM 1 ppm
HIGH LEVEL (0.1%) HYDRAZINE	< 2 HOUR RECOVERY TO 1 ppm SENSITIVITY

Hydrazine Risetime Apparatus

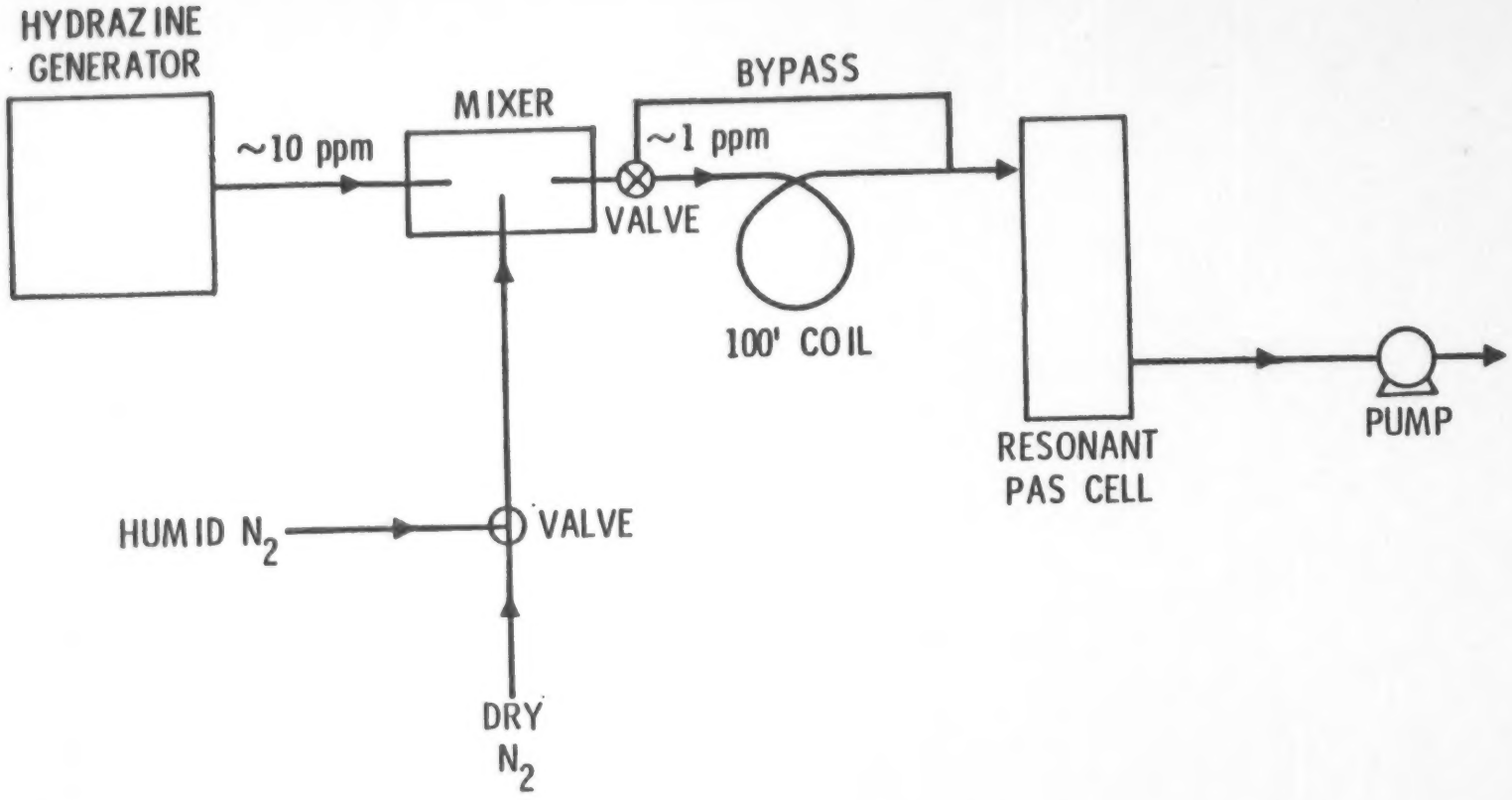

FIGURE C-1

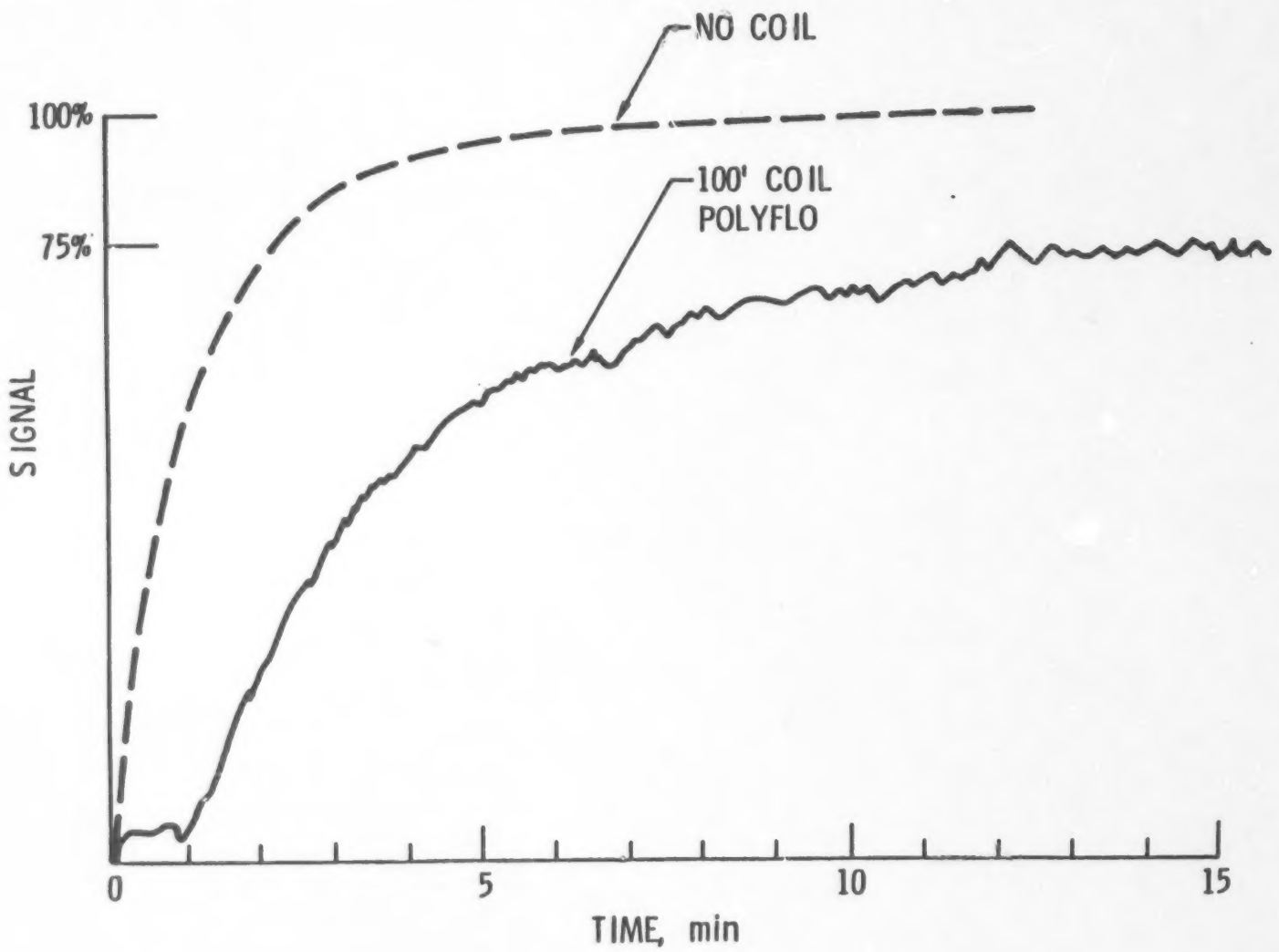
1 ppm Hydrazine Risetime
NO COIL
100' COIL
POLYFLO
100%
75%
SIGNAL
0
5
10
15
TIME, min

FIGURE C-2

APPENDIX D

CO_2 LASER ABSORPTION SPECTRA OF VOLATILE CONSTITUENTS OF HAZARDOUS WASTE

ABSTRACT

CO_2 laser absorption cross-section data are reported for the toxic compounds acrylonitrile, allyl alcohol, methacrylonitrile, methyl methacrylate, carbonyl difluoride, methyl chloride, and methyl bromide. These data indicate that methyl chloride and methyl bromide should be detectable by the CO_2 laser photoacoustic technique at concentrations of 250 and 100 ppb, respectively, in the presence of water vapor and other anticipated interferences in the ambient air. The other five compounds should be detectable in the ambient air at concentrations of 25 ppb or below by the photoacoustic method.

I. INTRODUCTION

CO_2 laser-based spectroscopic detection methods can provide highly specific detection of toxic organic compounds in multicomponent air samples. The $C^{12}O_2^{16}$ laser has an output (Ref. D-1) of more than 100 discretely tunable wavelengths between 9.1 and 11.0 μm. Laser output at wavelengths as long as 12.0 μm can be obtained from other CO_2 isotopic species. The CO_2 laser spectral output thus conveniently overlaps the wavelength region where: (a) absorptive interferences due to water vapor and other atmospheric constituents are minimized (Ref. D-2), and (b) most organic compounds possess moderate to strong absorption bands due to skeletal stretch or deformation vibrational modes (Ref. D-3). The wavelength positions, intensities, and shapes of absorption bands due to these modes are particularly dependent upon the size, geometry, and type of bonding in a molecule. Organic molecules, even without resolvable rotational structure, thus generally possess unique CO_2 laser absorption signatures (Refs. D-4 through D-7). Molecules with resolvable rotational structure within the CO_2 laser region will possess highly characteristic absorption signatures due to the random wavelength coincidences between the molecule's absorption features and the CO_2 laser lines (Refs. D-1, D-8).

This report presents data needed to assess the capability of the $C^{12}O_2^{16}$ laser photoacoustic technique to detect low ppb levels of acrylonitrile, allyl alcohol, methacrylonitrile, methyl methacrylate, methyl chloride, methyl bromide, and carbonyl difluoride in multicomponent ambient air samples. These compounds are among the many organic substances for which near real-time, low-ppb-level detection are desired. These substances are workplace inhalation hazards. Acrylonitrile is a suspected carcinogen (Ref. D-9). Repeated low-level exposure to the other compounds may cause severe lung, kidney, or nervous system damage (Refs. D-10, D-11). The first four compounds are used extensively in the plastics, fiber, or rubber industries (Refs. D-12, D-13). Methyl bromide is commonly used as a fumigant.

Each of the seven compounds are among possible volatile constituents of hazardous chemical waste (Ref. D-14). Sensitive detection of these vapors may be needed as part of waste site cleanup operations.

Vapor-phase absorption cross-section data as a function of $C^{12}O_2^{16}$ laser wavelength are reported here for the aforementioned compounds. The determination of the concentrations of species in an air sample by CO_2 laser spectroscopic techniques requires a library of such absorption cross-section data for the compounds of interest as well as for absorbing interferences in the sample. With these data, the concentrations of the n absorbing sample components can be determined by measuring sample absorption at $m \geq n$ different laser wavelengths and solving a set of n simultaneous equations. Cross-section data as a function of laser wavelength are also required for compounds to be detected and possible interferences to estimate the expected detection sensitivities of these compounds by a particular CO_2 laser spectroscopic method. The cross-section data measured for the foregoing seven compounds are used here to estimate their expected ambient air detection sensitivities by the CO_2 laser photoacoustic technique.

$C^{12}O_2^{16}$ laser absorption cross-section data of the type obtained in this study have been measured in previous studies for several different gases whose trace detection are of interest. These include the atmospheric constituents ammonia (Refs. D-8, D-15 through D-17), ethylene (Refs. D-8, D-15, D-16, D-18), and ozone (Refs. D-8, D-19), the hydrazine-based rocket fuels and some of their air oxidation products (Ref. D-4), and various toxic industrial compounds (Refs. D-5 through D-7, D-15).

II. EXPERIMENTAL

The absorption cross sections $\sigma(\lambda)$ reported here were determined by measuring the transmittance $T(\lambda)$ of CO_2 laser light of different wavelengths λ through a gas cell and by then evaluating the relationship $T(\lambda) = \exp[-\sigma(\lambda)pL]$. Here p represents the pressure (in atmospheres) of the absorbing compound, and L represents the path length of the absorption cell in centimeters. All measurements were performed at room temperature (298 K). The cross-section measurements were carried out on mixtures containing low pressures of the compound of interest in 1-atm pressure of synthetic air (80% N_2/20% O_2) to model the collisional broadening of the absorption lines of these compounds that would occur in the ambient air. Three or more transmittance measurements were made at each laser wavelength for a given gas mixture. Three or more sets of spectral measurements using different gas fills were generally performed for each compound studied. The $T(\lambda)$ values were corrected for the small transmittance losses that occur at the cell windows. These losses were determined by performing transmission measurements through the cell when filled with synthetic air only.

The compounds studied are highly polar. Cross-section measurements were thus performed in absorption cells designed to minimize sample losses on cell walls due to adsorption or surface catalyzed degradation reactions. Measurements were performed with either or both of two different 5-liter spherical glass cells of low surface-to-volume ratio (0.28 cm^{-1}). The inside walls of one cell were entirely coated with paraffin to form a nonpolar surface. The inside walls of the other cell were left uncoated. These cells were equipped with zinc selenide windows at Brewster's angle and had optical path lengths of 32.98 and 33.95 cm, respectively. An MKS Instruments, Inc. Baratron pressure gauge with a 310 BH-10 pressure head was used to measure the steady-state pressure of the sample gas in a cell after the gas was present for several minutes. The cross-section data obtained with the coated and uncoated cells

for even the most polar species studied were found to be in very good agreement with each other. This indicates that negligible sample losses occurred in these cells.

The optical arrangement used in the measurements was similar to that used in our previous studies (Refs. D-4, D-5). A waveguide $C^{12}O_2^{16}$ laser was employed that was tunable over ~ 18 wavelengths in each of its 9.4- and 10.4-μm band P and R branches. The laser intensity incident on the cell was maintained below 1.5 W (beam diam ~ 2 mm) to avoid absorption saturation effects.

High purity commercial compounds and research purity (99.9995%) nitrogen and oxygen were employed in the study. The CO_2 laser absorption spectra obtained for these compounds were found to be consistent with their corresponding low-resolution standard spectra (Ref. D-20). All samples were degassed at liquid nitrogen temperature prior to use.

III. RESULTS AND DISCUSSION

Table D-1 summarizes the vapor phase $C^{12}O_2^{16}$ laser absorption cross-section data obtained for acrylonitrile [CH_2=CHCN], allyl alcohol [CH_2=$CHCH_2OH$], methacrylonitrile [CH_2=$C(CH_3)CN$], methyl methacrylate [CH_2=$C(CH_3)CO_2CH_3$], methyl chloride, methyl bromide, and carbonyl difluoride when buffered to a total pressure of 1 atm with 80% N_2/20% O_2. The cross-section data obtained for acrylonitrile and allyl alcohol are plotted in Fig. D-1, while the methacrylonitrile and methyl methacrylate data are displayed in Fig. D-2. The results for methyl chloride and methyl bromide are shown in Fig. D-3. Fig. D-4 shows the results for carbonyl difluoride. From these figures it is observed that these compounds can be readily distinguished from each other by their CO_2 laser absorption spectra. As discussed more fully below, this is possible even though some of these compounds are structurally similar and possess absorption bands in the 9- to 11-μm region due to some of the same vibrational modes.

A. CO_2 LASER ABSORPTION SPECTRA FOR VINYL- AND VINYLIDENE-SUBSTITUTED COMPOUNDS

Vibrational modes associated with the vinyl [CH_2= CH-] groups on acrylonitrile and allyl alcohol and the vinylidene [CH_2=$C(CH_3)$-] groups on methacrylonitrile and methyl methacrylate give rise to strong absorption bands within the 9- to 11-μm wavelength region. For vinyl compounds, this absorption is due to two different out-of-plane C-H bond deformation modes. These modes have been characterized as an in-phase trans CH=CH wag vibration and a CH_2 wag vibration (Refs. D-21, D-22). For vinylidene compounds, the CH_2 wag contributes to absorption in the CO_2 laser region (Ref. D-22).

The CO_2 laser absorption spectrum of acrylonitrile in Fig. D-1 consists of weak absorption within the laser 9.4-μm band R-branch, but moderate strength, highly structured absorption throughout the laser 10.4-μm band. The series of sharp peaks result from the presence of resolvable rotational structure in the vinyl group absorption bands due to the trans CH=CH wag vibration and the CH_2 wag vibration. In acrylonitrile vapor, strong Q-branch

Table D-1. Absorption Cross Sections ($cm^{-1}atm^{-1}$) of Selected Toxic Compounds[a]

$C^{12}O_2^{16}$ laser 9.4 μm ($00^0 1 - 02^0 0$) band		Acrylonitrile[b]	Allyl Alcohol[c]	Methyl Methacrylate[d]	Methacrylonitrile[e]	Methyl Bromide[f]	Methyl Chloride[g]	Carbonyl Difluoride[h]
R(34)	9.201			0.18				0.35
R(32)	9.210		0.87	0.24 ± 0.03	0.01	0.023 ± 0.001		0.47 ± 0.04
R(30)	9.219	0.49	0.80	0.20 ± 0.01	0.02	0.024 ± 0.006	0.079±0.011	0.42 ± 0.02
R(28)	9.229	0.50±0.20	0.74 ± 0.01	0.14 ± 0.03	0.04 ± 0.01	0.016 ± 0.001	0.042±0.002	0.45 ± 0.05
R(26)	9.239	0.60±0.19	0.75 ± 0.01	0.13 ± 0.03	0.03 ± 0.03	0.023 ± 0.001	0.054±0.002	0.41 ± 0.02
R(24)	9.250	0.65±0.02	0.72 ± 0.02	0.18 ± 0.03	0.04 ± 0.04	0.014 ± 0.004	0.046±0.001	0.29 ± 0.07
R(22)	9.260	0.67±0.12	0.70 ± 0.02	0.19 ± 0.02	0.03 ± 0.01	0.035 ± 0.008	0.080±0.009	0.23
R(20)	9.271	0.58±0.11	0.72 ± 0.04	0.17 ± 0.03	0.03 ± 0.03	0.042	0.071±0.001	0.25 ± 0.05
R(18)	9.282	0.61±0.02	0.71 ± 0.01	0.16 ± 0.01	0.05 ± 0.02	0.022 ± 0.007	0.047±0.007	0.22
R(16)	9.293	0.55±0.05	0.73 ± 0.03	0.16 ± 0.02	0.04 ± 0.04	0.026 ± 0.001	0.085±0.002	0.16
R(14)	9.305	0.61±0.10	0.77 ± 0.07	0.16 ± 0.01	0.03 ± 0.03	0.011		0.21
R(12)	9.317	0.37±0.17	0.69 ± 0.01	0.17 ± 0.02	0.04 ± 0.01	0.019 ± 0.005		
R(10)	9.329	0.47±0.17	0.79 ± 0.01	0.13 ± 0.00				
P(10)	9.473	0.55±0.06	2.24 ± 0.06	0.14 ± 0.01	0.02 ± 0.01	0.028 ± 0.002	0.107±0.002	0.07
P(12)	9.488	0.44±0.13	2.77 ± 0.07	0.14 ± 0.03	0.05 ± 0.03	0.039 ± 0.006	0.120±0.002	0.08 ± 0.03
P(14)	9.504	0.40±0.10	3.33 ± 0.07	0.15 ± 0.01	0.04 ± 0.03	0.032 ± 0.004	0.089±0.008	0.07 ± 0.05
P(16)	9.520	0.47±0.11	3.92 ± 0.08	0.19 ± 0.04	0.06 ± 0.06	0.067 ± 0.001	0.087±0.001	0.08 ± 0.01
P(18)	9.536	0.49±0.13	4.54 ± 0.05	0.18 ± 0.02	0.09 ± 0.07	0.030 ± 0.001	0.084±0.010	0.05
P(20)	9.553	0.46±0.12	5.17 ± 0.07	0.22 ± 0.02	0.13 ± 0.08	0.029 ± 0.011	0.130±0.006	0.06 ± 0.05
P(22)	9.569	0.59±0.07	5.60 ± 0.04	0.25 ± 0.07	0.11 ± 0.09	0.043 ± 0.005	0.117±0.002	0.05
P(24)	9.586	0.56±0.12	5.75 ± 0.14	0.31 ± 0.03	0.09	0.061 ± 0.013	0.053±0.001	0.02
P(26)	9.604	0.58±0.06	5.24 ± 0.06	0.41 ± 0.03	0.11 ± 0.03	0.038 ± 0.007	0.409±0.006	0.05 ± 0.01
P(28)	9.621	0.58±0.12	4.89 ± 0.08	0.59 ± 0.03	0.13 ± 0.05	0.048 ± 0.003	0.173±0.019	0.03 ± 0.00
P(30)	9.639	0.45±0.06	4.53 ± 0.07	1.01 ± 0.06	0.18 ± 0.02	0.079 ± 0.012	0.086 ±0.003	0.02 ± 0.02
P(32)	9.658	0.61±0.13	5.70 ± 0.11	1.43 ± 0.09	0.17 ± 0.01	0.061 ± 0.008	0.104±0.004	0.04 ± 0.01
P(34)	9.676	0.53±0.12	6.00	1.64 ± 0.07	0.22 ± 0.01	0.088 ± 0.010	0.329±0.003	0.04
P(36)	9.695	0.51	6.04 ± 0.01	1.51 ± 0.04	0.22	0.082 ± 0.014	0.140	

Table D-1. Absorption Cross Sections ($cm^{-1}atm^{-1}$) of Selected Toxic Compounds[a] (Continued)

$C^{12}O_2^{16}$ laser 10.4 μm
($00^0 1 - 10^0 0$) band

Transition	λ (μm)	Acrylonitrile[b]	Allyl Alcohol[c]	Methyl Methacrylate[d]	Methacrylonitrile[e]	Methyl Bromide[f]	Methyl Chloride[g]	Carbonyl Difluoride[h]
R(38)	10.135			0.67 ± 0.05	0.05			
R(36)	10.147	1.91	3.07	0.65 ± 0.04	0.11 ± 0.10	0.166 ± 0.008		
R(34)	10.158	2.68±0.10	2.76 ± 0.02	0.63 ± 0.03	0.11 ± 0.01	0.162 ± 0.010	0.090±0.016	2.55 ± 0.08
R(32)	10.170	2.83±0.09	2.81 ± 0.04	0.65 ± 0.02	0.10 ± 0.00	0.214 ± 0.016	0.080±0.006	3.04 ± 0.18
R(30)	10.182	1.87±0.05	2.64 ± 0.04	0.59 ± 0.05	0.08 ± 0.02	0.095 ± 0.012	0.062±0.004	3.31 ± 0.05
R(28)	10.194	2.55±0.02	2.69 ± 0.00	0.53 ± 0.02	0.08 ± 0.02	0.125 ± 0.005	0.053±0.004	3.56 ± 0.18
R(26)	10.207	1.92±0.05	2.53 ± 0.03	0.50 ± 0.06	0.09 ± 0.01	1.018 ± 0.100	0.057±0.014	4.51 ± 0.11
R(24)	10.219	2.42±0.23	2.33 ± 0.03	0.42 ± 0.04	0.12	0.338 ± 0.004	0.210±0.003	4.30 ± 0.14
R(22)	10.233	2.07±0.03	2.21 ± 0.02	0.36 ± 0.03	0.11 ± 0.02	0.182 ± 0.007	0.078±0.005	5.48 ± 0.05
R(20)	10.247	2.14±0.01	2.07 ± 0.05	0.36 ± 0.06	0.10 ± 0.03	0.213 ± 0.011	0.040±0.006	5.15 ± 0.01
R(18)	10.260	2.39±0.34	1.91 ± 0.02	0.32 ± 0.02	0.13 ± 0.02	0.181 ± 0.016	0.061±0.005	4.47 ± 0.17
R(16)	10.274	2.74±0.12	1.80 ± 0.03	0.30 ± 0.05	0.14 ± 0.02	0.143 ± 0.015	0.071±0.006	5.17 ± 0.15
R(14)	10.289	3.57±0.44	1.72 ± 0.00	0.26 ± 0.05	0.18 ± 0.07	0.604 ± 0.039	0.089±0.001	4.92 ± 0.20
R(12)	10.303	4.85±0.12	1.83 ± 0.04	0.32 ± 0.07	0.19 ± 0.03	0.231 ± 0.010	0.086±0.004	3.51 ± 0.10
R(10)	10.318	3.59±0.27	1.71 ± 0.02	0.31 ± 0.01	0.17 ± 0.02	0.191 ± 0.014	0.027±0.005	3.50 ± 0.25
R(8)	10.334	2.28±0.01	1.63 ± 0.05	0.30	0.25 ± 0.03	0.196		
R(6)	10.349				0.21			
P(6)	10.453				0.36 ± 0.04			
P(8)	10.476		1.86 ± 0.01	1.95 ± 0.07	0.77 ± 0.04			
P(10)	10.494	3.71±0.31	2.03 ± 0.03	2.09 ± 0.13	1.04 ± 0.05	0.214 ± 0.012	0.031±0.005	3.79 ± 0.06
P(12)	10.513	4.17±0.26	2.19 ± 0.04	2.44 ± 0.09	1.26 ± 0.03	0.140 ± 0.008	0.023±0.008	3.89 ± 0.12
P(14)	10.532	2.37±0.22	2.30 ± 0.02	2.70 ± 0.09	1.47 ± 0.05	0.662 ± 0.013	0.018±0.008	3.94 ± 0.09
P(16)	10.551	2.26±0.05	2.46 ± 0.01	3.78 ± 0.02	1.73 ± 0.05	0.178 ± 0.006	0.025±0.007	3.75 ± 0.09
P(18)	10.571	2.61±0.36	2.60 ± 0.01	3.86 ± 0.01	1.91 ± 0.06	0.141 ± 0.005	0.027±0.007	3.40 ± 0.06
P(20)	10.591	1.81±0.11	2.73 ± 0.04	4.06 ± 0.20	2.10 ± 0.02	0.195 ± 0.007	0.024±0.013	2.88 ± 0.08
P(22)	10.611	1.92±0.11	2.87 ± 0.03	4.74 ± 0.21	2.20 ± 0.05	0.681 ± 0.037	0.024±0.014	2.79 ± 0.04

Table D-1. Absorption Cross Sections ($cm^{-1}atm^{-1}$) of Selected Toxic Compounds[a] (Concluded)

$C^{12}O_2$:6 laser 10.4 μm
(00°1 - 10°0) band

Transition	λ(μm)	Acrylonitrile[b]	Allyl Alcohol[c]	Methyl Methacrylate[d]	Methacrylonitrile[e]	Methyl Bromide[f]	Methyl Chloride[g]	Carbonyl Difluoride[h]
P(24)	10.632	1.96±0.106	2.90 ± 0.04	6.79 ± 0.13	2.24 ± 0.02	0.178 ± 0.015	0.029±0.011	2.19 ± 0.05
P(26)	10.653	2.40±0.17	3.07 ± 0.05	5.13 ± 0.18	2.35 ± 0.03	0.152 ± 0.004	0.023±0.012	1.82 ± 0.07
P(28)	10.674	3.76±0.07	3.18 ± 0.06	4.73 ± 0.09	2.31 ± 0.01	0.152 ± 0.010	0.020±0.009	1.64 ± 0.04
P(30)	10.696	1.71±0.15	3.20 ± 0.07	4.30 ± 0.13	2.33 ± 0.05	1.037 ± 0.019	0.009±0.008	1.31 ± 0.08
P(32)	10.718	1.57±0.05	3.51 ± 0.06	3.73 ± 0.06	2.39 ± 0.04	0.190 ± 0.019	0.009±0.003	0.91 ± 0.02
P(34)	10.741	2.28±0.31	3.51 ± 0.03	3.31 ± 0.01	2.21 ± 0.04	0.116 ± 0.015	0.010±0.008	0.76 ± 0.01
P(36)	10.764	1.49±0.02	3.41 ± 0.03	3.12 ± 0.09	2.48 ± 0.07	0.104 ± 0.004	0.011±0.003	0.57 ± 0.03
P(38)	10.787	1.34±0.04	3.65 ± 0.07	2.71 ± 0.07	13.48± 0.13	0.296 ± 0.018		0.38
P(40)	10.810		3.68 ± 0.14	2.35 ± 0.01	3.28 ± 0.09			
P(42)	10.834			1.76 ± 0.01				

[a]The acrylonitrile cross-sections decrease with increasing acrylonitrile pressure, probably due to self-complexing. These cross-sections are extrapolated zero-pressure values. The acrylonitrile cross-section uncertainties correspond to one stardard deviation. The cross-sections for the other compounds vary negligibly with sample pressure and are averages of replicate measurements. The uncertainties in these cross-sections are probable error values. Measurements were made at the following sample pressures when buffered to 760 Torr with 80% N_2/20% O_2; [b]2.01-, 3.03-, 4.41-, 5.28-, and 6.49-Torr acrylonitrile (linear least squares fit); [c]3.92-, 4.31-, 4.66-, 4.96-Torr allyl alcohol; [d]0.961-, 0.974-, 2.08-, 4.67-, 7.38-, 8.53- Torr methyl methacrylate; [e] 0.900-, 1.33-, 1.74-, 2.30-, 5.69-, 7.64-Torr methacrylonitrile, [f]1.12-, 2.80-, 3.03-, 6.81-, Torr carbonyl difluoride; [g] 9.89-, 9.96-, 16.61-, 18.77- Torr methyl bromide; [h]8.39-, 28.69-, 38.44- Torr methyl chloride.

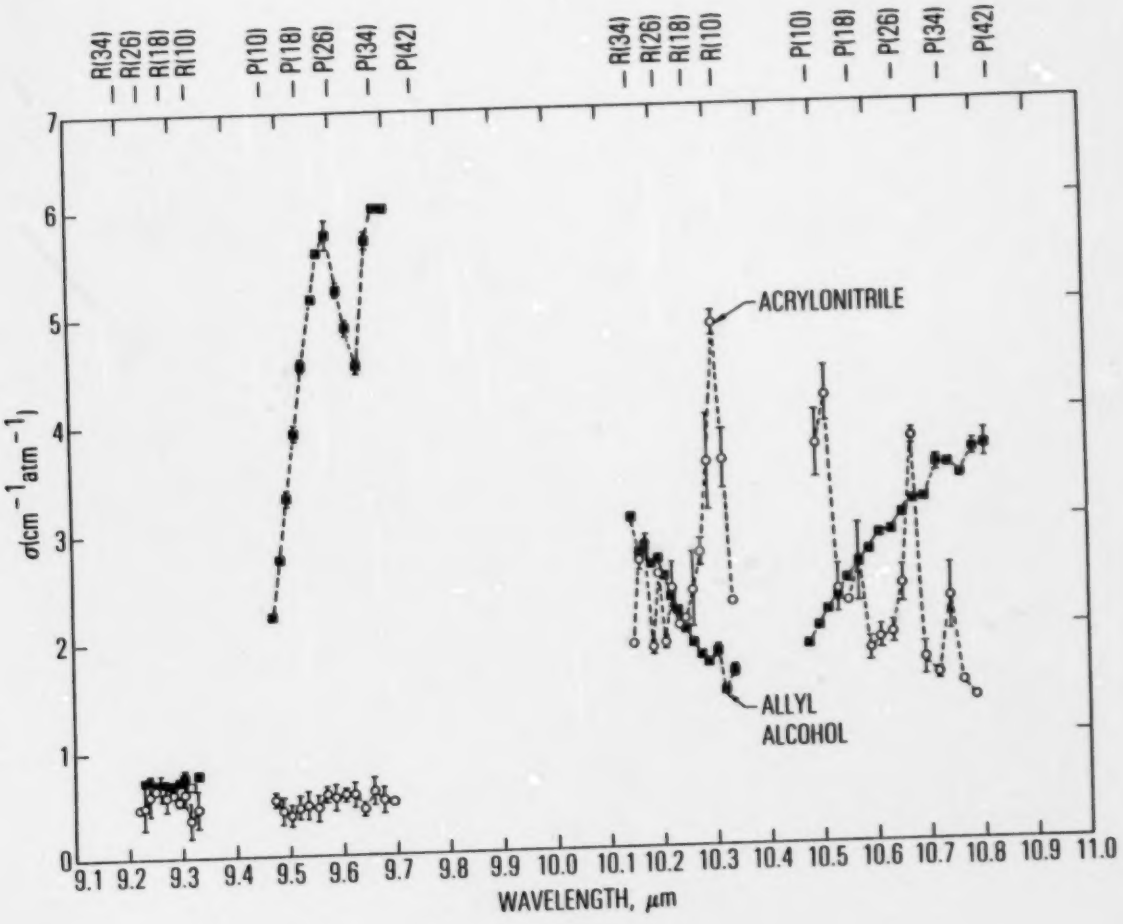

Figure D-1. CO_2 Laser Absorption Spectra of Acrylonitrile and Allyl Alcohol

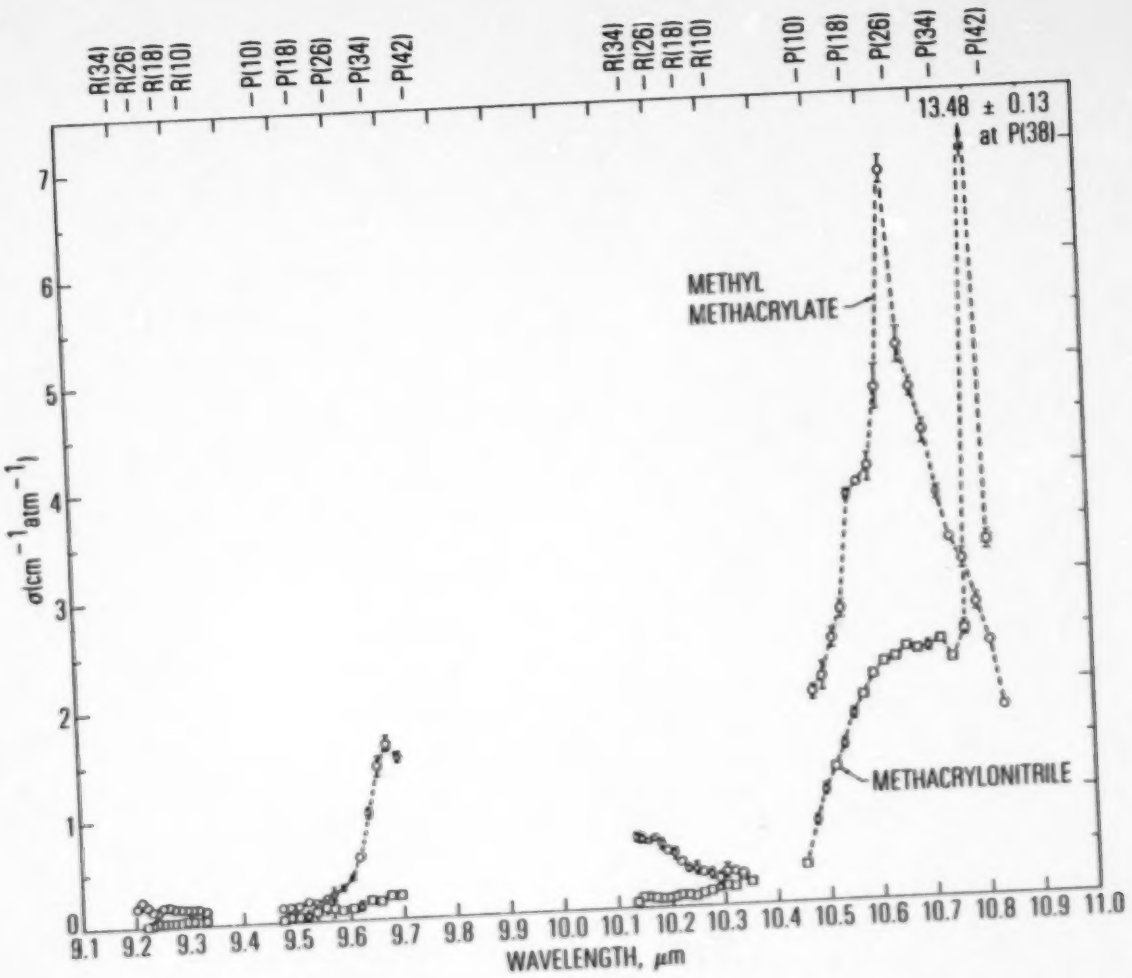

Figure D-2. CO_2 Laser Absorption Spectra of Methyl Methacrylate and Methacrylonitrile

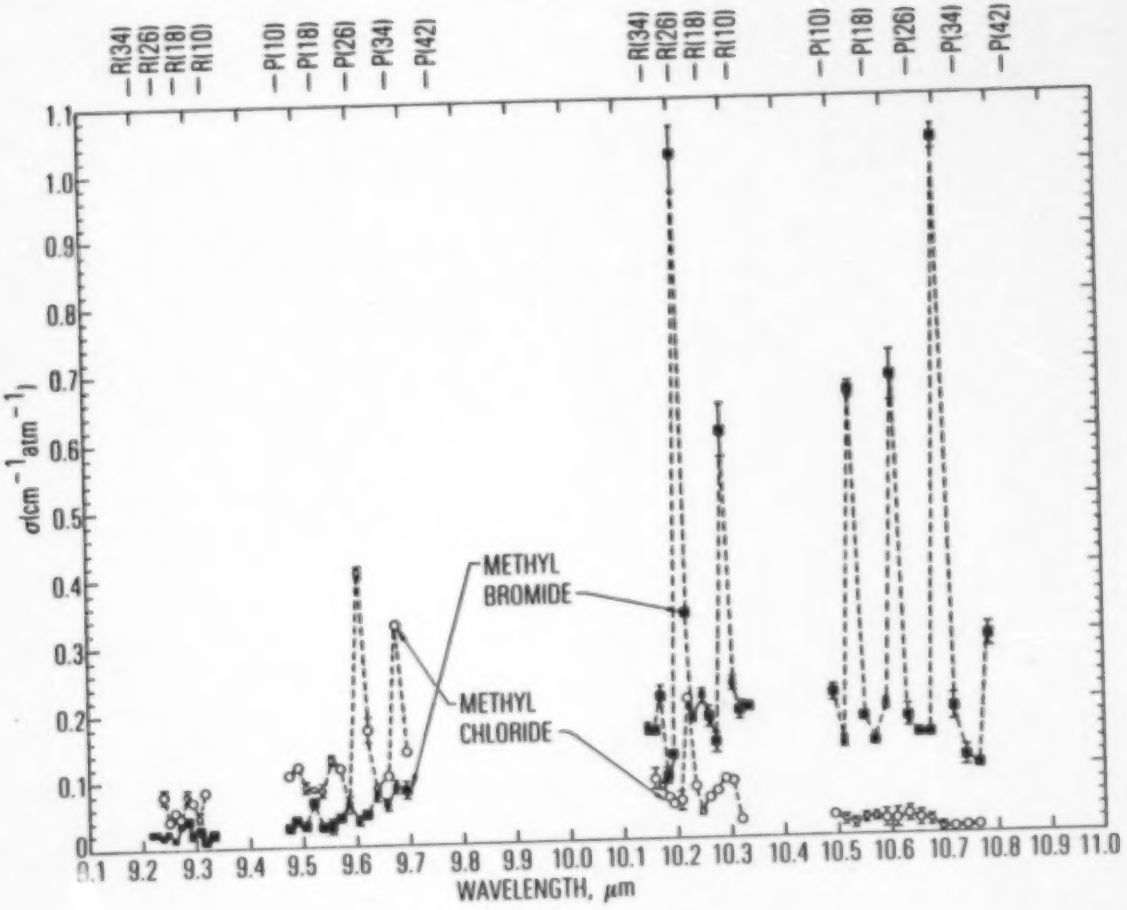

Figure D-3. CO_2 Laser Absorption Spectra of Methyl Bromide and Methyl Chloride

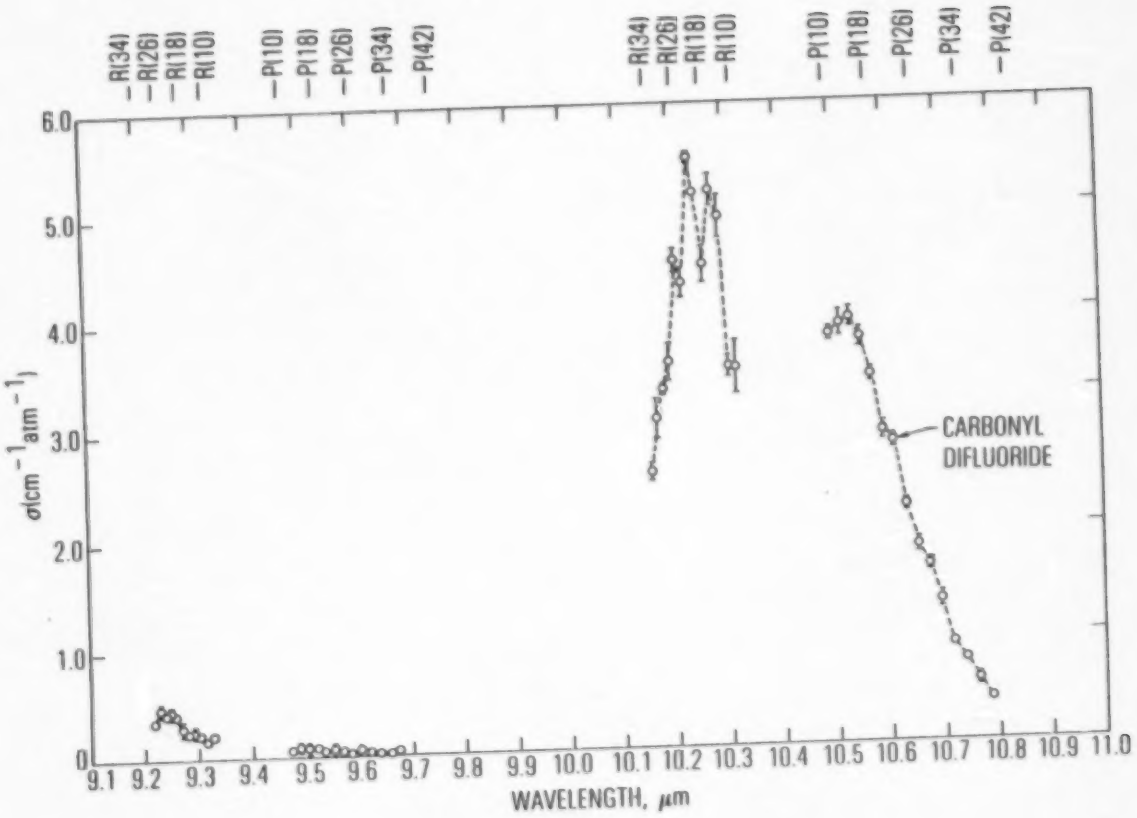

Figure D-4. CO_2 Laser Absorption Spectrum of Carbonyl Difluoride

features in absorption bands due to these modes are located near 10.29 and 10.47 μm, respectively (Ref. D-21). The most intense absorption peak observed in the acrylonitrile spectrum in Fig. D-1 corresponds to the near wavelength coincidences of the laser 10.4-μm band R12 line with the 10.29-μm Q-branch feature. The weak absorption for acrylonitrile within the laser 9.4-μm band R-branch is due to a CH_2 rocking vibrational band centered at 9.14 μm (Refs. D-23, D-24).

Allyl alcohol is observed in Fig. D-1 to possess moderate to strong absorption within the P-branches of both the 9.4- and 10.4-μm CO_2 laser bands. Vibrational assignments have not been made for allyl alcohol. Results for other vinyl compounds (Ref. D-21) suggest that allyl alcohol's trans CH=CH wag vibrational band is located near 10.03 μm, while its CH_2 wag vibrational band has a maximum near 10.84 μm. These bands, which are significantly shifted from the corresponding bands in acrylonitrile, contribute primarily to absorption within the laser 10.4-μm band R- and P-branches, respectively. Based on assignments for other unsaturated alcohols, it appears that the laser 9.4-μm band P-branch absorption is due to an allyl alcohol C-O stretching band with a maximum near 9.71 μm (Ref. D-3).

Methacrylonitrile is observed in Fig. D-2 to possess weak absorption within the laser 9.4-μm band R-branch and moderate to strong absorption within the laser 10.4-μm band P-branch. R- and Q-type rotational branch absorption contours can be observed for methacrylonitrile in the 10.4- to 10.8-μm region. This band has been assigned to the vinylidene group CH_2 wag (Ref. D-25). The R-branch absorption shoulder has a cross-section maximum of about 2.4 cm^{-1} atm^{-1}. The sharp Q-branch absorption feature has a cross section of about 13.6 cm^{-1} atm^{-1} at the laser 10.4-μm band P38 line. The P38 line apparently is nearly in resonance with this Q-branch feature. The weak absorption within the laser 9.4-μm band R-branch results from the high frequency absorption tail of a CH_3 group rocking mode (Ref. D-25).

The CO_2 laser absorption spectrum of methyl methacrylate is observed in Fig. D-2 to consist of weak to moderate strength absorption within the laser

features in absorption bands due to these modes are located near 10.29 and 10.47 μm, respectively (Ref. D-21). The most intense absorption peak observed in the acrylonitrile spectrum in Fig. D-1 corresponds to the near wavelength coincidences of the laser 10.4-μm band R12 line with the 10.29-μm Q-branch feature. The weak absorption for acrylonitrile within the laser 9.4-μm band R-branch is due to a CH_2 rocking vibrational band centered at 9.14 μm (Refs. D-23, D-24).

Allyl alcohol is observed in Fig. D-1 to possess moderate to strong absorption within the P-branches of both the 9.4- and 10.4-μm CO_2 laser bands. Vibrational assignments have not been made for allyl alcohol. Results for other vinyl compounds (Ref. D-21) suggest that allyl alcohol's trans CH=CH wag vibrational band is located near 10.03 μm, while its CH_2 wag vibrational band has a maximum near 10.84 μm. These bands, which are significantly shifted from the corresponding bands in acrylonitrile, contribute primarily to absorption within the laser 10.4-μm band R- and P-branches, respectively. Based on assignments for other unsaturated alcohols, it appears that the laser 9.4-μm band P-branch absorption is due to an allyl alcohol C-O stretching band with a maximum near 9.71 μm (Ref. D-3).

Methacrylonitrile is observed in Fig. D-2 to possess weak absorption within the laser 9.4-μm band R-branch and moderate to strong absorption within the laser 10.4-μm band P-branch. R- and Q-type rotational branch absorption contours can be observed for methacrylonitrile in the 10.4- to 10.8-μm region. This band has been assigned to the vinylidene group CH_2 wag (Ref. D-25). The R-branch absorption shoulder has a cross-section maximum of about 2.4 cm^{-1} atm^{-1}. The sharp Q-branch absorption feature has a cross section of about 13.6 cm^{-1} atm^{-1} at the laser 10.4-μm band P38 line. The P38 line apparently is nearly in resonance with this Q-branch feature. The weak absorption within the laser 9.4-μm band R-branch results from the high frequency absorption tail of a CH_3 group rocking mode (Ref. D-25).

The CO_2 laser absorption spectrum of methyl methacrylate is observed in Fig. D-2 to consist of weak to moderate strength absorption within the laser

9.4-μm band P-branch and moderate to strong absorption within the laser 10.4-μm band P-branch. The latter absorption results from a band centered at 10.65 μm that has been assigned to the vinylidene group CH_2 wag vibration (Ref. D-22). This band is located at shorter wavelength than the corresponding band in methacrylonitrile. Assignments have not been made for the 9.4-μm P-branch absorption. Based on assignments for other methyl esters and vinyl compounds, this absorption is likely due to bands resulting from either or both a CH_3 group rocking mode and the $O-CH_3$ bond stretching mode. Both bands should be centered near 9.85 μm.

B. CO_2 LASER ABSORPTION SPECTRA FOR METHYL CHLORIDE, METHYL BROMIDE, AND CARBONYL DIFLUORIDE

The CO_2 laser absorption spectra of methyl chloride and methyl bromide are compared in Fig. D-3. The absorption in the CO_2 laser region for each compound has been attributed essentially to a $H_3{\equiv}C-X$ (X is Cl or Br) bending vibration (Ref. D-26). The CH_3Br^{79} absorption band is centered at longer wavelength (10.50 μm) than the CH_3Cl^{35} band (9.85 μm) due to mass effects. Resolvable rotational structure in the bands of both compounds result in highly characteristic CO_2 laser absorption spectra. The CO_2 laser absorption spectra of these compounds can be readily distinguished from each other and from those of other chlorinated and brominated compounds (Refs. D-3, D-5, D-6).

Carbonyl difluoride is observed in Fig. D-4 to exhibit weak absorption within the CO_2 laser 9.4-μm band, but an absorption band with R-,Q-, and P-rotational branch contours of moderate-to-strong intensity within the laser 10.4-μm band. The latter absorption band is due to a vibration that results in the in-phase stretching of the C-F bonds in carbonyl difluoride (Ref. D-27). The carbonyl difluoride CO_2 laser absorption spectrum can be easily distinguished from those of other fluorinated compounds (Refs. D-3, D-6).

C. EXPECTED CO_2 LASER PHOTOACOUSTIC DETECTABILITIES OF TOXIC COMPOUNDS IN THE AMBIENT AIR

The minimum vapor phase concentration at which a particular compound can be detected in the absence of interferences by the CO_2 laser photoacoustic method is given by the expression

$$P_{min} = (\alpha_{min})/[\sigma(\lambda)] \qquad (D-1)$$

Here α_{min} represents the minimum detectable absorption coefficient of the CO_2 laser photoacoustic detector, and $\sigma(\lambda)$ is the absorption cross section of the compound to be detected at the CO_2 laser monitoring wavelength. The minimum detectable absorption coefficients obtained with nonresonant (Ref. D-28) and resonant (Ref. D-29) photoacoustic cells designed to minimize window absorption are currently 10^{-10}–10^{-9} cm^{-1}. Based upon the absorption cross-section maxima observed in Figs. D-1 through D-4, the following interference-free detectabilities would be expected using a detection system with an α_{min} value of 10^{-9} cm^{-1}: acrylonitrile (0.25 ppb), allyl alcohol (0.20 ppb), methacrylonitrile (0.07 ppb), methyl methacrylate (0.15 ppb), methyl chloride (2.5 ppb), methyl bromide (1.0 ppb), and carbonyl difluoride (0.20 ppb).

CO_2 laser absorption cross sections for water vapor are quite small, 10^{-4} cm^{-1} atm^{-1} (Refs. D-18, D-30). However, because of its high concentration in the ambient air, water vapor is the most important interference to the trace detection of species in air samples by CO_2 laser spectroscopic methods. The CO_2 laser absorption spectrum of water vapor consists of a few sharp absorption peaks superimposed on a broad continuous background. Absorption strengths of $\sim 10^{-6}$ cm^{-1} are obtained throughout most of the CO_2 laser region for air samples containing 15 Torr of water vapor (i.e., at ~ 70% RH at 23°C). For air samples with 5 Torr of water vapor, this absorption is reduced to $\sim 4 \times 10^{-7}$ cm^{-1} (Refs. D-18, D-30).

The use of absorption measurements that are carefully ratioed to the sharp water peaks should allow the characteristic absorption profiles in Figs. D-1 through D-4 to be recognizable at absorption strengths as small as 10% of the continuous water vapor background absorption (Refs. D-4, D-5). Thus, for air samples containing 15 Torr of water vapor, the α_{min} value in Eq. (D-1) would increase to $\sim 10^{-7}$ cm^{-1} and the CO_2 laser photoacoustic detection limits listed previously would be expected to increase by a factor of ~ 100. Table D-2 compares the detection limits that would be expected in air samples containing 15 Torr water vapor and no other interferences with the current or proposed threshold limit values (Ref. D-11) for these compounds in work place

Table D-2. Comparison of Expected CO_2 Laser Photoacoustic Detectabilities[a] of Selected Toxic Vapors to Work Place Standards for These Compounds

Compound	CO_2 laser Wavelength λ(μm)	Transition	σ(λ) ($cm^{-1}atm^{-1}$)	P'min = α'min/[σ(λ)][b] (atm, ppb)	Current threshold limit values (TLV's) in workplace air[11]
Acrylonitrile	10.303	R(12)	4.85 ± 0.12	21	2-ppm OSHA[c] 8-h time-weighted average (TWA), OSHA-cancer hazard
	10.513	P(12)	4.17 ± 0.26	24	
Allyl Alcohol	9.695	P(36)	6.04 ± 0.01	17	2-ppm OSHA 8-h TWA
	10.718	P(32)	3.51 ± 0.06	28	
Methacrylonitrile	10.718	P(32)	2.39 ± 0.04	42	1-ppm NIOSH[d] recommended 8-h TWA
	10.787	P(38)	13.48 ± 0.13	7	
Methyl Methacrylate	10.632	P(24)	6.79 ± 0.13	15	100-ppm OSHA 8-h TWA (ACGIH[e] may recommend lower TLV)
	10.718	P(32)	3.73 ± 0.06	27	
Methyl Chloride	9.604	P(26)	0.409 ± 0.008	250	100-ppm OSHA 8-h TWA 50-ppm ACGIH recommended 8-h TWA
	10.219	R(24)	0.210 ± 0.003	480	
Methyl Bromide	10.207	R(26)	1.02 ± 0.10	10	20-ppm OSHA ceiling level 5-ppm NIOSH 8-h TWA
	10.696	P(30)	1.04 ± 0.02	10	
Carbonyl Difluoride	10.233	R(22)	5.48 ± 0.05	18	2-ppm MIOSH 8-h TWA (ACGIH may recommend lower TLV)
	10.532	P(14)	3.94 ± 0.09	25	

[a] Estimated detection limit in air samples containing 15-Torr water vapor and no other interferences.
[b] Assumes an effective minimum detectable absorptivity value α'_{min} of 10^{-7} cm^{-1}. This value is 10% of the water continuum background absorption for air samples containing 15-Torr water vapor. P'min value expressed in parts of vapor per billion parts of air by volume at 25°C and 760 Torr pressure.
[c] Occupational Safety and Health Administration.
[d] National Institute of Occupational Safety and Health.
[e] American Conference of Governmental Industrial Hygienists.

air. The expected photoacoustic detection limits for these compounds in high-humidity air samples are observed in Table D-2 to be a factor of 50 or more below their most stringent current or recommended threshold limit values.

As in our earlier studies (Refs. D-4, D-5), an analysis of the spectral properties and possible concentrations of inorganic and organic pollutants found in urban air suggests that these pollutants should not significantly increase the photoacoustic detection limits estimated for the toxic compounds in Table D-2 in the presence of water vapor only. Based on the uniqueness of the CO_2 laser spectral signatures observed for the compounds studied here, it is further expected that the detection limits listed in Table D-2 should not significantly increase if these compounds are to be monitored in multi-component ambient air mixtures of each other or compounds of similar structure.

IV. CONCLUSIONS

The absorption cross-section data determined for the hazardous compounds acrylonitrile, allyl alcohol, methacrylonitrile, methyl methacrylate, methyl chloride, methyl bromide, and carbonyl difluoride indicate that each of these compounds can be readily distinguished from each other and from possible interferences in the ambient air by CO_2 laser spectroscopic detection techniques. It was estimated in Section III that the CO_2 laser photoacoustic method should be capable of detecting, even in the presence of 15-Torr water vapor, methyl chloride and methyl bromide at the 250- and 100-ppb levels, respectively. The other five compounds were estimated to be detectable at concentrations of 25-ppb or lower by the photoacoustic method under these conditions. Because each of the seven compounds possess highly characteristic CO_2 laser absorption spectra, it is further expected that they should be detectable by the CO_2 laser photoacoustic method at similar low levels in multicomponent mixtures of each other or in the presence of typical air pollutants. These concentrations are well below current or anticipated new work-place standards for these compounds.

REFERENCES

D-1. R. Beck, W. English, and K. Gürs, Table of Laser Lines in Gases and Vapors, Vol. 2, Springer, Berlin (1978).

D-2. R. A. McClatchey, W. S. Benedict, S. A. Clough, D. E. Burch, R. F. Calfee, K. Fox, L. S. Rothman, and J. S. Garing, AFCRL Atmospheric Absorption Line Parameters Compilation, AFCRL-TR-73-0096, Bedford, Mass. (1973).

D-3. C. J. Pouchert, The Aldrich Library of Infrared Spectra, Edition III, Aldrich Chemical Co, Inc., Milwaukee (1981).

D-4. G. L. Loper, A. R. Calloway, M. A. Stamps, and J. A. Gelbwachs, Appl. Opt. 19, 2726 (1980).

D-5. G. L. Loper, G. R. Sasaki, and M. A. Stamps, Appl. Opt. 21, 1648 (1982).

D-6. B. D. Green and J. I. Steinfeld, Environ. Sci. Technol. 10, 1134 (1976); Appl. Opt. 15, 1688 (1976).

D-7. P. Anderson and U. Persson, Appl. Opt. 23, 192 (1984).

D-8. R. R. Patty, G. M. Russwurm, W. A. McClenny, and D. R. Morgan, Appl. Opt. 13, 2850 (1974).

D-9. IARC Monographs on the Evaluation of Carcinogenic Risk of Chemicals to Man, 19, 73 (1979); and 28, 151 (1982). (World Health Organization, International Agency for Research on Cancer, Lyon, France).

D-10. N. I. Sax, Dangerous Properties of Industrial Materials, 6th edition, Van Nostrand Reinhold, New York (1984).

D-11. R. L. Tatken and R. J. Lewis, Sr., eds., Registry of Toxic Effects of Chemical Substances, U. S. Dept. of Health and Human Services (National Institute for Occupational Safety and Health) Publication No. 83-107 (U. S. GPO, Washington, D.C., 1983).

D-12. R. E. Kirk, D. F. Othmer, M. Grayson, and D. Eckroth, Kirk-Othmer Encyclopedia of Chemical Technology, John Wiley and Sons, Inc., New York (1978).

D-13. A. McRae and L. Whelchel, eds., Toxic Substances Control Source Book Aspen Systems Corp., Rockville, Md. (1978).

D-14. "Hazardous Constituents of Waste Streams," Appendix VIII, Federal Register, Vol. 46, pp. 27477-480 (20 May 1981).

D-15. A. Mayer, J. Comera, H. Charpentier, and C. Jaussaud, Appl. Opt. 17, 391 (1978); Appl. Opt. 19, 1572 (1980).

D-16. U. Perrson, B. Marthinsson, J. Johansson, and S. T. Eng, Appl. Opt. 19, 1711 (1980).

D-17. R. J. Brewer and C. W. Bruce, Appl. Opt. 17, 3746 (1978).

D-18. G. L. Loper, M. A. O'Neill, and J. A. Gelbwachs, Appl. Opt., 22, 3701 (1983).

D-19. R. T. Menzies, Appl. Opt. 15, 2597 (1976).

D-20. Sadtler Standard Spectra, Gases and Vapors, Vol 1, Sadtler Research Laboratories, Philadelphia (1972).

D-21. W. J. Potts and R. A. Nyquist, Spectrochim. Acta 15, 679 (1959).

D-22. J. R. Cowles, W. O. George, and W. G. Fateley, JCS Perkin Trans. II, 396 (1975).

D-23. F. Halverson, R. F. Stamm, and J. J. Whalen, J. Chem. Phys., 16, 808 (1948).

D-24. I. Kanesaka, K. Miyawaki, and K. Kawai, Spectrochimica Acta, 32A, 195 (1976).

D-25. J. Bragin, K. L. Kizer, and J. R. Durig, J. Mol. Spectry. 38, 289 (1971).

D-26. G. Herzberg, Molecular Spectra and Molecular Structure II. Infrared and Raman Spectra of Polyatomic Molecules, D. Van Nostrand Co., Inc., Princeton, N. J. (1956), p 315.

D-27. A. H. Nielsen, T. G. Burke, P. J. H. Woltz, and E. A. Jones, J. Chem. Phys., 20 596 (1952); J. Overend and J. R. Scherer, J. Chem. Phys., 32, 1296 (1960).

D-28. C. K. N. Patel and R. J. Kerl, Appl. Phys. Lett. 30, 578 (1977); T. F. Deaton, D. A. Depatie, and T. W. Walker, Appl. Phys. Lett. 26, 300 (1975); M. S. Shumate, U. S. Patent 4,067,653 (10 January 1978).

D-29. C. F. Dewey, Jr., R. D. Kamm, and C. E. Hackett, Appl. Phys. Lett. 23, 633 (1973); C. W. Bruce, B. Z. Sojka, B. G. Hurd, W. R. Watkins, K. O. White, and Z. Derzko, Appl. Opt. 15, 2970 (1976); R. M. Gerlach and N. M. Amer, J. Appl. Phys. 23, 319 (1980).

D-30. M. S. Shumate, R. T. Menzies, J. S. Margolis, and L. G. Rosengren, Appl. Opt. 15, 2480 (1976); J. C. Peterson, M. E. Thomas, R. J. Nordstrom., E. K. Damon, and R. K. Long, Appl. Opt. 18, 834 (1979).